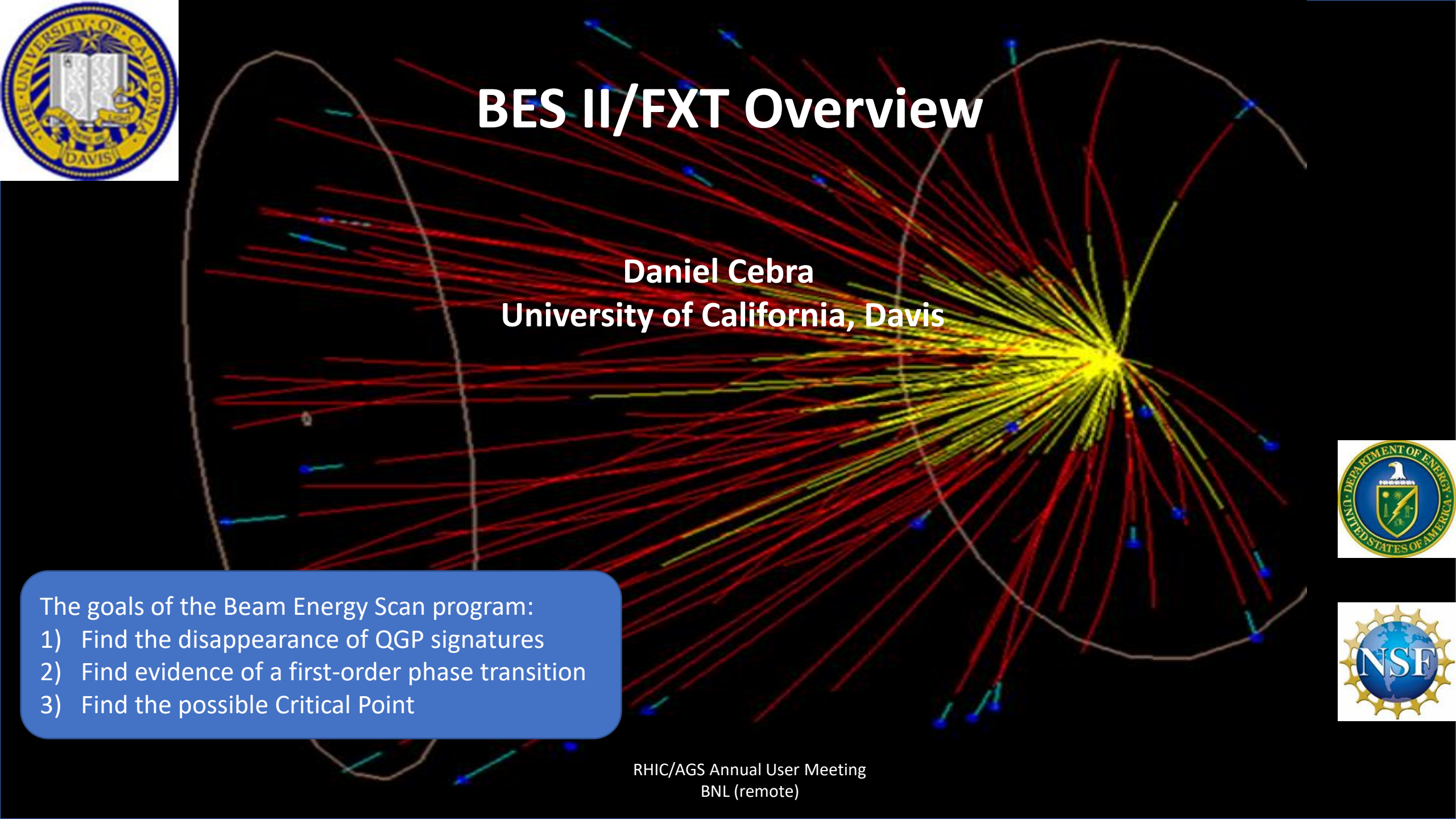

BES II/FXT Overview

Daniel Cebra
University of California, Davis

The goals of the Beam Energy Scan program:
1) Find the disappearance of QGP signatures
2) Find evidence of a first-order phase transition
3) Find the possible Critical Point

RHIC/AGS Annual User Meeting
BNL (remote)

Motivation for Energy Scans

Onset of deconfinement; nature of the phase transition; Critical Point; Partonic Matter

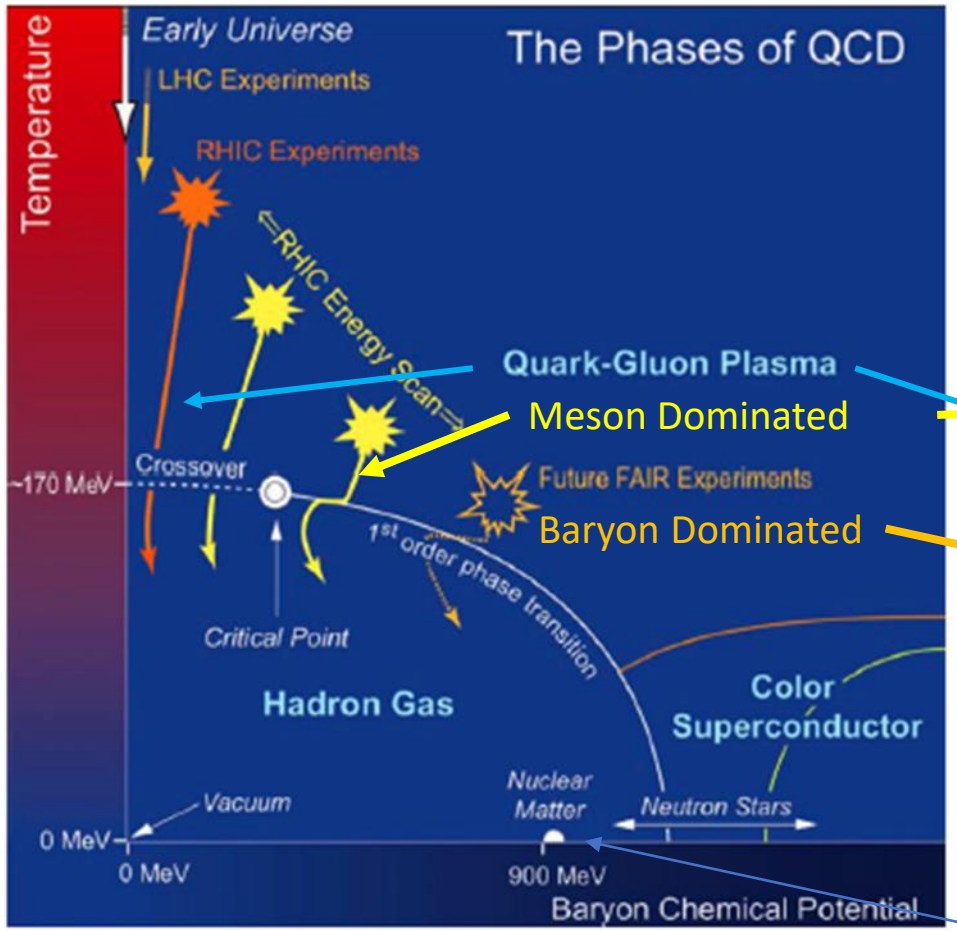

The goal of the energy scans is to study regions of the QCD which exhibit different behaviors and the transitions between such regions

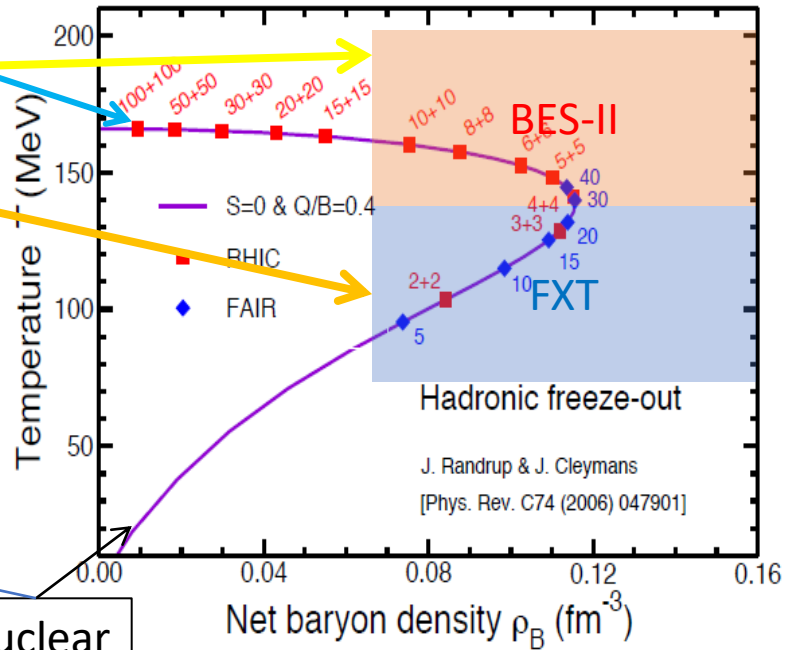

There is strong motivation to study both the baryon and meson dominated regions

Nuclear Matter

BES-II Whitepaper 2014

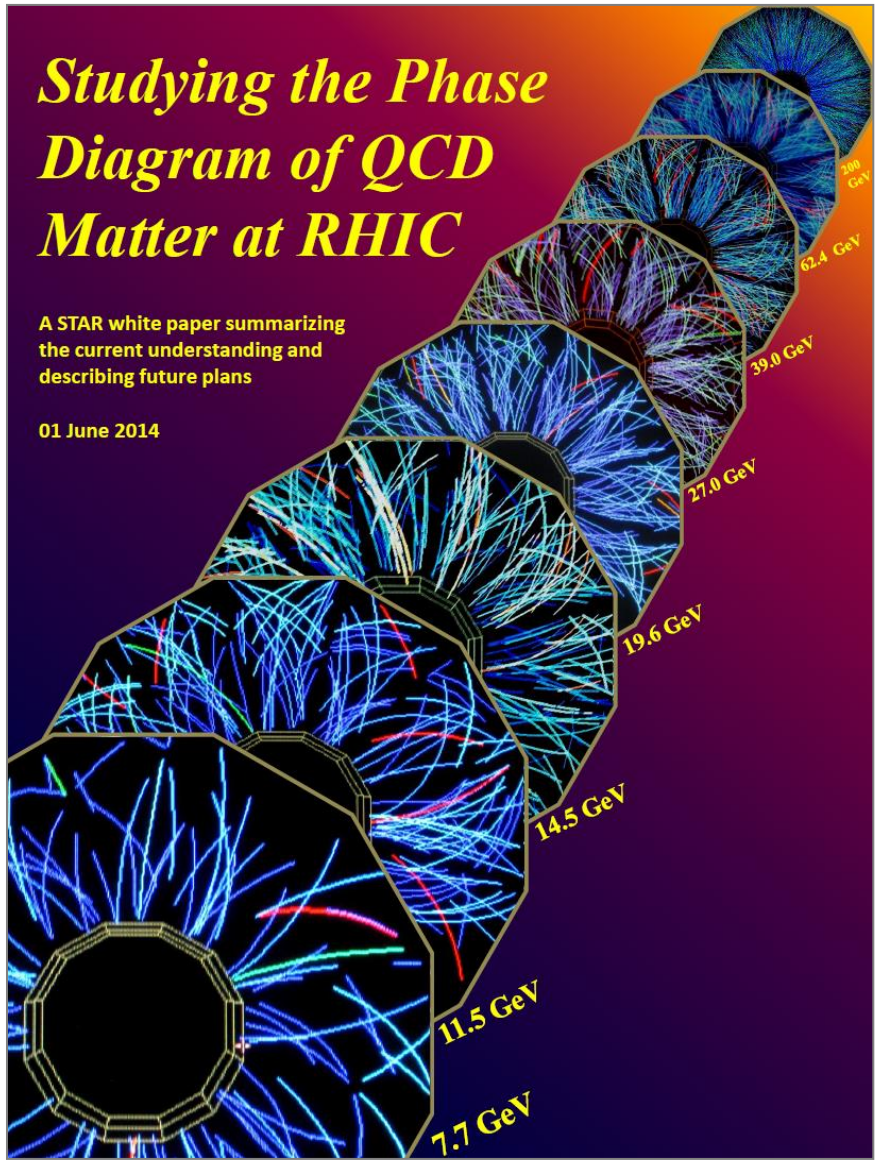

Beam Energy Scan II (2018-2021)

Select the most important energy range
➔ 3 to 20 GeV (**Add fixed-target program**)

Improve significance
➔Long runs, higher luminosity (**electron cooling**)

Refine the signals
➔ Detector improvements (**iTPC, eTOF, EPD**)

STAR Beam Energy Scan II – Mapping the QCD Phase Diagram
The Experimental Plan

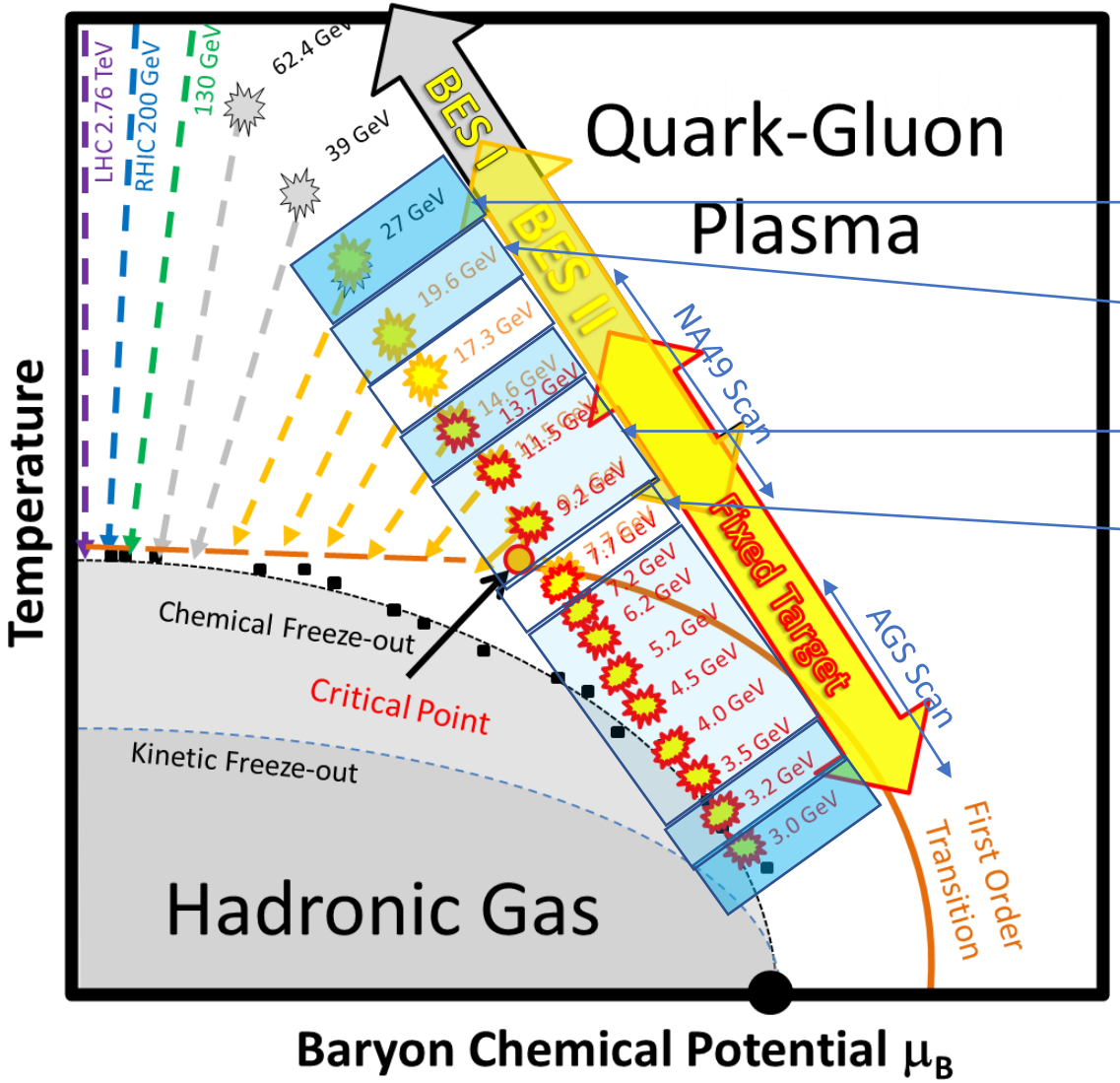

Go from easiest to hardest

Run 18 -- 27 GeV, FXT 3.0, FXT 7.2
Beams are accelerated

Run 19 – 19.6, 14.6, FXT 3.2 GeV
No acceleration in RHIC

Run 20 – 11.5, 9.2, six FXT energies
Needs cooling at 9.2 GeV

Run 21 – 7.7, 17.3 GeV Collider
FXT 9.2, 11.5, 13.5, hi stats at FXT 3

The plan went well, all items in red were extra

The BESII collider program maps the approach to the transition from the QGP side of the QCD phase diagram.

The FXT program maps the baryon-rich side of the phase diagram

- There are a lot of data.
- All collider energies have 10-20 times higher statistics compared to BES-I
- All FXT energies have at least 100 million events (500 million at 7.2 eV, 2 billion at 3.0 GeV)

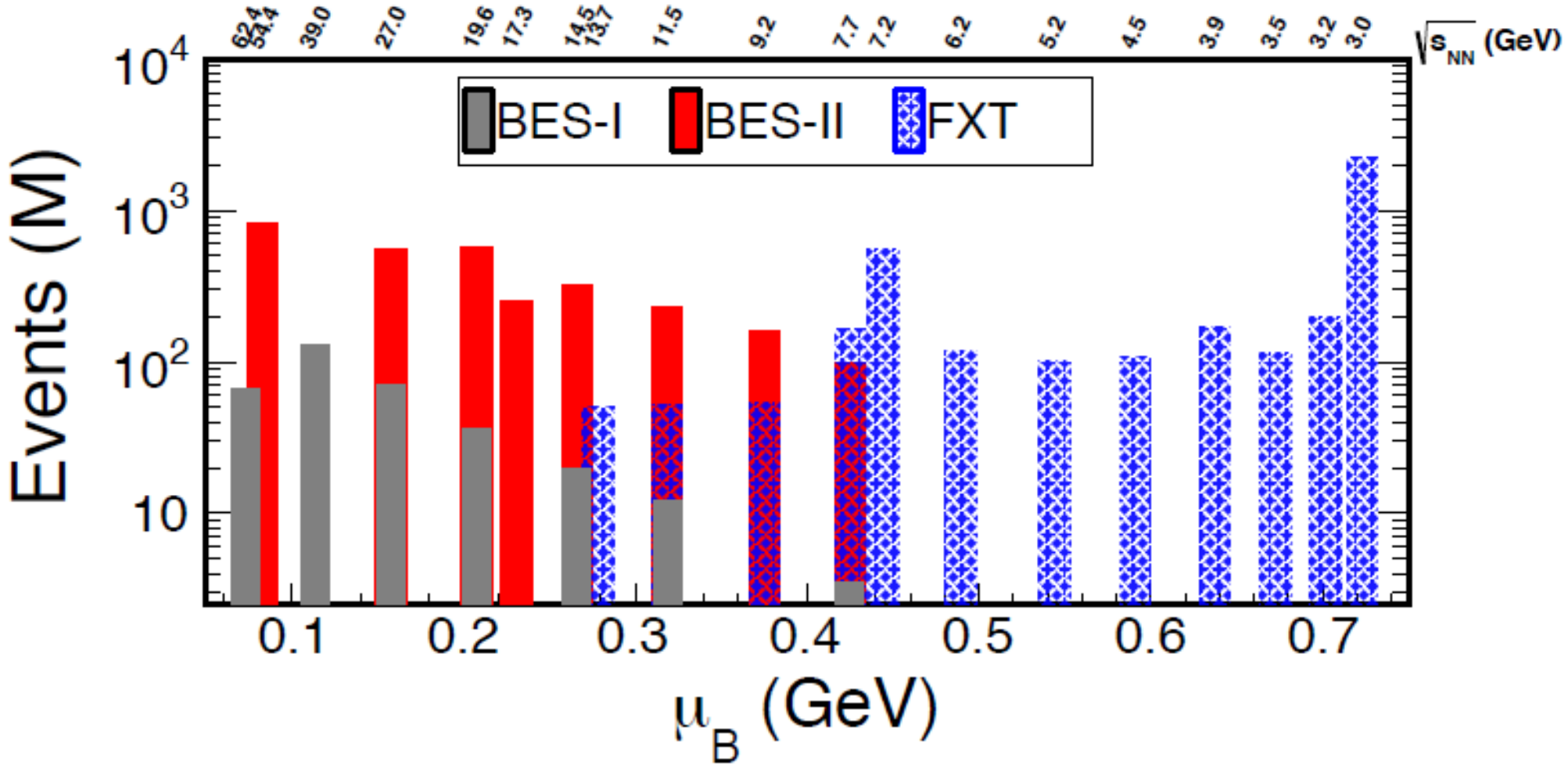

Fixed-Target (FXT) Program at STAR

- Test run with gold target in 2015
- First physics runs at $\sqrt{s_{NN}}$ = 3.0 GeV and 7.2 GeV in 2018
- Now have data at $\sqrt{s_{NN}}$ of 3.0, 3.2, 3.5, 3.9, 4.5, 5.2, 6.2, 7.2, and 7.7 GeV **(and 9.2, 11.5, and 13.7 GeV)**

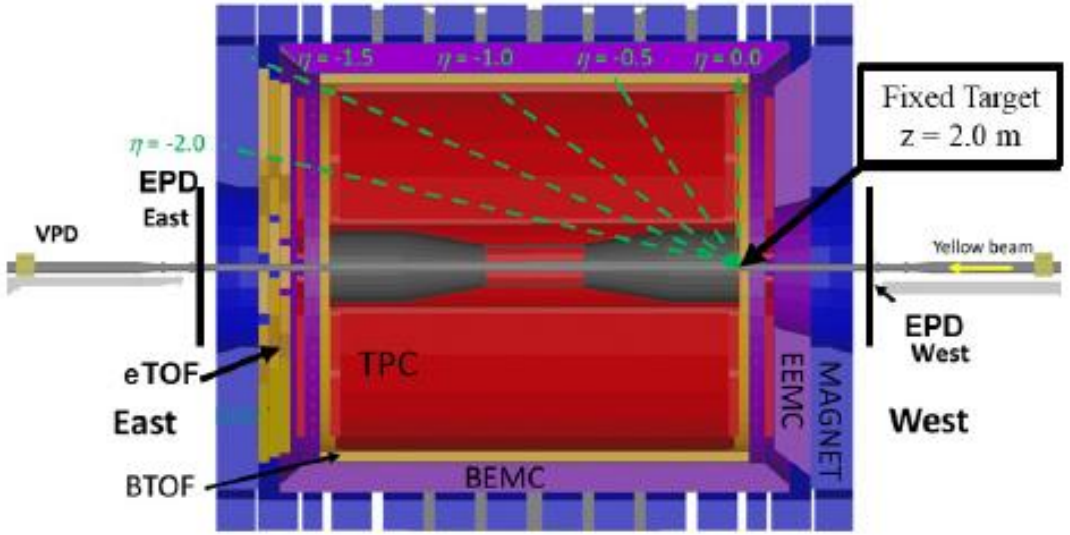

Challenges for FXT

- Shifting asymmetric acceptance wrt midrapidity
- At 7.7 GeV midrapidity moves to edge of Time Projection Chamber (TPC) acceptance
- Boost at higher energies shifts PID to rely more on TOF than TPC identification

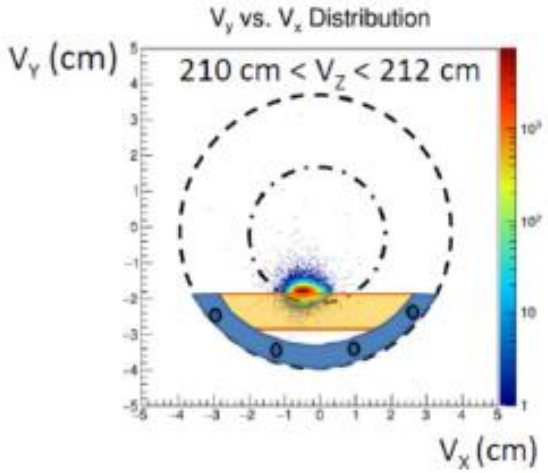

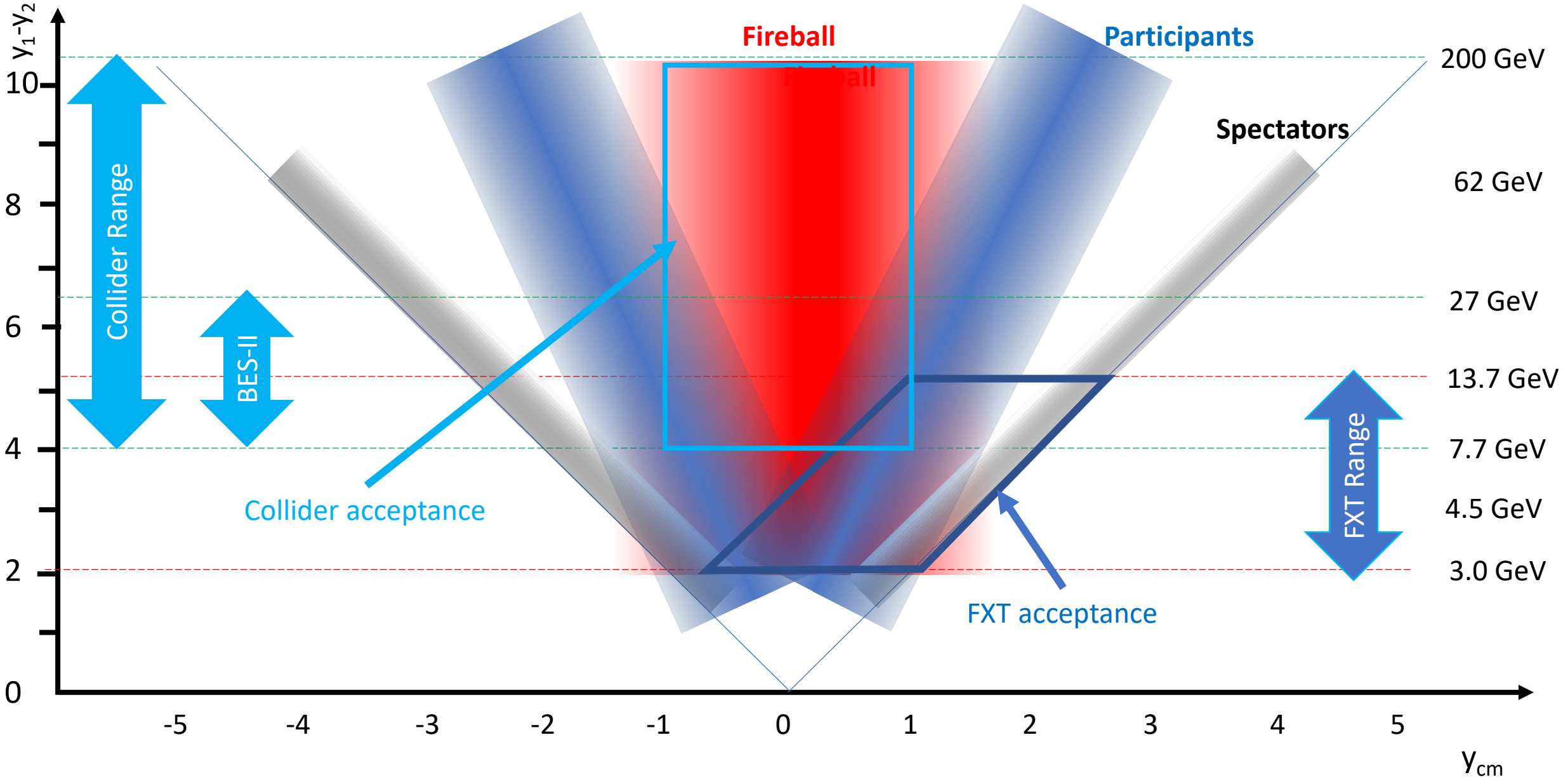

The FXT part of the program is dominated by participant baryons, while the collider part sees mostly the fireball

The Path to Publication

- Data Acquisition ← Weekly QA of FastOffline and HLT
- Calibration, Production — STAR Software Team
- Run-by-Run QA — QA Board Meetings every Friday
- Centrality — Centrality Definition Meetings Tuesday
- Physics Analysis — Analysis teams should report regularly in PWG ➔ Chaired by Conveners
- Paper Proposal Preview — PAs present paper proposal to PWGC
- God Parent Committee
- Collaboration Review

Overall Status

Acquisition of the BES-II/FXT data went very well, even leaving some time for some opportunity systems.

Calibration, Production, and Post-production QA take some time, but teams are in place and data sets are becoming available for the analysis teams.

2018	Start	Stop	Good	Target	Calib/Prod	RbyR QA	Centrality	Analysis
27 GeV	May 10th	June 17th	555 M	700 M	Produced	Completed	Completed	Published 7
3.0 FXT	May 30th	June 4th	258 M	100 M	Produced	Completed	Completed	Published 9
7.2 FXT	June 11th	June 12th	155 M	none	Produced	Completed	Completed	Status ?
2019	**Start**	**Stop**	**Good**	**Target**	**Calib/Prod**	**RbyR QA**	**Centrality**	**Analysis**
19.6 GeV	Feb 25th	April 3rd	582 M	400 M	Produced	Completed	Completed	Preliminary
14.6 GeV	April 4th	June 3rd	324 M	310 M	Produced	Completed	Completed	Preliminary
3.9 FXT	June 18th	June 18th	52.7 M	50 M	Produced	Completed	Completed	Preliminary
3.2 FXT	June 28th	July 2nd	200.6 M	200 M	Produced	Completed	Completed	Preliminary
7.7 FXT	July 8th	July 9th	50.6 M	50 M	Produced	Completed		Preliminary
200 GeV	July 11th	July 12th	138 M	140 M	Produced	Completed	Completed	
2020	**Start**	**Stop**	**Good**	**Target**	**Calib/Prod**	**RbyR QA**	**Centrality**	**Analysis**
11.5 GeV	Dec 10th	Feb 24th	235 M	230 M	Produced			Preliminary
7.7 FXT	Jan 28th	Jan 29th	112.5 M	100 M	Produced	Completed		Preliminary
4.5 FXT	Jan29th	Feb 1st	108 M	100 M	Produced	Completed		Preliminary
6.2 FXT	Feb 1st	Feb 2nd	118 M	100 M	Produced	Completed		
5.2 FXT	Feb 2nd	Feb 3rd	103 M	100 M	Produced	Completed		
3.9 FXT	Feb 4th	Feb 5th	117 M	100 M	Produced	Completed	In progress	Preliminary
3.5 FXT	Feb 13th	Feb 14th	115.6 M	100 M	Produced	Completed	In progress	Preliminary
9.2 GeV	Feb 24th	Sep 1st	161.8 M	160 M	Produced	Ready		Preliminary
7.2 FXT	Sep 12th	Sep 14th	317 M	None				
2021	**Start**	**Stop**	**Good**	**Target**	**Calib/Prod**	**RbyR QA**	**Centrality**	**Analysis**
7.7 GeV	Jan 31st	May 1st	100.9 M	100 M	Produced	Completed	In progress	Preliminary
3.0 FXT	May 1st	June 28th	2103 M	2.0 B				
9.2 FXT	May 6th	May 6th	53.9 M	50 M				
11.5 FXT	May 7th	May 7th	51.7 M	50 M				
13.7 FXT	May 8th	May 8th	50.7 M	50 M				
17.3 GeV	May 25th	June 7th	256.1 M	250 M				
7.2 FXT	June 3rd	July 3rd	88.6 M	None				

The only published results are from 2018 data.

Results from the 19.6, 14.6, and 200 GeV data sets will be shown at QM2023.

The full FXT energy scan data have been produced and completed Quality Assurance. Results from 3.2, 3.5, and 3.9 will be shown at QM2023.

7.7 GeV Collider data have been given a high priority. Results will be shown at QM2023.

Overview of Analysis Status by Topic

Physics Analysis	Status of Analyses
Rapidity Dependent Spectra	In-prep 3.0 GeV, QM2023 3.2, 7.7-54.4 GeV
Multi-strange Baryons	Published 3 GeV, QM2023 3.2 GeV
Hyper-nuclei	Published 3 GeV, QM2023 3.2-4.5 GeV
R_{CP} up to p_T = 5 GeV/c	Physics Working Group
Lambda Polarization	Published 3, 19.6 and 27 GeV,
Femtoscopy	QM2023 3.0-4.5 GeV
Directed Flow	Published 3 GeV, QM2023 3.0-7.7, 27 GeV
Elliptic Flow	Published 3 and 27 GeV, QM2023 3.0-3.9, 7.7-19.6 GeV
Chiral Magnetic Effect	Published 27 GeV, QM2023 7.7, 14.6, 19.6
Net-proton Kurtosis	Published 3 GeV, QM2023 7.7, 14.6, 19.6
Di-leptons	QM2022 27 GeV, QM2023 14.6, 19.6 GeV
J/psi Production	QM2023 14.6, 19.6, 27 GeV

Later talks by:

Yevhenia Khyzhniak

Cameron Racz

Zhiwan Xu

Zach Sweger

Zaochen Ye

*** All results that *might* be shown at QM2023 are subject to collaboration approval

Results

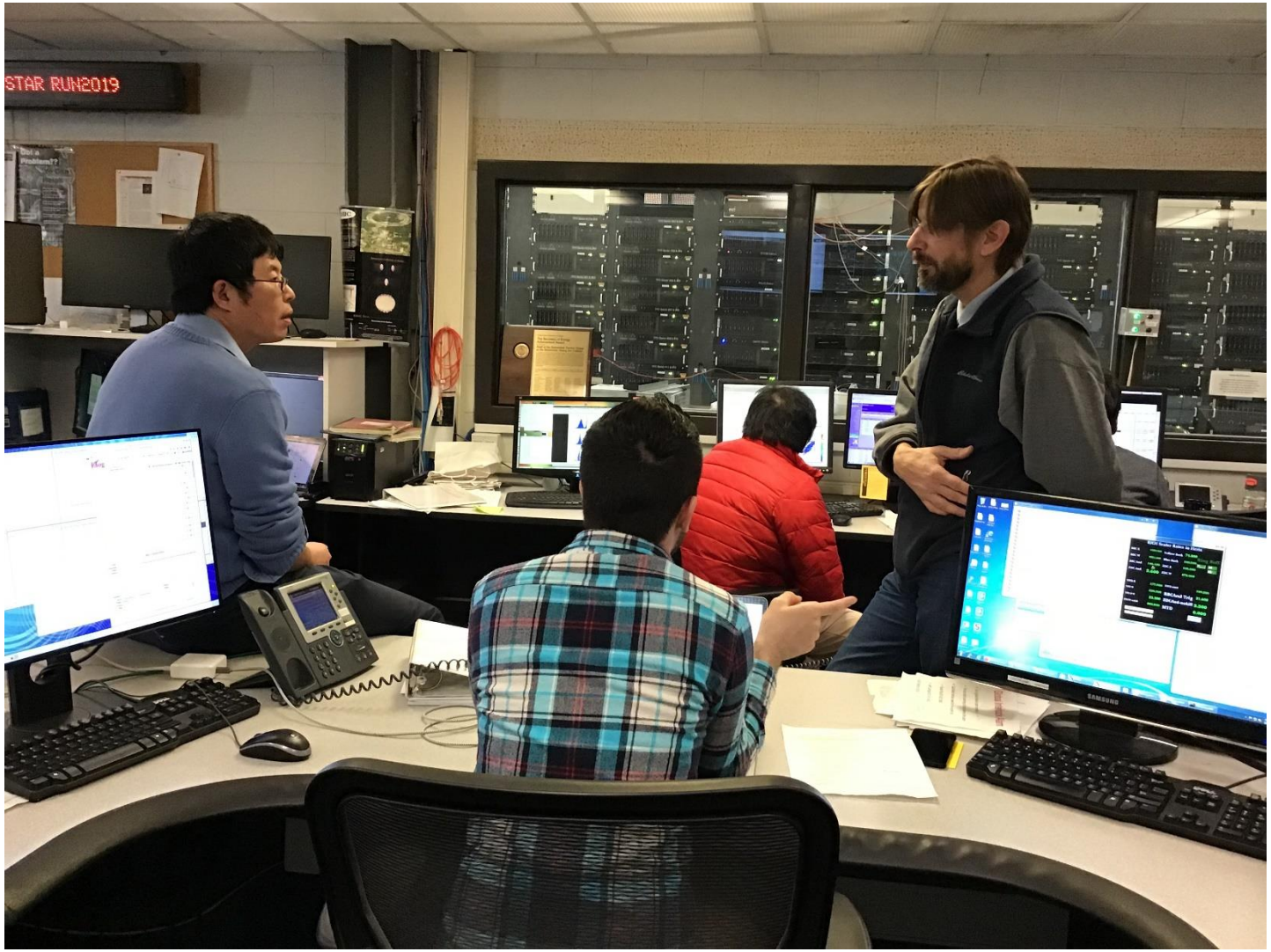

Particle Production at $\sqrt{s_{NN}}$ = 3.0 and 27 GeV

Spectra and rapidity densities have been measured for:

- π^+
- π^-
- K^+
- K^0_S
- K^-
- ϕ
- P
- Λ
- Ξ
- d
- t
- h
- α
- $^3_\Lambda H$
- $^4_\Lambda H$
- $^4_\Lambda He$

QM2023: results at 7.7-27 GeV

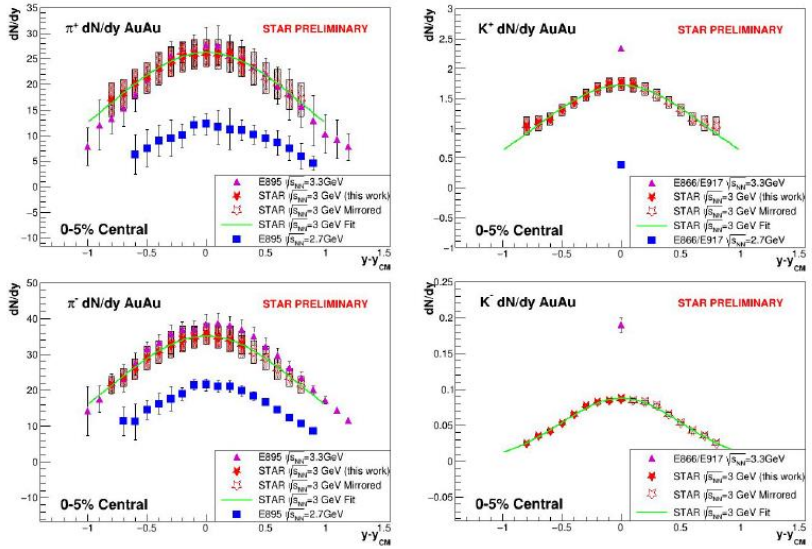

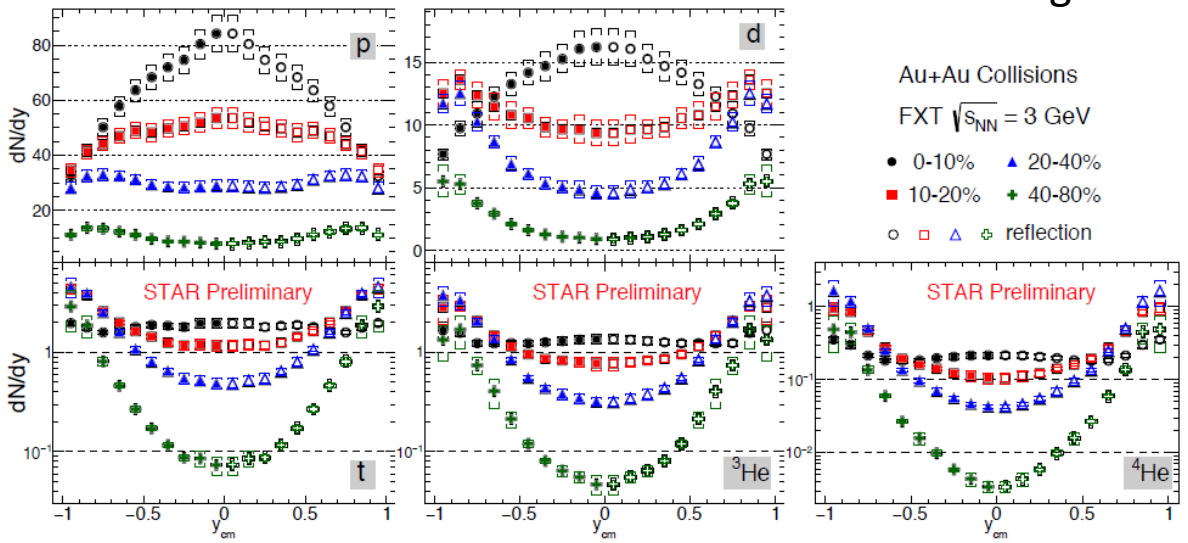

Spectra require detailed calculations of efficiency, backgrounds, and feed-down.

3.0 GeV spectra were show at QM2022 and are currently in collaboration review.

27 GeV spectra will be published with other collider energies.

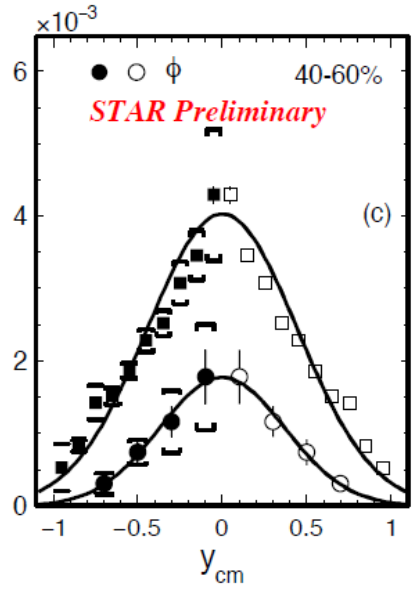

Lessons learned from spectra and rapidity densities at 3 GeV:

- The low p_T pions are strongly effected by the coulomb potential of the source.
- The charged kaons mostly comes from associated production.
- The Heinz blast wave needs to be modified to work in an environment which is not boost invariant.
- We need a better understanding of stopping.
- Light nuclei and produced through coalescence.
- Strange particle production is not well represented by UrQMD.

Further lessons that can be learned at 3 GeV:

With rapidity densities for almost all particles, we can add up the total charge, baryon number (and energy) to test conservation. ➔ We note that our total baryon number exceeds the number of participants predicted by the two component Glauber Model for all centralities.

➔ **Is something wrong? Efficiencies? Low p_T extrapolation? Maybe Glauber is "wrong"?**

Can We use multiplicity and the Glauber Model to Measure Cross-sections (centrality bins)?

- In our methodology, we “measure” cross sections by comparing the observed multiplicity distributions to those expected using the two component (N_{part} and N_{coll}) negative binomial.

- The challenge is always what fraction of the cross section are you missing at low multiplicity.

- We performed a number of test to convince ourselves that the Glauber method was OK for centrality bins.
  - Comparison to E895 ➔ Fractions of total cross section are OK.
  - Study of HADES analysis ➔ Glauber matches their multiplicity distributions.
  - Study of Zero-bias triggered data ➔ Our understanding of the trigger bias is OK.
  - Comparison Glauber to UrQMD ➔ **Predicts significantly more participating nucleons.**

  ➔ Centralities (fractions of the total inelastic cross section) using Glauber are fine, but N_{part} and N_{coll} are questionable at FXT energies.

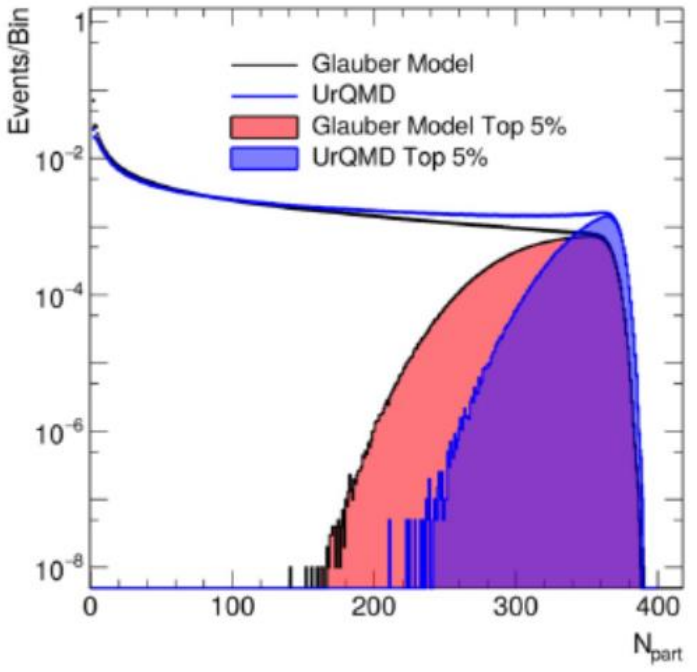

Study of identified hadrons in Au+Au collisions at $\sqrt{s_{NN}}$ = 27 GeV

27 GeV Spectra were measured in BES-I, what is new, what do we learn?

➔ Extend the rapidity coverage ➔ **Both μ_B and μ_S are seen to change with rapidity**

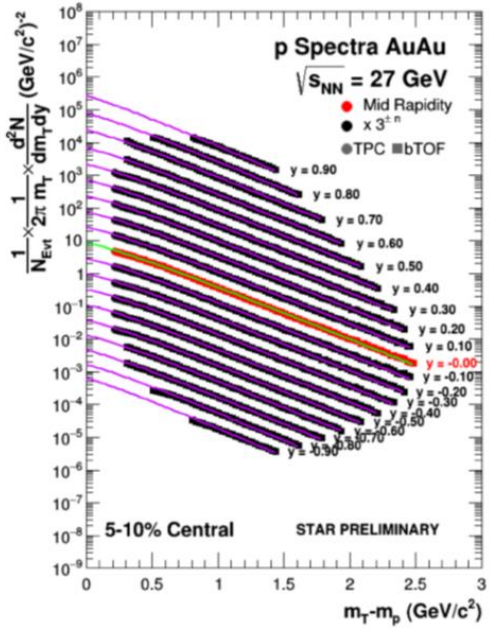

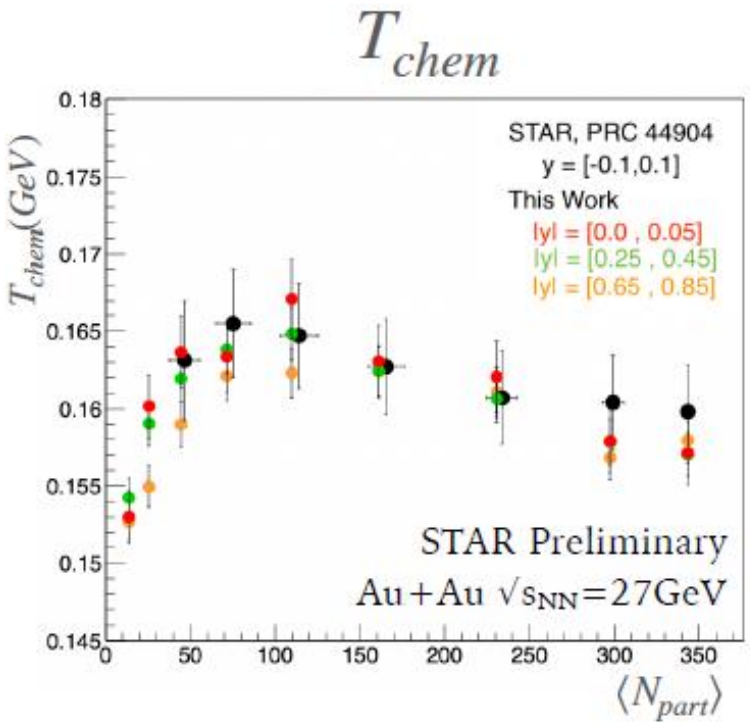

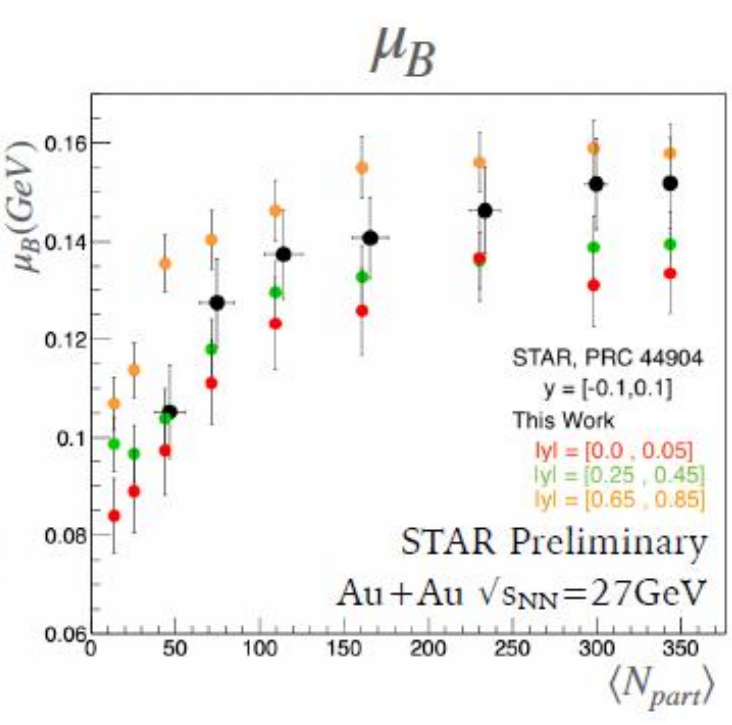

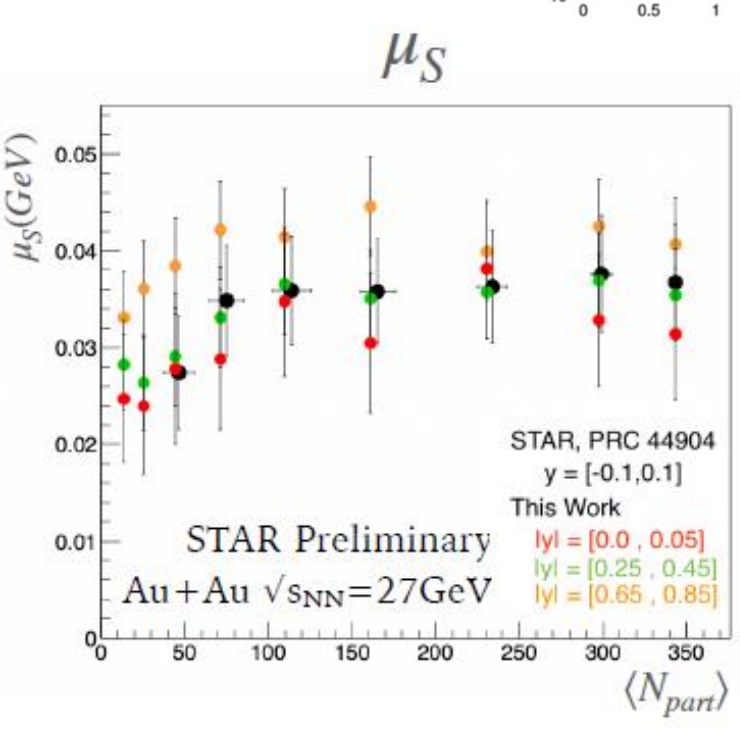

Hyper-nuclei $\sqrt{s_{NN}}$ = 3.0

QM2023: results at 3.2-4.5 GeV

Does being bound within a nucleus stabilize or de-stabilize a hyperon?

The lifetimes of the two hyper-nuclei are both 20% lower than the free Lambda lifetime.

Phys. Rev. Lett. 128 (2022) 202301

Hyper-triton

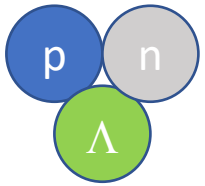

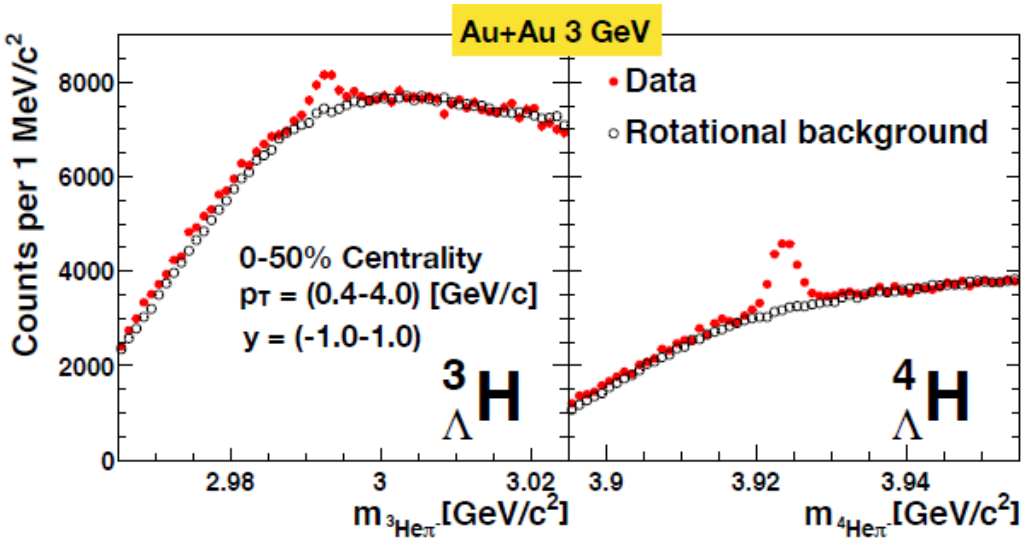

Hyper-^{4}H

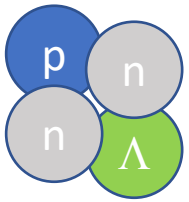

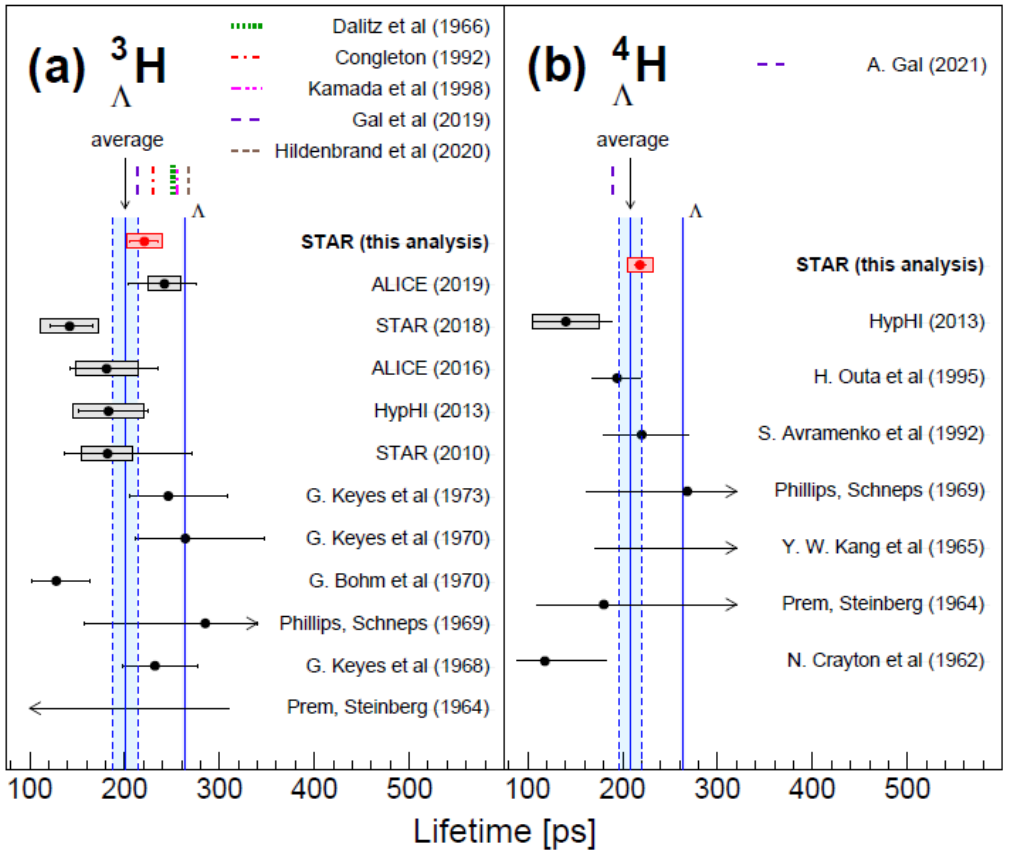

Production of hyper-nuclei occurs through coalescence. The hyperon yield rises with energy whereas the nucleon yield drops. The should be a maximum of production within the range of the FXT program.

Phys. Rev. Lett. 128 (2022) 202301

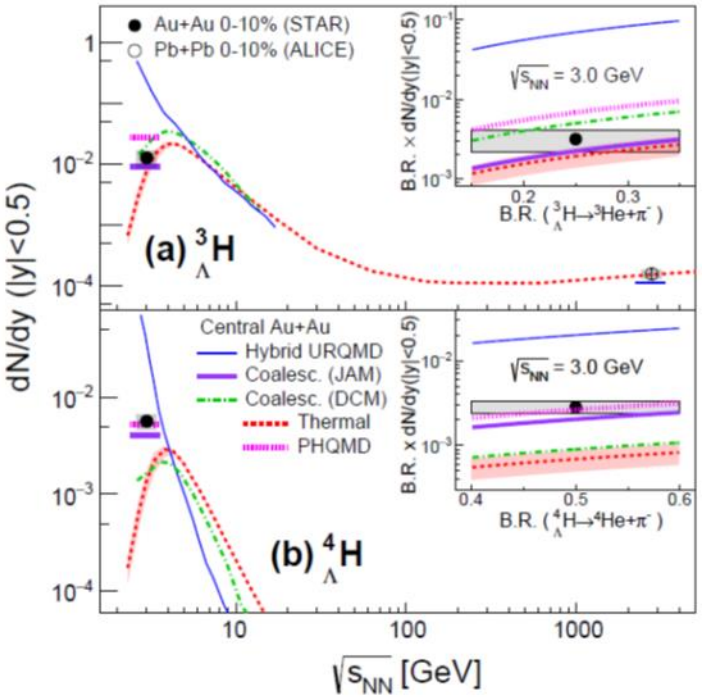

The masses and the binding energies of the mirror hypernuclei, 4HL and 4HeL, are measured at 3 GeV.

The binding energies and excited states are extracted.

Provides a new avenue to study the Charge Symmetry Breaking in heavy-ion collision experiments.

Phys. Lett. B **834** (2022) 137449

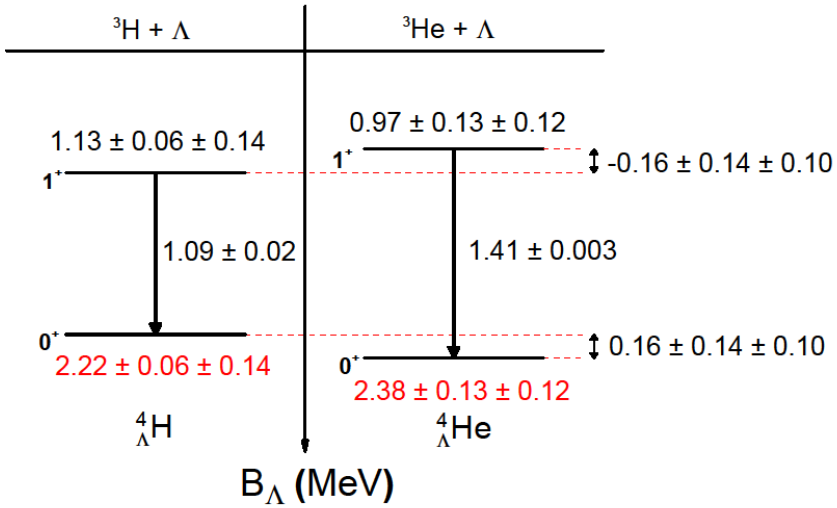

The flows of hyper-nuclei and light nuclei are similar and follow the same mass scaling suggesting the coalescence is the dominate production mechanism.

Phys. Rev. Lett. 130 (2023) 212301

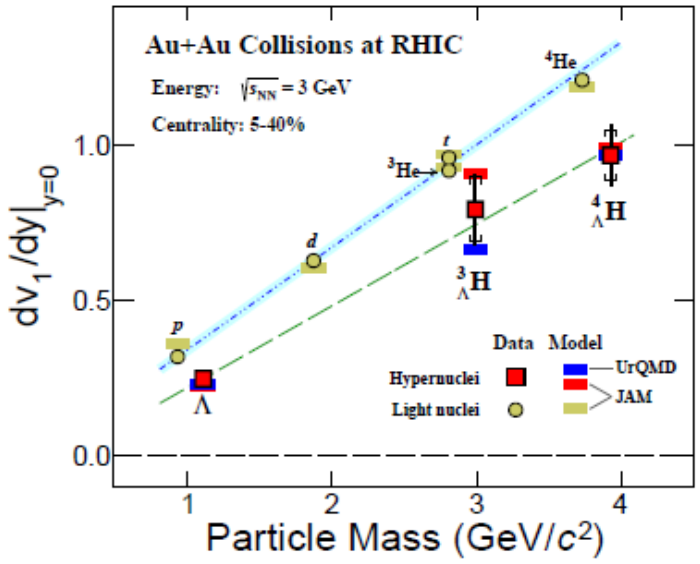

Global Polarization at $\sqrt{s_{NN}}$ = 3.0, 19.6, and 27 GeV

Lambda polarizations are expected to be sensitive to the vortical flow structure of the QGP.

- Significant polarization is seen at 3.0 GeV.
- At 19.6 and 27 GeV, the Lambda and anti-Lambda polarizations are very similar, placing an upper limit on the late-stage magnetic filed.

Phys. Rev. C **104** (2021) 61901

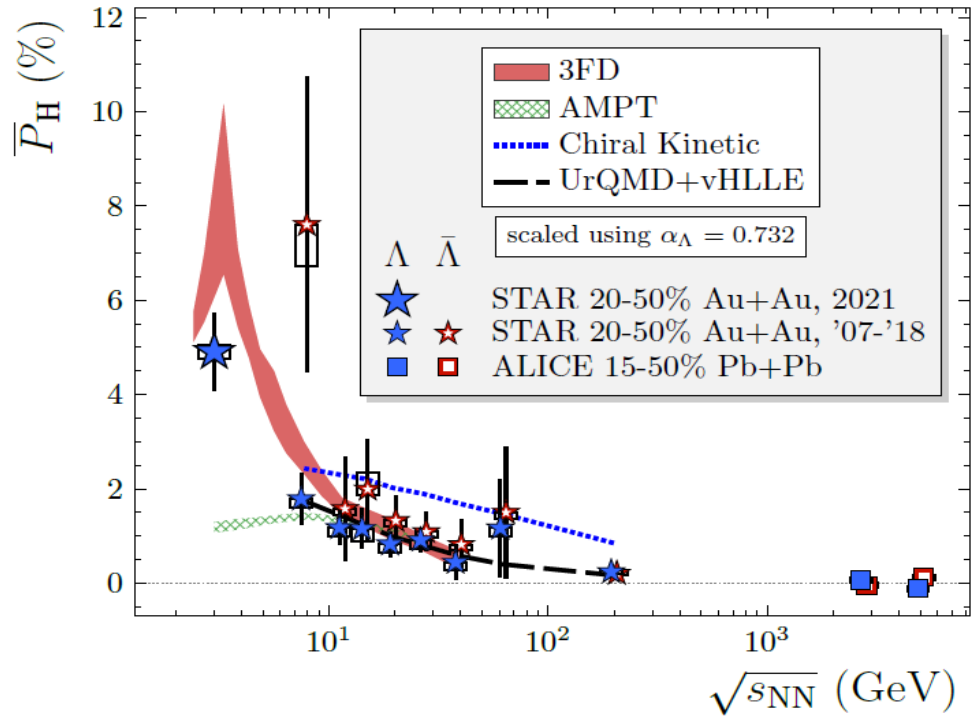

2305.08705 [nucl-ex]

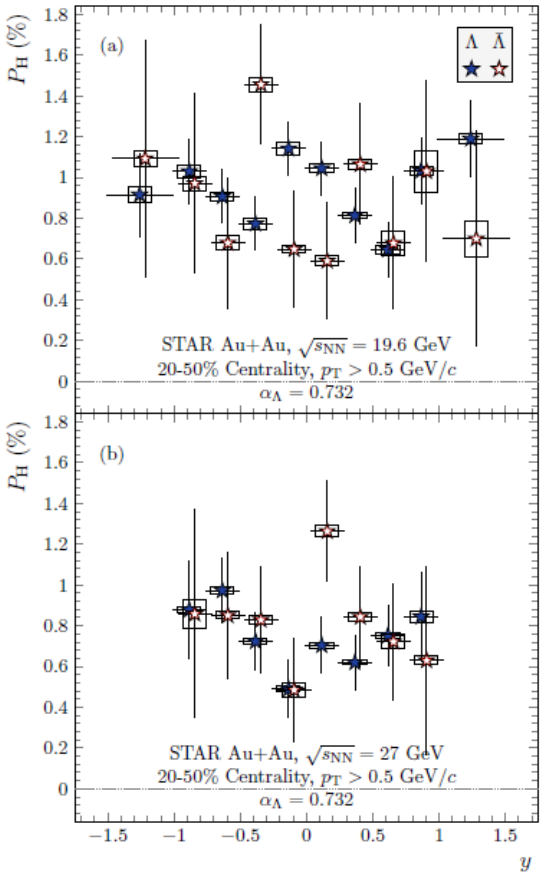

Femtoscopy at $\sqrt{s_{NN}}$ = 4.5 GeV

See later talk by Yevhenia Khyzhniak

QM2023: results at 3.0-4.5 GeV

The tilt angle and the volume of the source are sensitive to the compressibility, and hence to the first order phase boundary.

Kaon and light nuclei femtoscopy results are in collaboration review. Pion and kaon results at FXT energies will be shown at QM2023.

Here, I show the results from the 4.5 GeV test run.

This illustrates the asHBT

With the higher statistics in the BES-II/FXT data sets one can also resolve the tilt angle

Phys. Rev. C **103** (2021) 34908

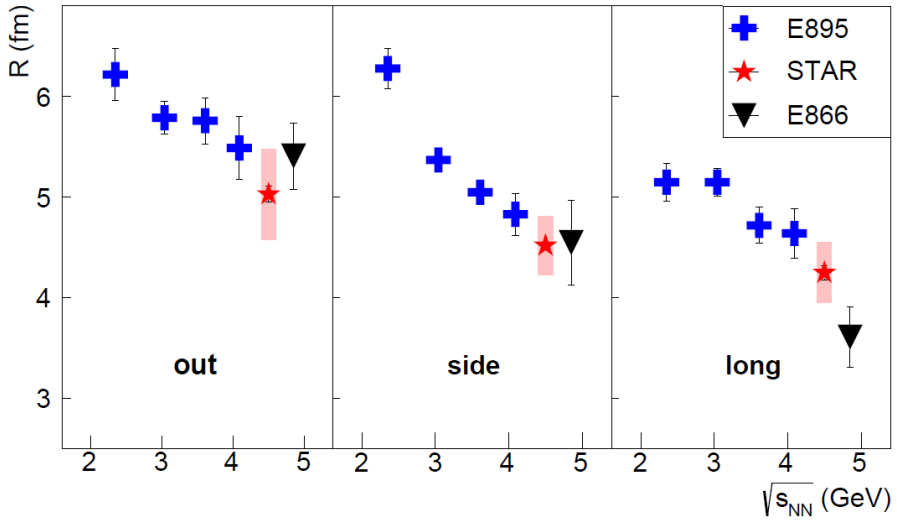

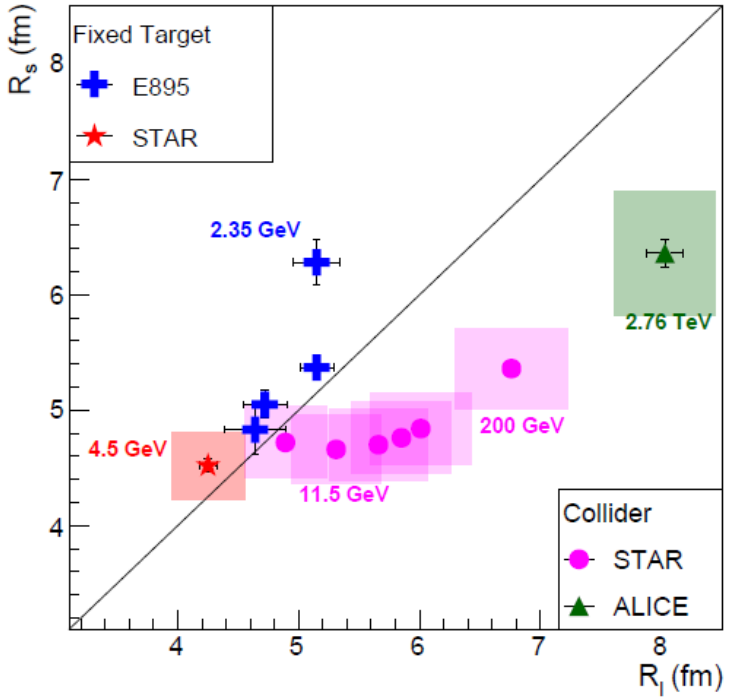

Flow results at $\sqrt{s_{NN}}$ = 3.0 GeV

See later talk by Cameron Racz

Directed and elliptic flow are sensitive to the onset of deconfinement.

QM2023: results at several FXT and COL energies

Phys. Lett. B 827 (2022) 137003

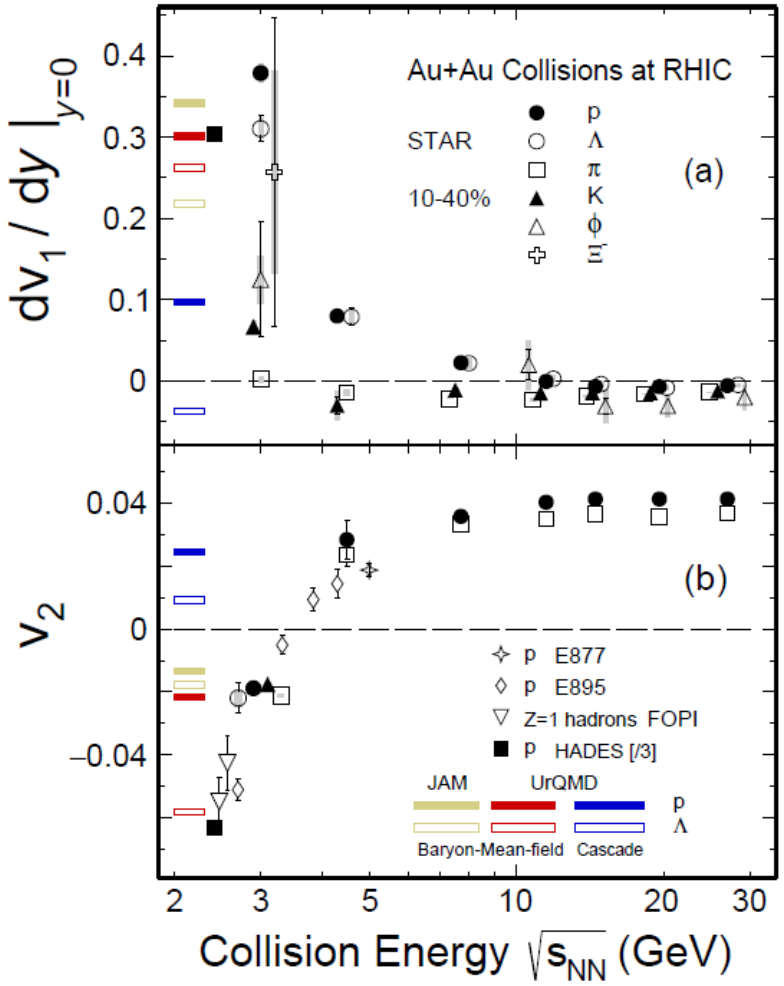

At 3.0 GeV, the NCQ scaling is absent, and all particle's v1's are positive. These results are reproduced by models which include a baryonic mean field, implying high baryon density state (not QGP).

Phys.Lett.B 827 (2022) 136941

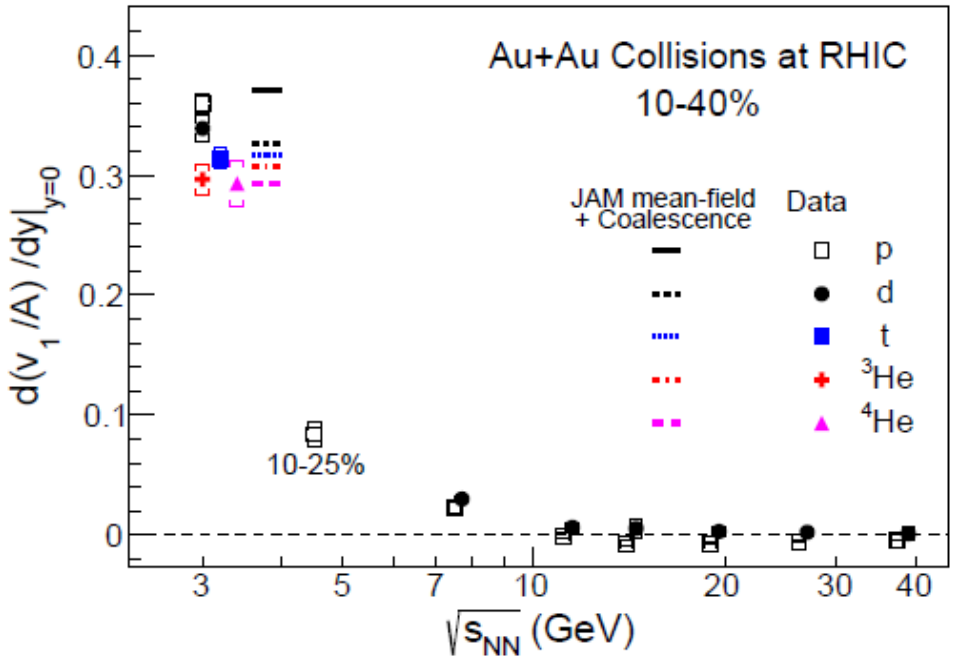

Chiral Magnetic Effect (CME) at 27 GeV

See later talk by Zhiwan Xu

QM2023: 7.7, 14.6, and 19.6 GeV results

Charge separation due to the large magnetic field is expected to be sensitive to the onset of deconfinement.

Phys. Lett. B 839 (2023) 137779

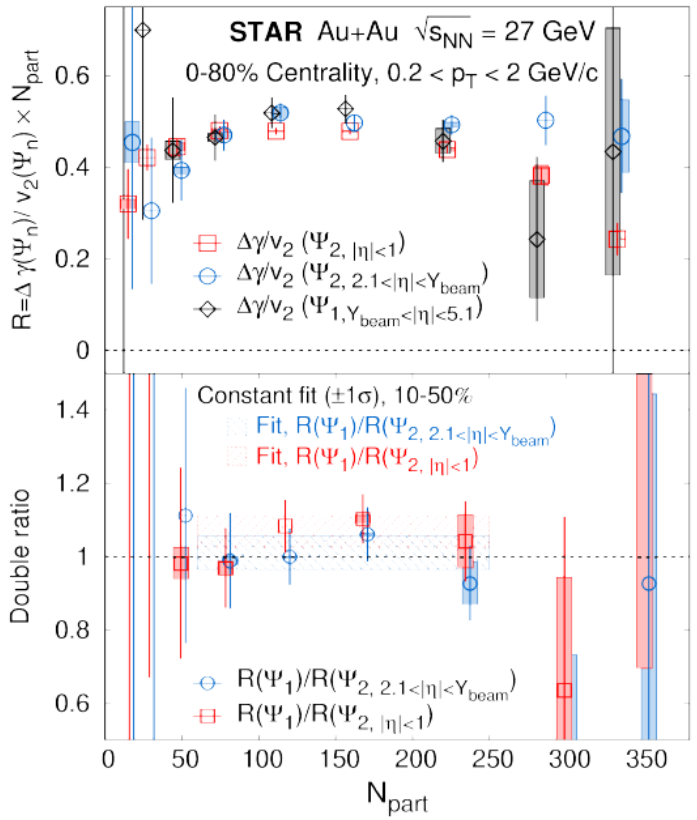

BES-II data has allowed study of charge separation with respect to the rection plane determined by the Event Plane Detector (EPD). This minimizes auto-correlations form using the same detector to determine the reaction plane and the charge separations.

The double ratio is found to be consistent with unity for all centralities. Which agrees with the expectations of the from a flow driven background scenario.

Proton Fluctuations – $\kappa\sigma^2$

See later talk by Zach Sweger

QM2023: 7.7, 14.6, and 19.6 GeV results

Fluctuations would indicate critical behavior.

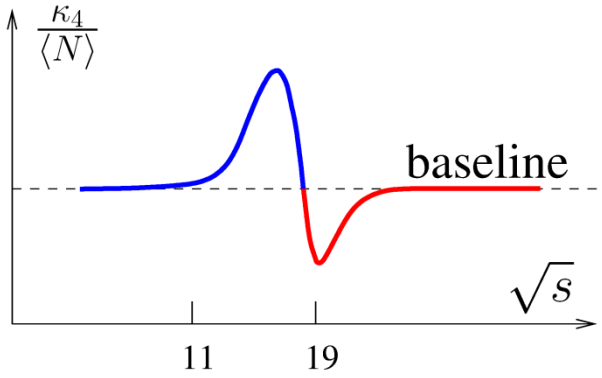

The results at 3.0 GeV are consistent with the UrQMD baseline, which is below unity due to baryon conservation.

Phys. Rev. Lett. 128 (2022) 202303

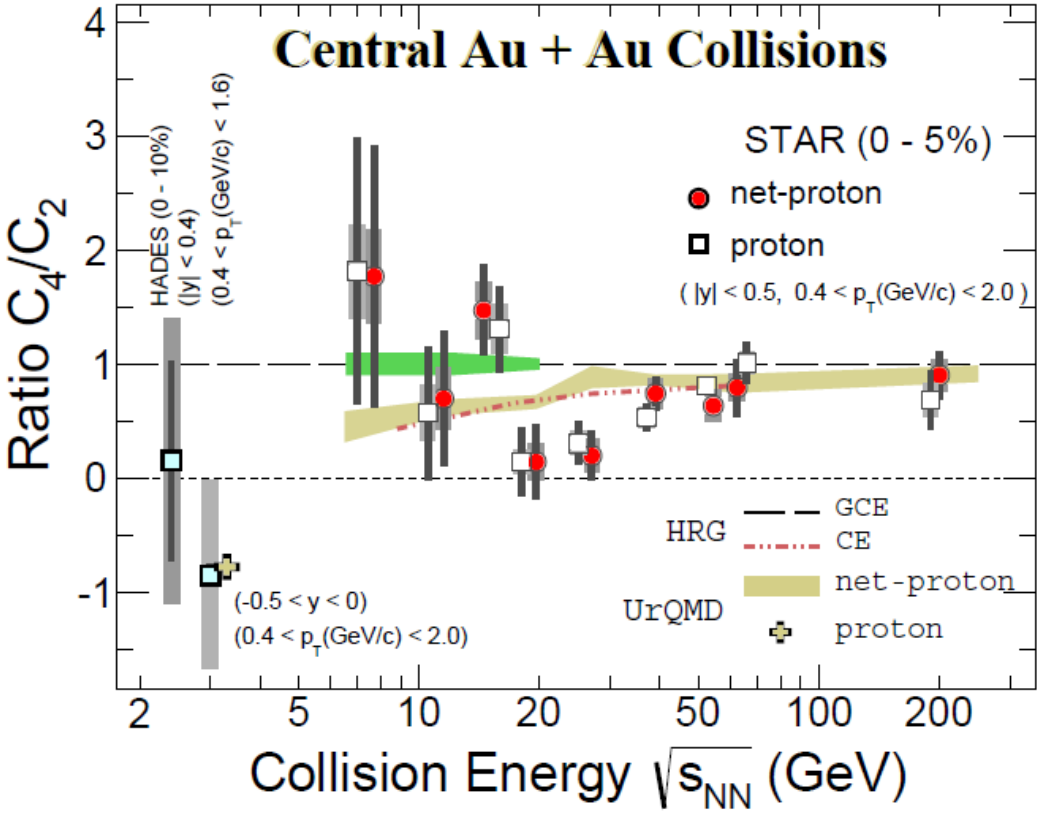

Dileptons (BES-I)

See later talk by Zaochen Ye

Dileptons are sensitive to the chiral nature of the phase transition

➔ Temperature in the LMR is representative of late stage of the collision

➔ Temperature in the IMR is representative of an early phase of the collision

QM2023: 14.6 and 19.6 GeV results

Phys. Rev. C **107** (2023) 0

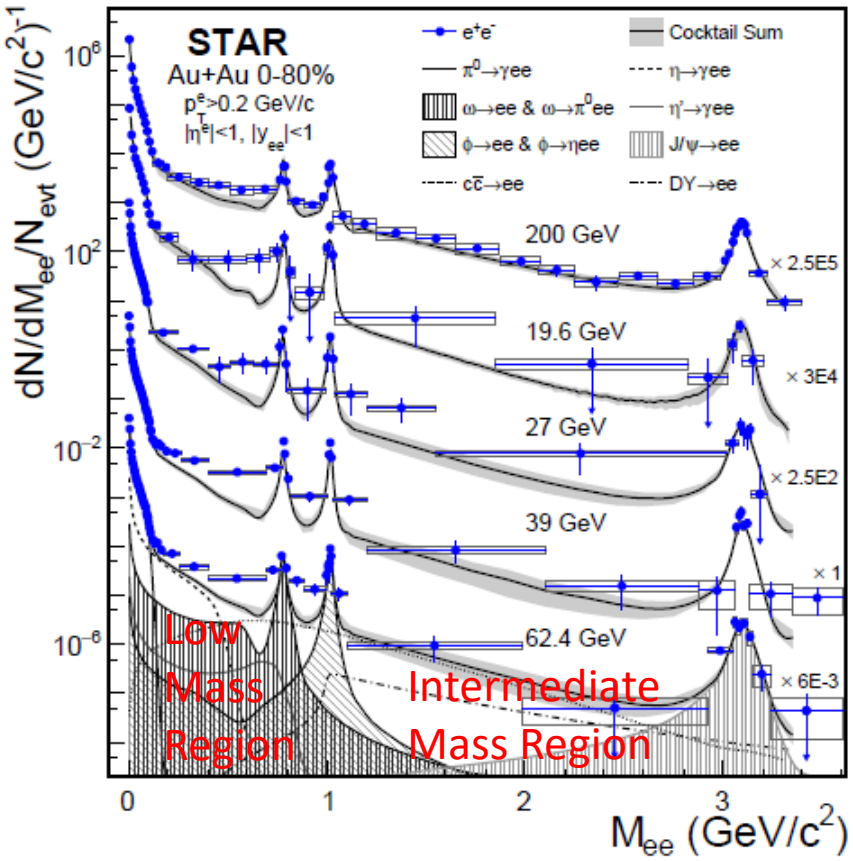

- The normalized yield is flat, at lower energies, it may increase with baryon density.

Phys. Rev. C **107** (2023) 0

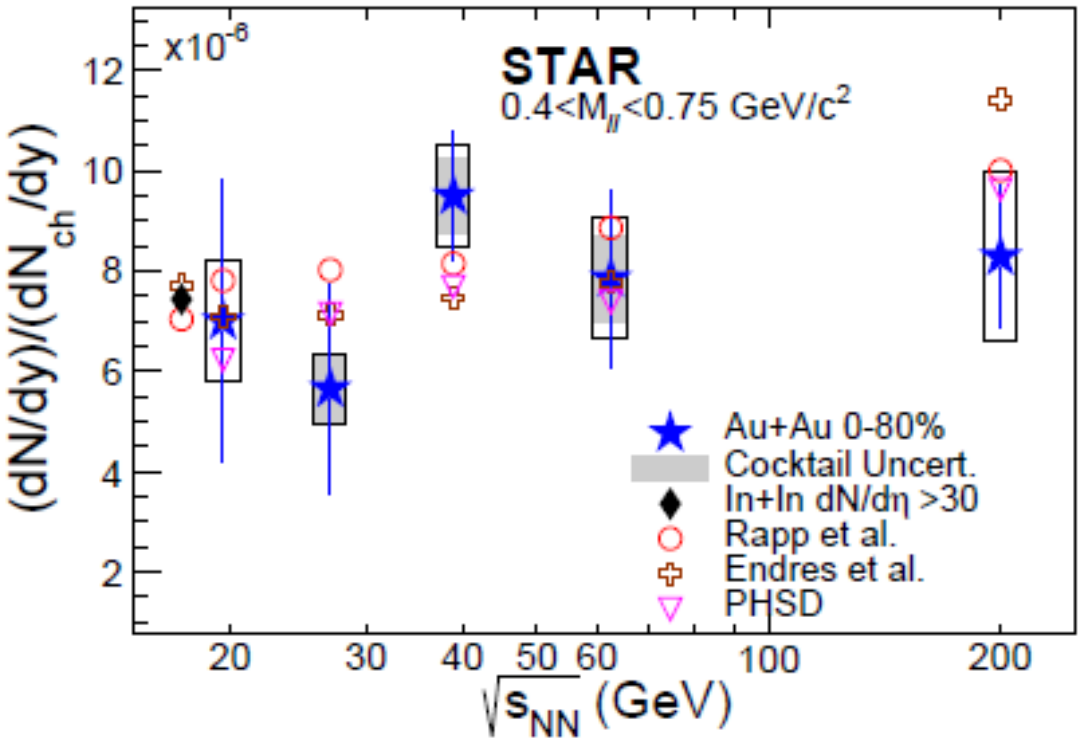

BES-II/FXT Physics Program 2018-2021

Physics Goals

The Onset of Deconfinement:

- High p_T suppression (R_{CP}) In Progress
- NCQ scaling of elliptic flow (ϕ and K mesons) ✓
- LPV through three particle correlators (CME) ✓
- Strangeness enhancement ✓
- Polarizations and alignments ✓

Compressibility ➔ First Order Phase Transition

- Directed flow ✓
- Tilt angle of the HBT source (asHBT) ✓
- The volume of the HBT source ✓
- The zero crossing of the elliptic flow (~6 AGeV) In Progress
- Volume measures from Coulomb potential ✓

Criticality:

- Higher moments ✓
- Particle ratio fluctuations In Progress

Chirality:

- Dilepton studies ✓

Hypernuclei:

- Lifetime of the hypertriton ✓

Online Event Display – Collider Event

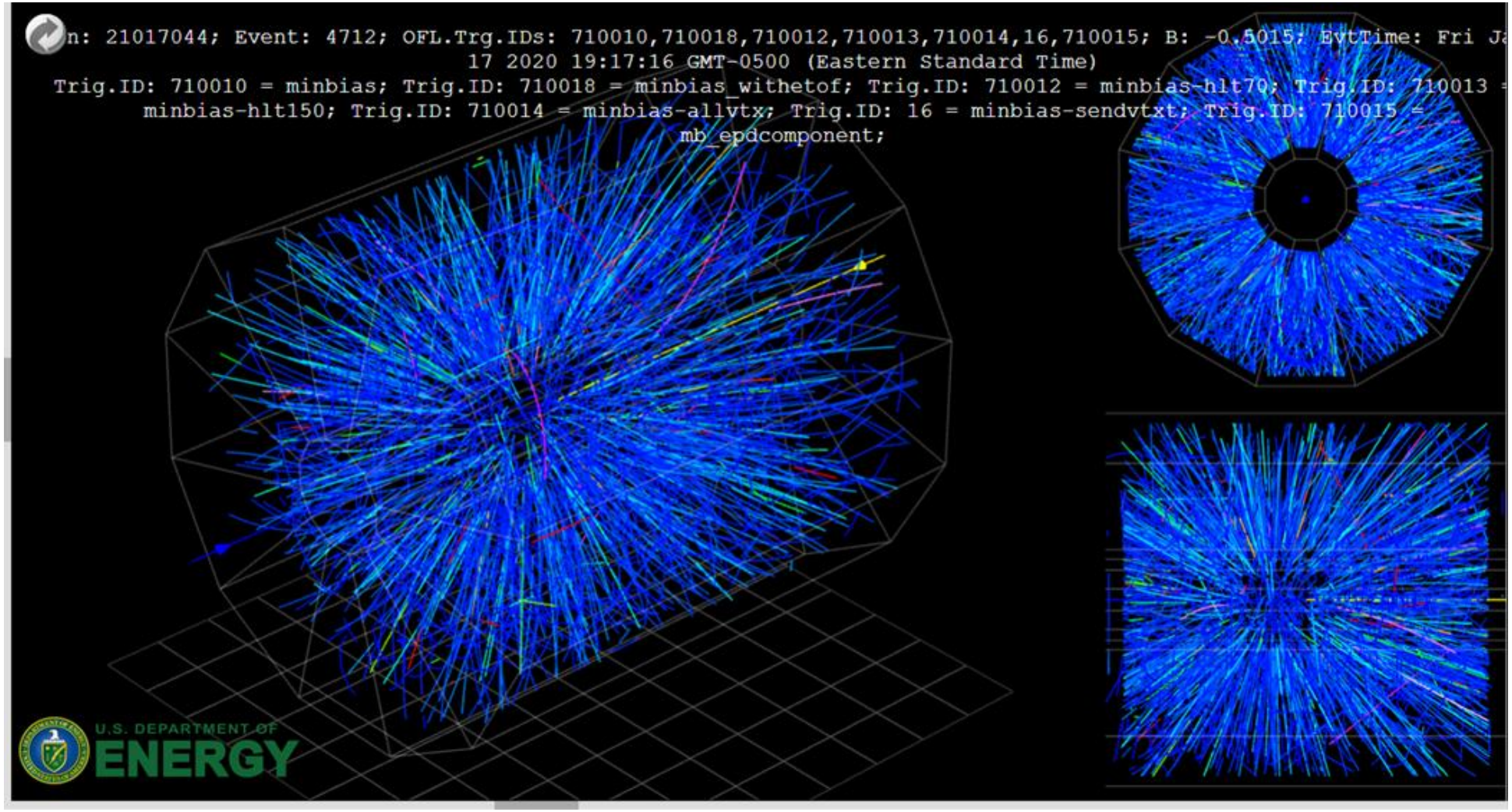

Online Event Display – FXT Event

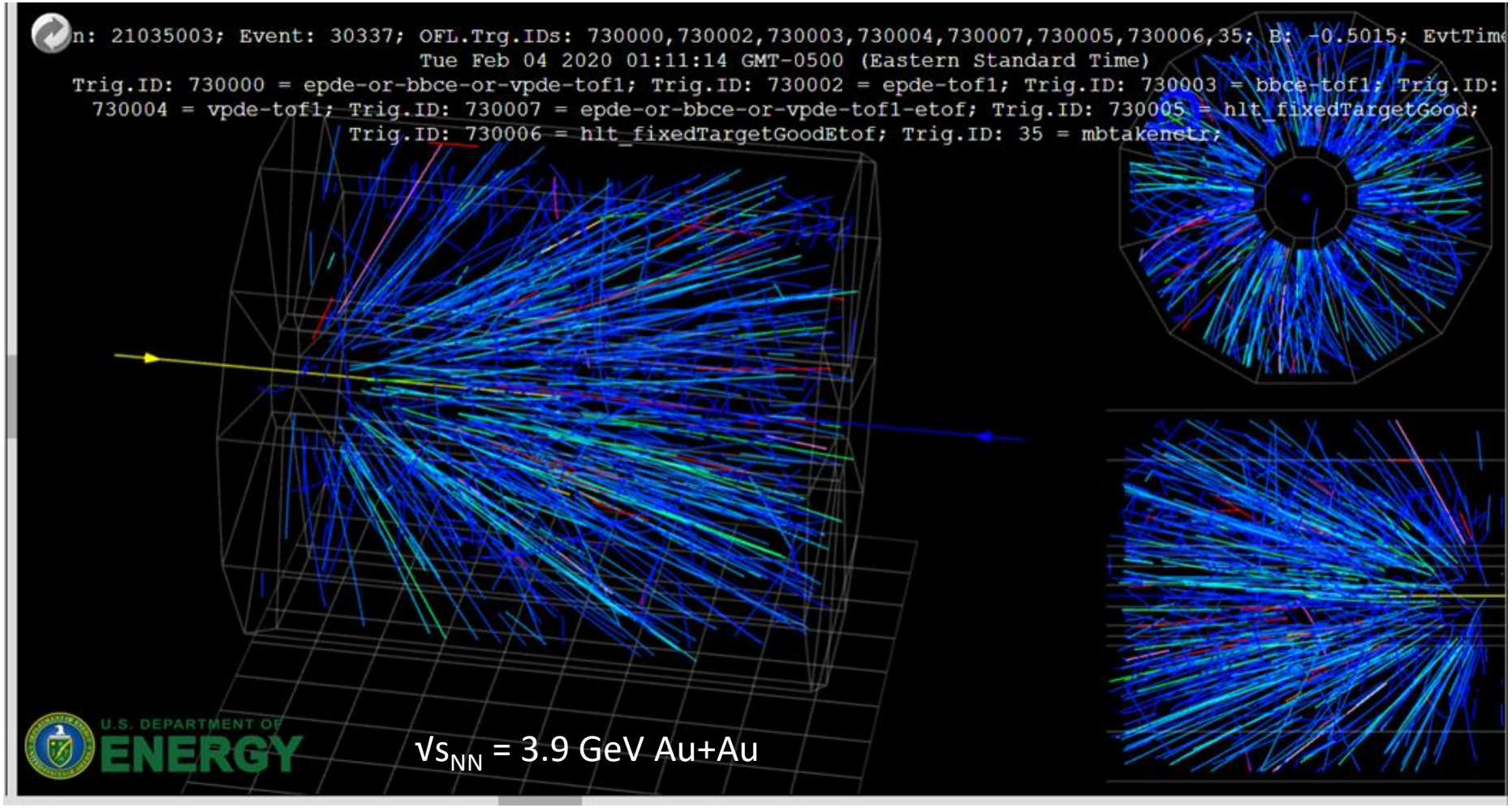

Summary

- Data taking for the STAR BES-II/FXT program was completed 2018 to 2021
- Au+Au collisions at seven collider and twelve FXT energies (with four FXT energies overlapping with the four lowest collider energies)
- Calibrations, data production and QA take time to get right and to date, only results from 3.0 and 27 GeV have been published. New results from 19.6, 14.6, and 7.7 COL and several FXT energies will be shown at QM2023
- Most analyses identified in the proposal are underway and teams are in place to complete the analysis of the additional energies when they become available

BACKUPS

BES-II Physics Goals and statistics

Total of 7 collider energies

Collision Energy (GeV)	7.7	9.1	11.5	14.5	19.6
μ_B (MeV) in 0-5% central collisions	420	370	315	260	205
Observables					
R_{CP} up to $p_T = 5$ GeV/c	-	-	160	125	92
Elliptic Flow (ϕ mesons)	80	120	160	160	320
Chiral Magnetic Effect	50	50	50	50	50
Directed Flow (protons)	20	30	35	45	50
Azimuthal Femtoscopy (protons)	35	40	50	65	80
Net-Proton Kurtosis	70	85	100	170	340
Dileptons	100	160	230	300	400
$>5\sigma$ Magnetic Field Significance	50	80	110	150	200
Required Number of Events	100	160	230	300	400

Added two energies: 17.3 and 27

Total of 12 FXT energies

$\sqrt{s_{NN}}$ (GeV)	3.0	3.2	3.5	3.9	4.5	5.2	6.2	7.7
Single Beam Energy (GeV)	3.85	4.55	5.75	7.3	9.8	13.5	19.5	31.2
μ_B (MeV)	721	699	666	633	589	541	487	420
Rapidity y_{CM}	1.06	1.13	1.25	1.37	1.52	1.68	1.87	2.10
Observables								
Elliptic Flow (kaons)	300	150	80	40	20	40	60	80
Chiral Magnetic Effect	70	60	50	50	50	70	80	100
Directed Flow (protons)	20	30	35	45	50	60	70	90
Femtoscopy (tilt angle)	60	50	40	50	65	70	80	100
Net-Proton Kurtosis	36	50	75	125	200	400	950	NA
Multi-strange baryons	300	100	60	40	25	30	50	100
Hypertritons	200	100	80	50	50	60	70	100
Requested Number of Events	300	100	100	100	100	100	100	100

Added four energies:
7.2, 9.2, 11.5, 13.5
Added high statistics at 3 GeV

Paper

Paper

Paper

Paper

Paper

Paper Lambda Polarization

Glauber Model

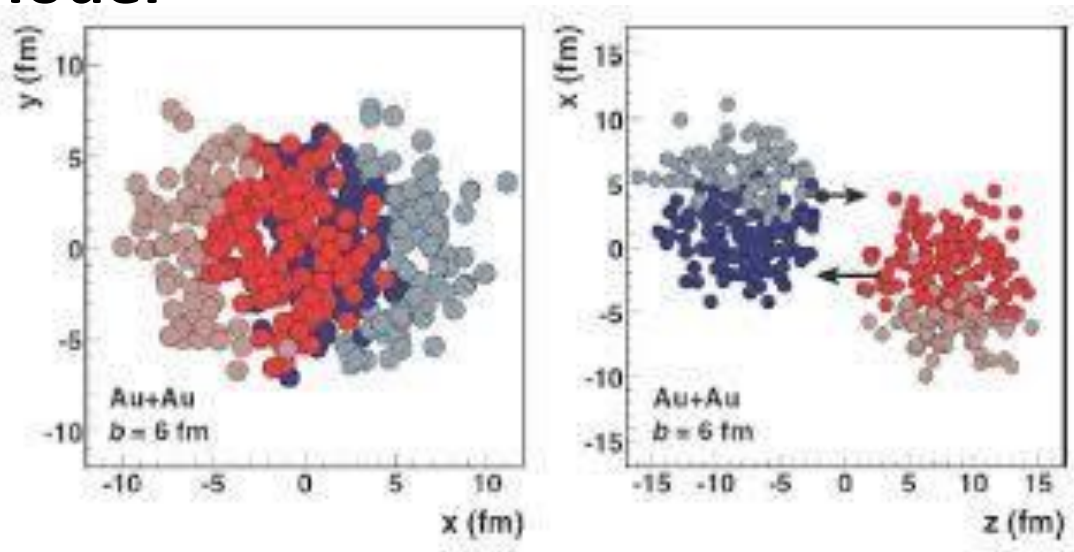

Glauber Model:

- Nucleons distributed with Woods-Saxon
- Nucleons do not scatter during collisions
- Collisions are determined by the inelastic σ_{pp}
- Particle production with negative binomial
- Crude hardness parameter (x)

➔ N = x Ncoll + (1-x) (Npart/2)

Basics:

- The Glauber model has been used to determine centrality by RHIC and LHC experiments since 2001
- The Glauber model considers particle production, not stopping of participant nucleons
- Hadron production in centered at the center-of-mass rapidity
- Closer to target rapidity, most charged hadrons are “stopped protons”
- Center-of-mass rapidity shifts through the FXT energy range ➔ Can not use RefMult

➔ **The basic question is, does the Glauber model work for the STAR FXT systems? [Centrality bins? N_{part}?]**

Should we worry about Glauber?

Inelastic, elastic, and total cross sections are very different.
At 3 GeV:

σ_{tot} = 42 mB
$\sigma_{inelatic}$ = 28 mB
$\sigma_{elastic}$ = 14 mB

pp and np cross sections are different.

Cross sections change rapidly with energy in the FXT regime.

Cross sections will change after each collision.

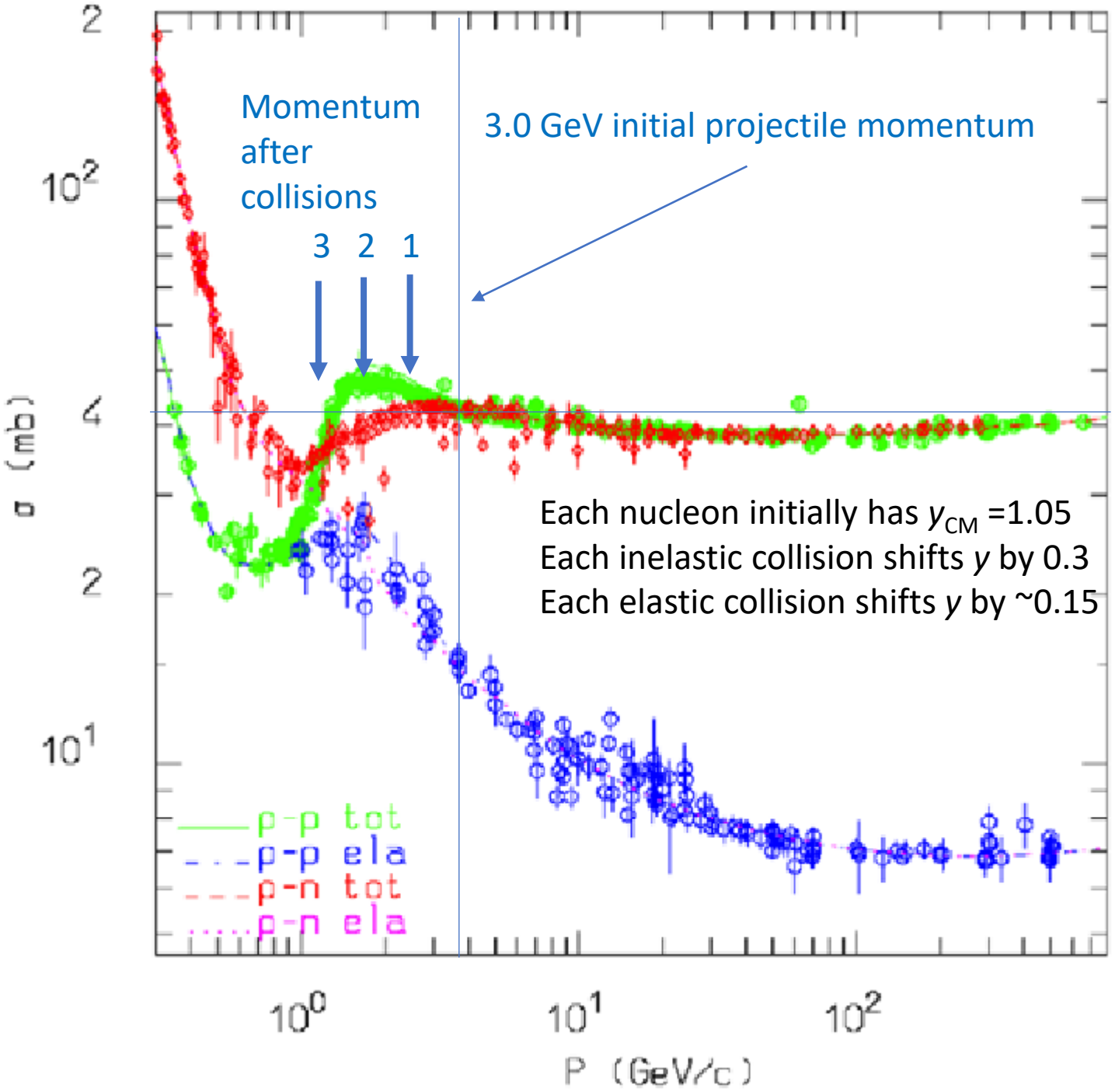

Comparison to Other Facilities

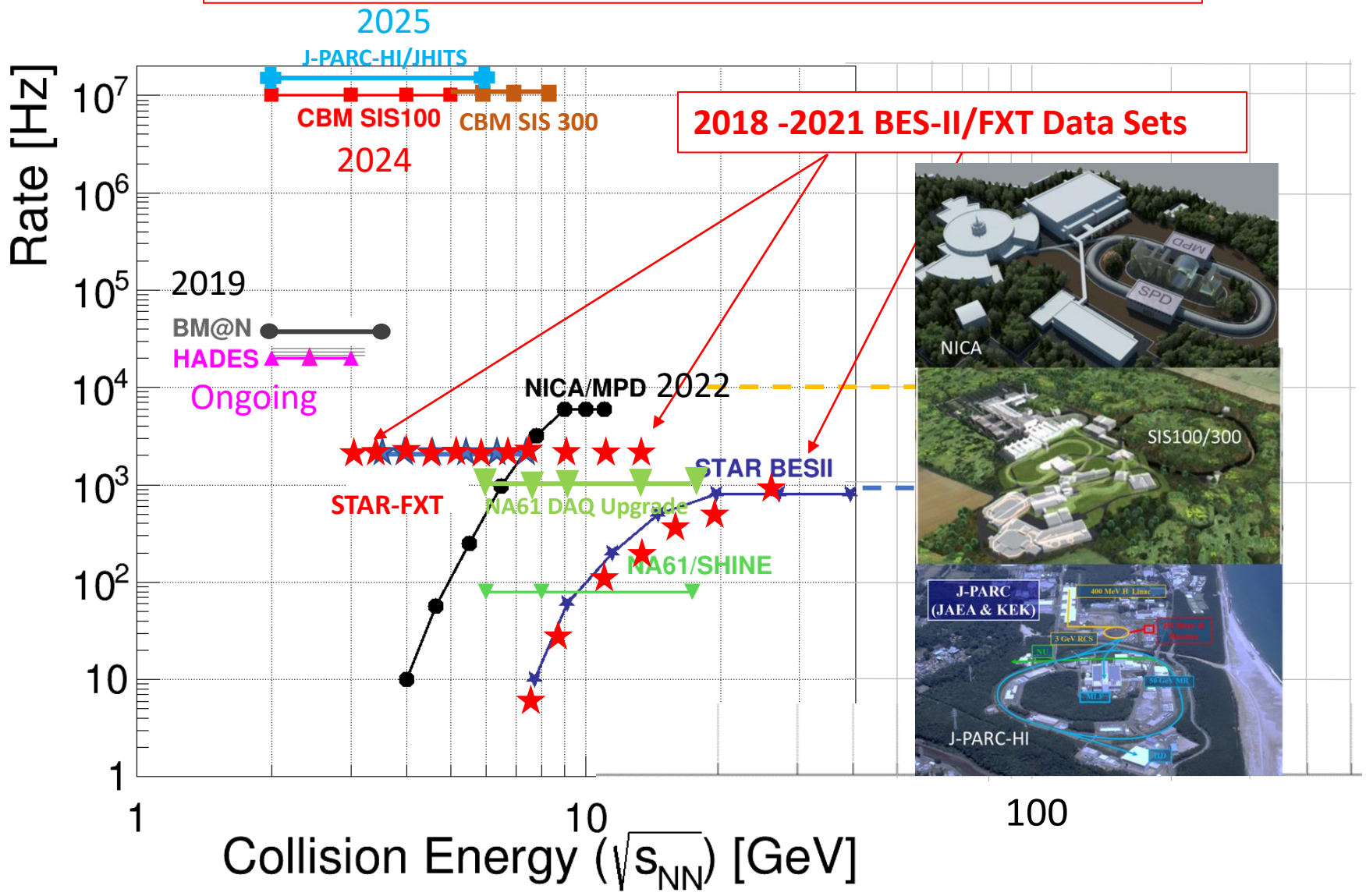

Beam E_T (GeV)	Beam E_k (AGeV)	Beam p_Z (GeV/c)	Rapidity y_{Beam}	$\sqrt{s_{NN}}$ (GeV)	Rapidity y_{CM}	Ch. Pot. μ_B (GeV)
3.85	2.92	3.73	2.10	3.0	1.05	721
4.59	3.66	4.50	2.28	3.2	1.13	699
5.75	4.82	5.67	2.51	3.5	1.25	666
7.3	6.4	7.25	2.75	3.9	1.37	633
9.8	8.9	9.44	3.04	4.5	1.52	589
13.5	12.6	13.5	3.37	5.2	1.68	541
19.5	18.6	19.5	3.73	6.2	1.87	487
26.5	25.6	26.5	4.04	7.2	2.02	443
31.2	30.3	31.2	4.20	7.7	2.10	420
44.5	43.6	44.5	4.56	9.2	2.28	372
70	69.1	70	5.01	11.5	2.51	316
100	99.1	100	5.37	13.7	2.69	276

LEReC inside RHIC tunnel at Interaction Region @ 2 o'clock (IR2)

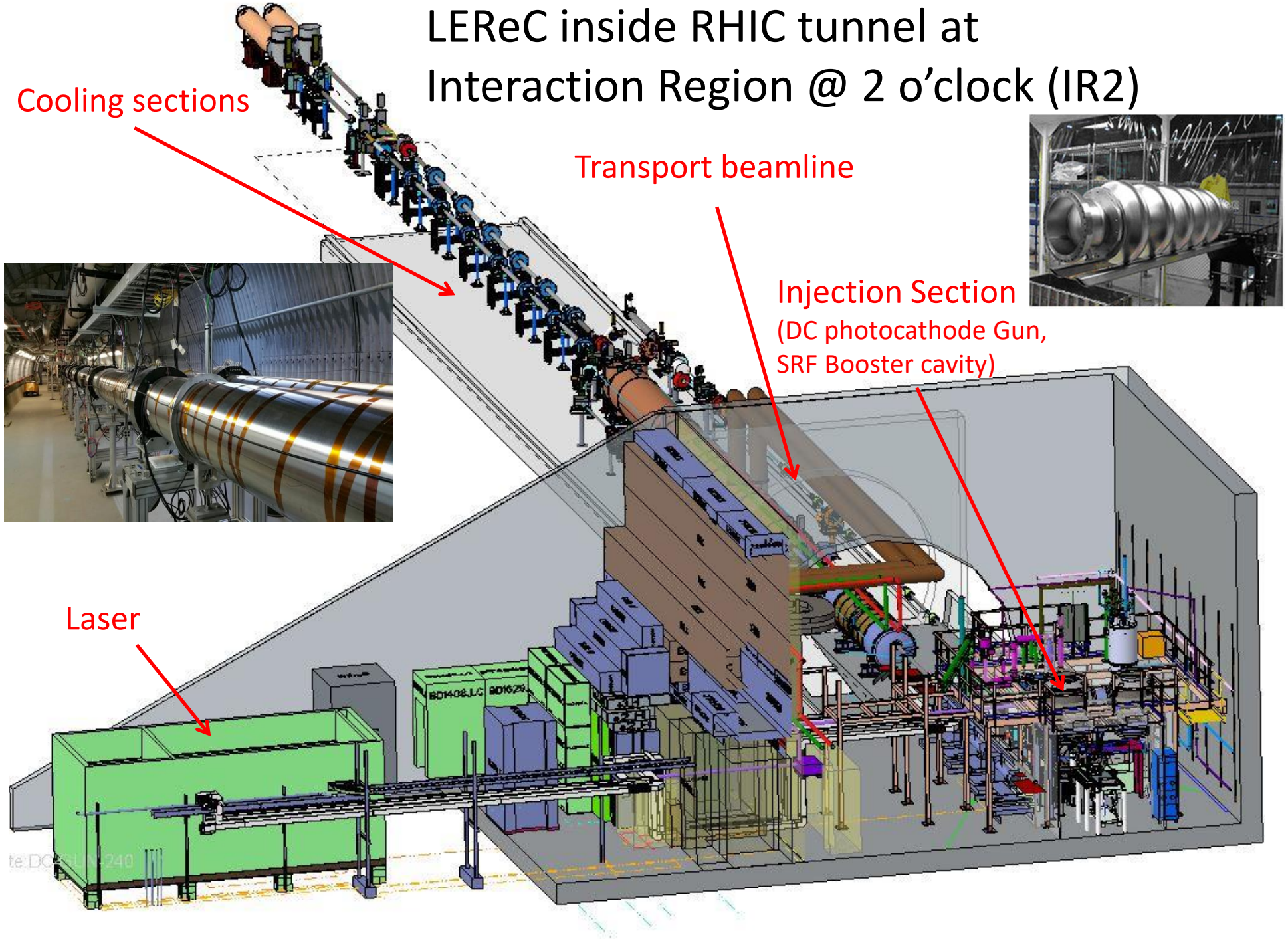

The STAR Detector Upgrades ➔ BES-II

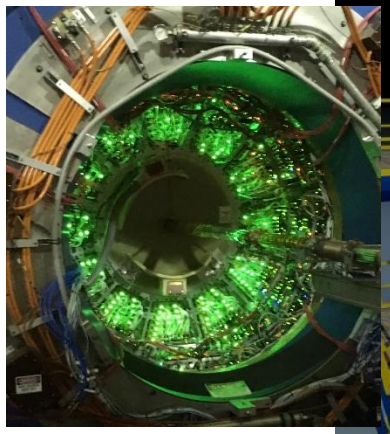

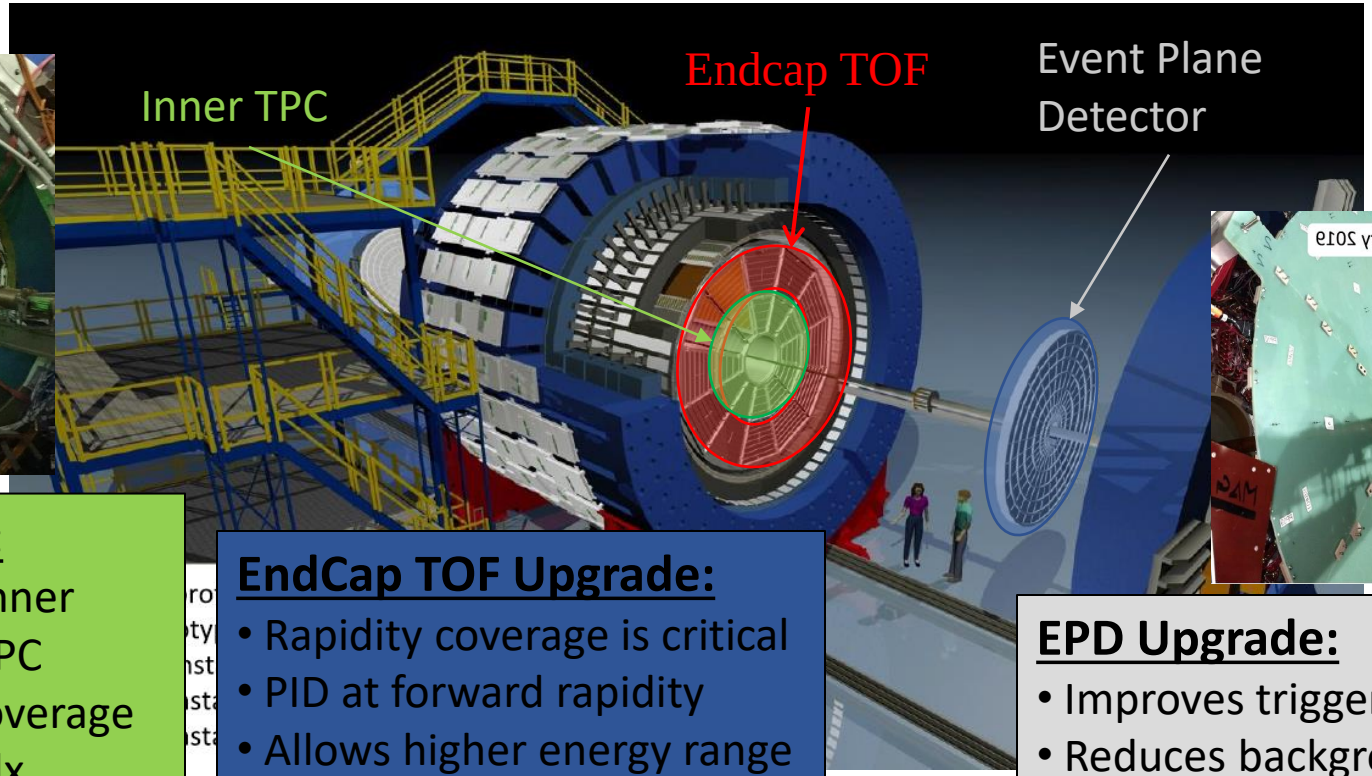

iTPC Upgrade:
- Rebuilds the inner sectors of the TPC
- Continuous Coverage
- Improves dE/dx
- Extends η coverage to 1.5 (2.2 for FXT)
- Lowers p_T cut-in from 125 MeV/c to 60 MeV/c
- Ready in 2019

EndCap TOF Upgrade:
- Rapidity coverage is critical
- PID at forward rapidity
- Allows higher energy range of FXT program
- CBM/FAIR
- Ready 2019

EPD Upgrade:
- Improves trigger
- Reduces background
- Allows a better and independent reaction plane measurement critical to BES and FXT
- Ready 2018

Installing the iTPC Upgrade

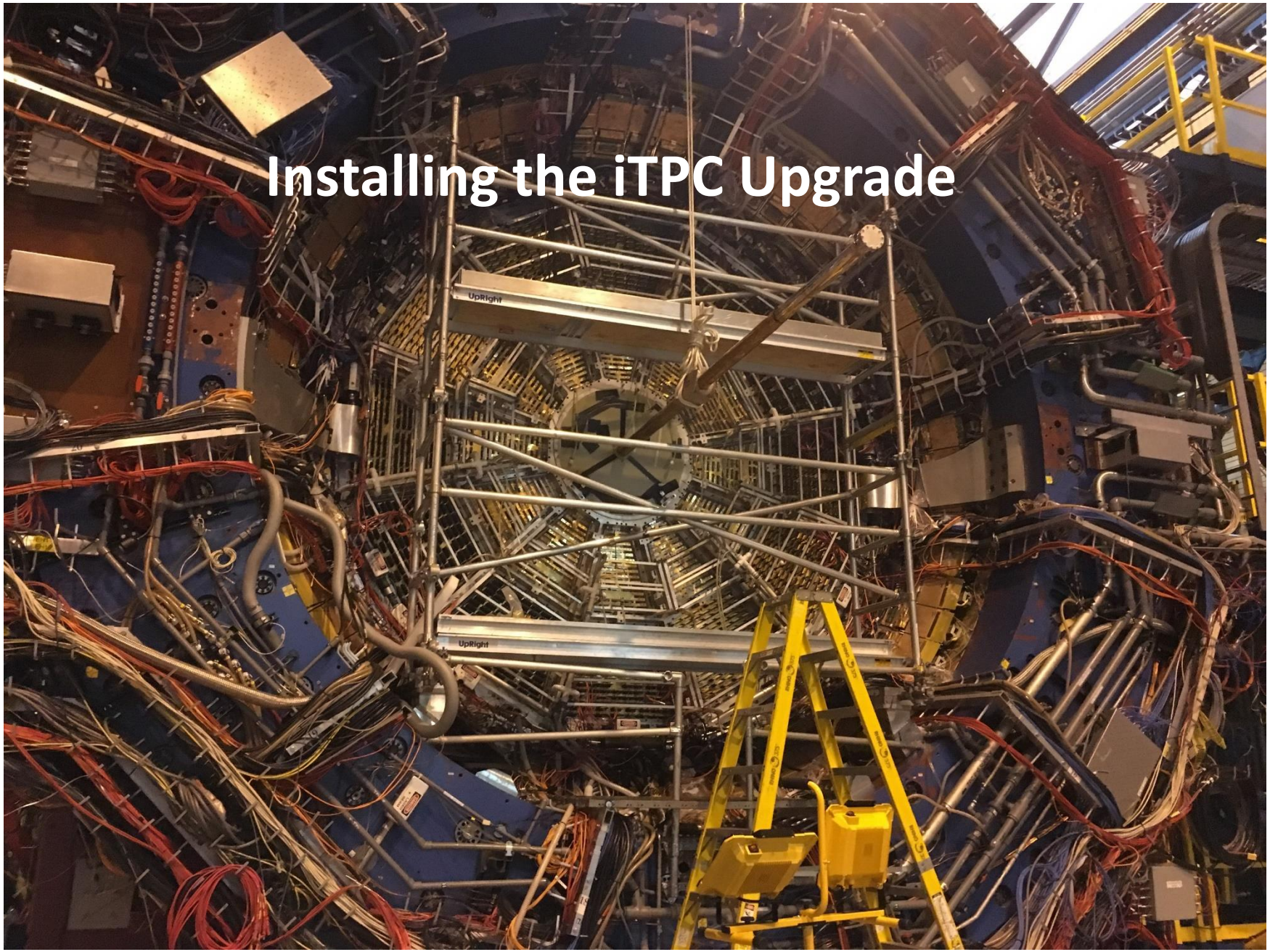

iTPC Upgrade – Current Performance

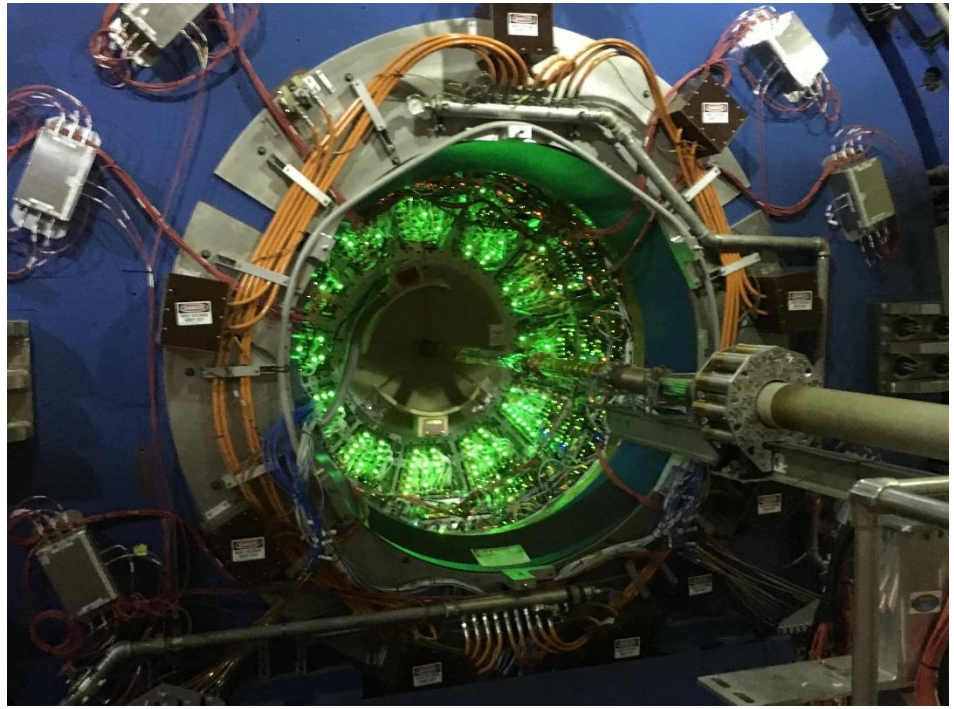

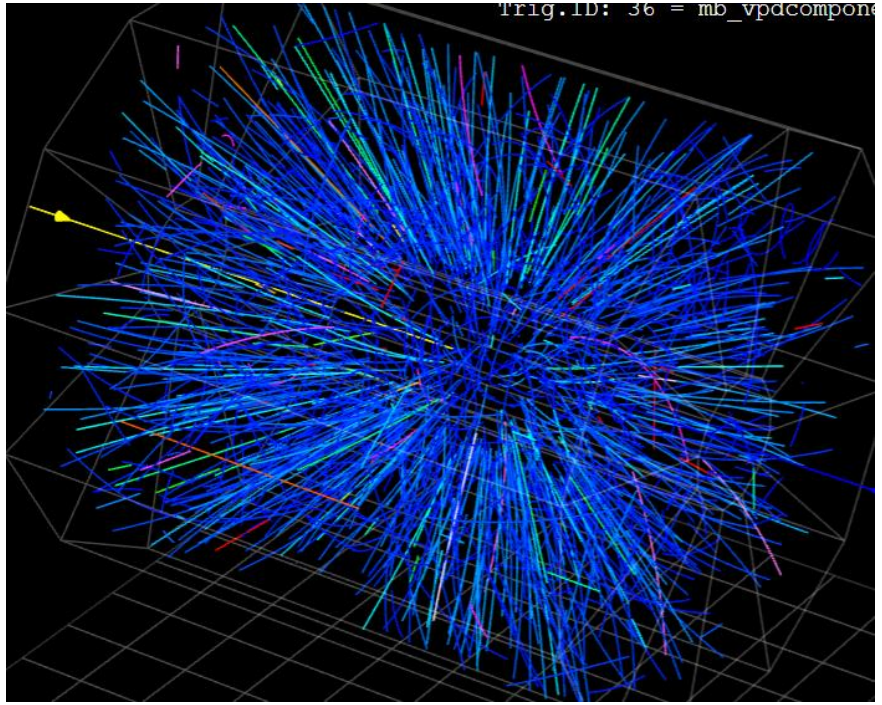

eTOF Upgrade – Current Performance

System time resolution ➔ 85 ps
Individual counter time resolution ➔ 65 ps

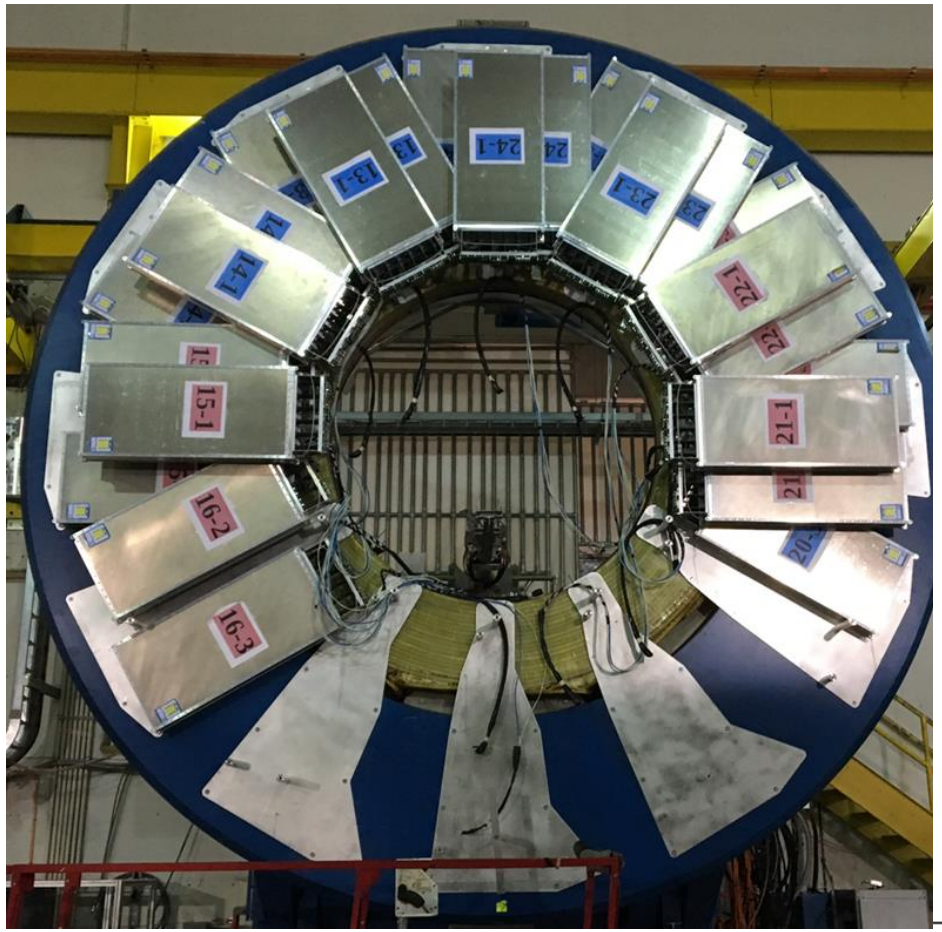

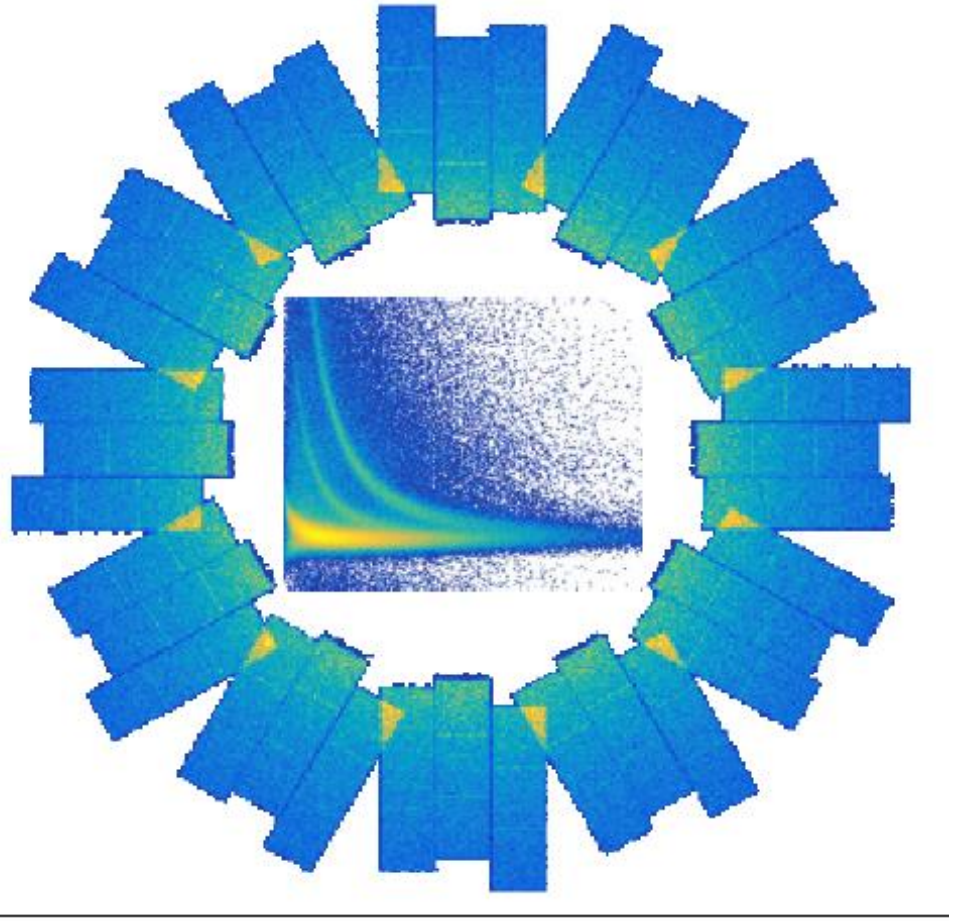

EPD Upgrade – Current Performance

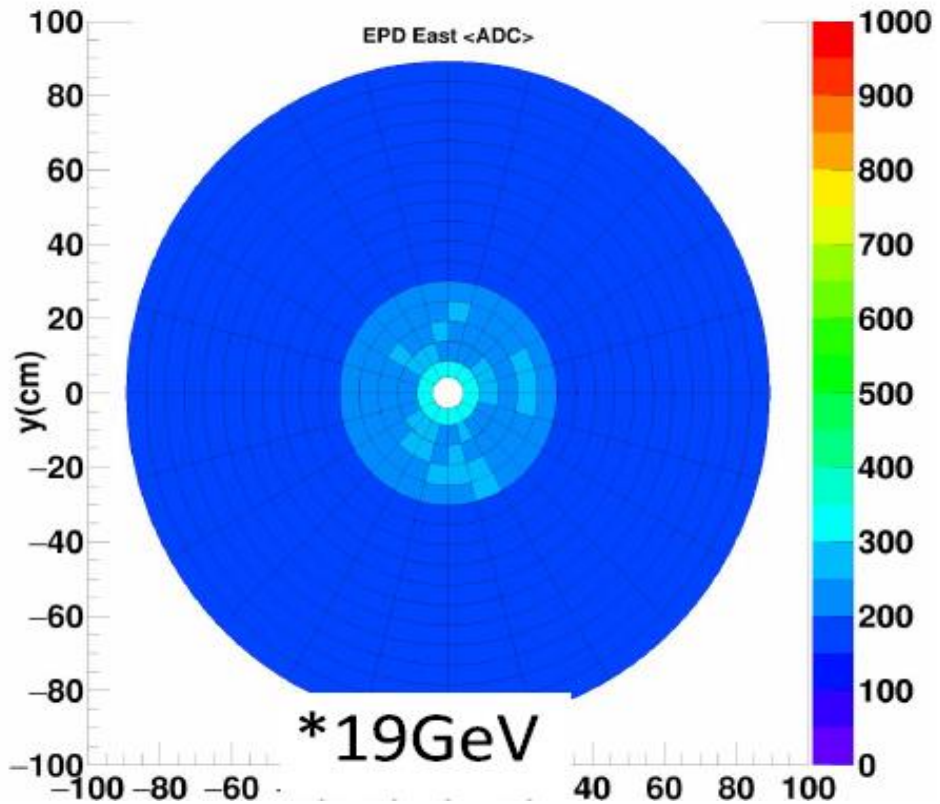

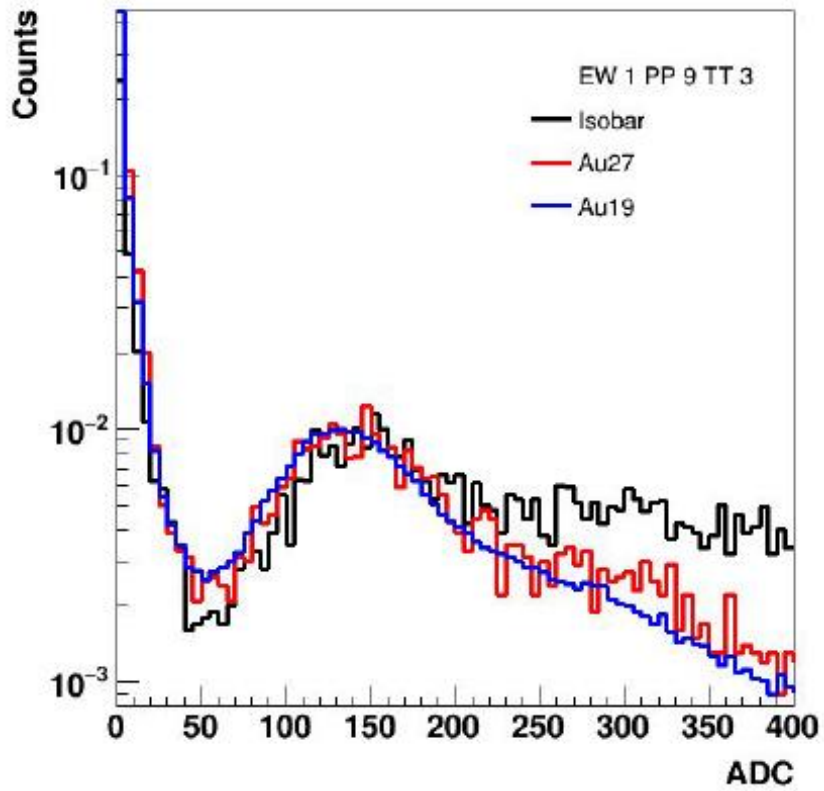

FXT Program

Collider Energy	Fixed-Target Energy	Single beam AGeV	Center-of-mass Rapidity	μ_B (MeV)
62.4	7.7	30.3	2.10	420
39	6.2	18.6	1.87	487
27	5.2	12.6	1.68	541
19.6	4.5	8.9	1.52	589
14.5	3.9	6.3	1.37	633
11.5	3.5	4.8	1.25	666
9.1	3.2	3.6	1.13	699
7.7	3.0	2.9	1.05	721

- Data rate is DAQ limited
- Would need 100 Million Events at each energy to make the sensitivity of BES-II
- Two days per energy

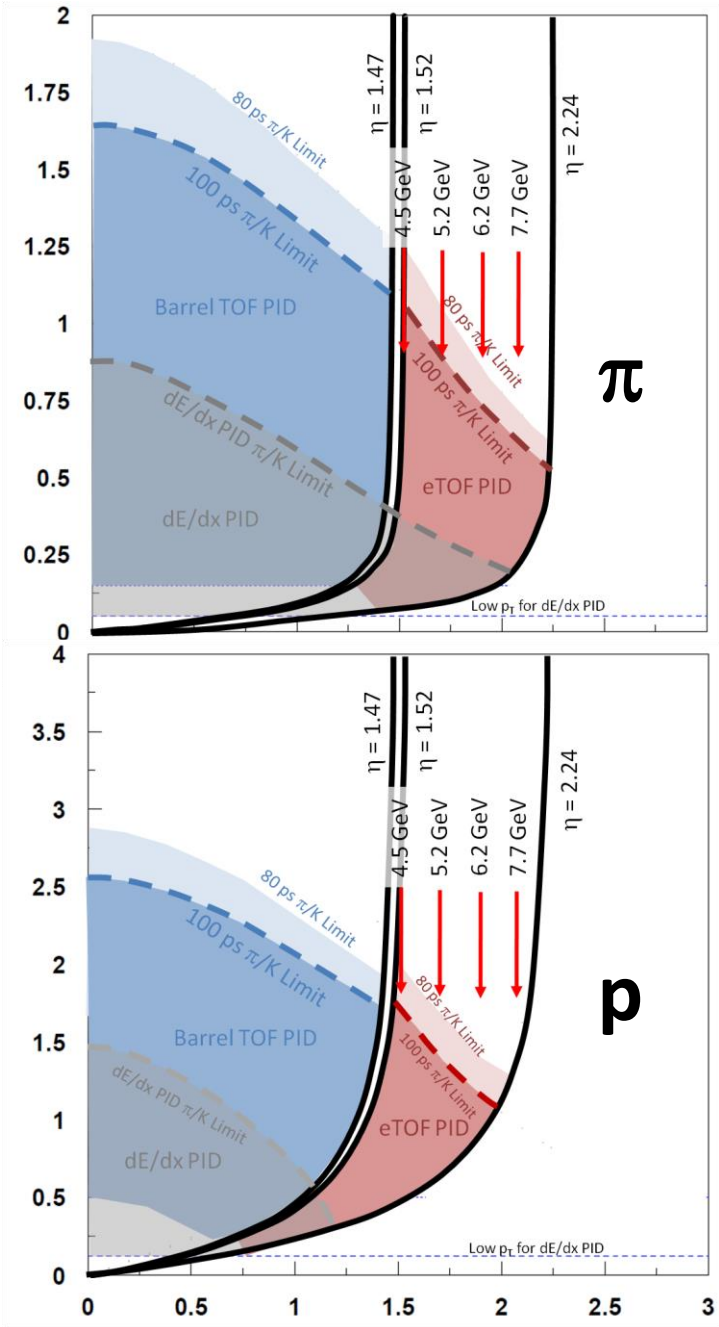

Fixed-Target Program Exp. Setup

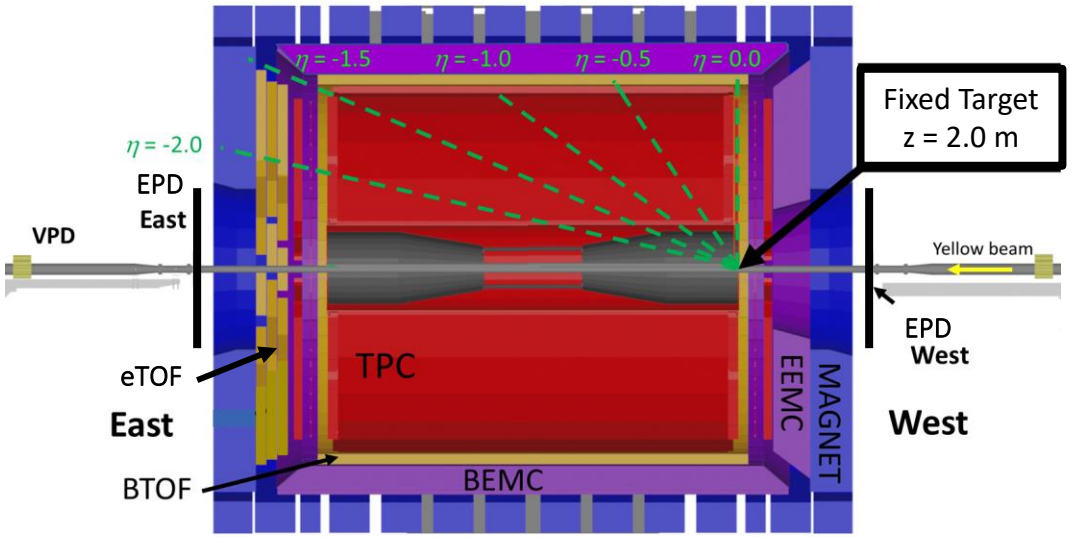

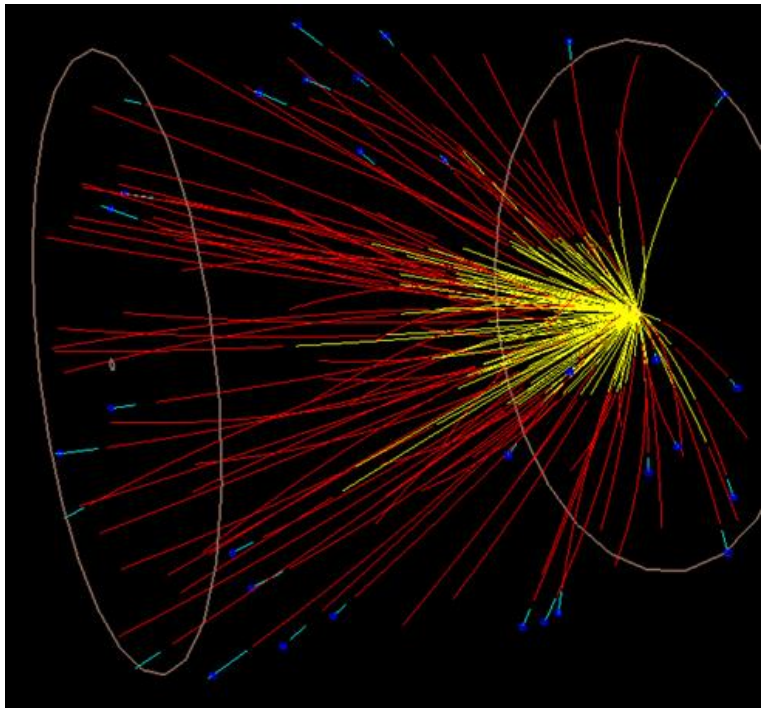

Gold Target:

- 250 μm foil
- 2 cm below the nominal beam axis
- 2 m from the center of STAR

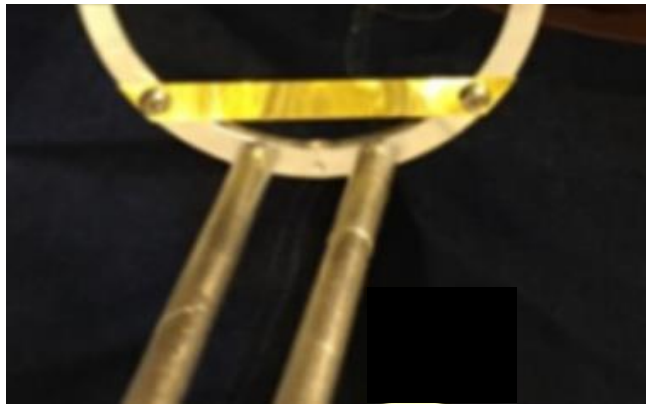

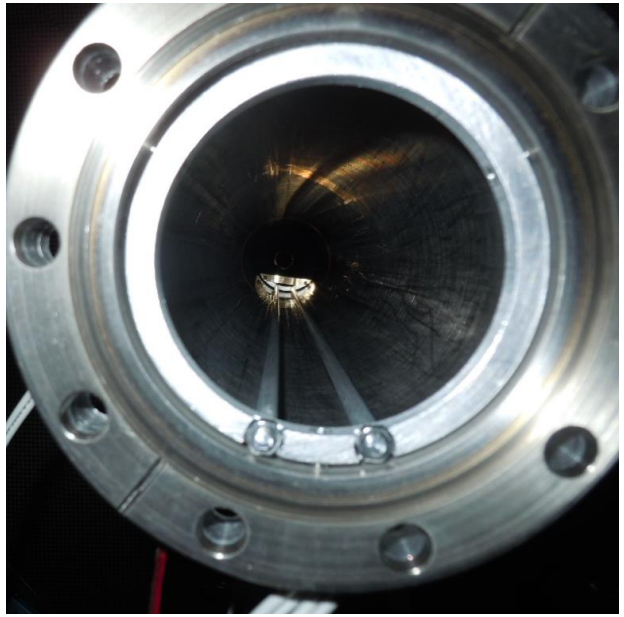

The Upgrades are Important for the FXT Program

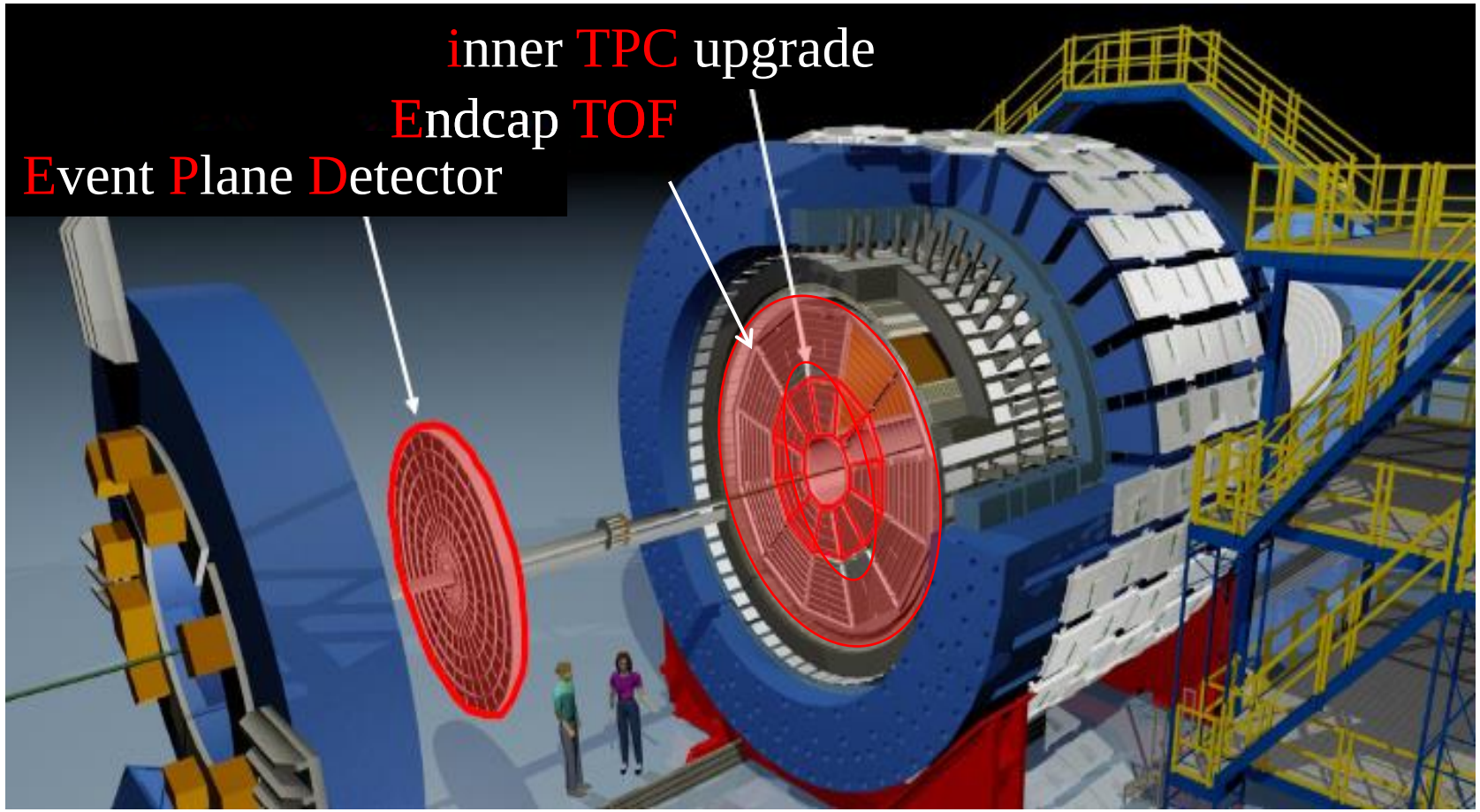

Detects Particles in the $0 < \eta < 2$ range

π, K, p, d, t, h, α through dE/dx and TOF

K^0_s, Λ, Ξ, Ω, ϕ, ${}^3_\Lambda H$, ${}^4_\Lambda H$ through invariant mass

Particle Identification

Because the tracks are longer, on average, for FXT events than for collider events, the resolutions for both dE/dx and 1/β are better in FXT mode than collider mode.

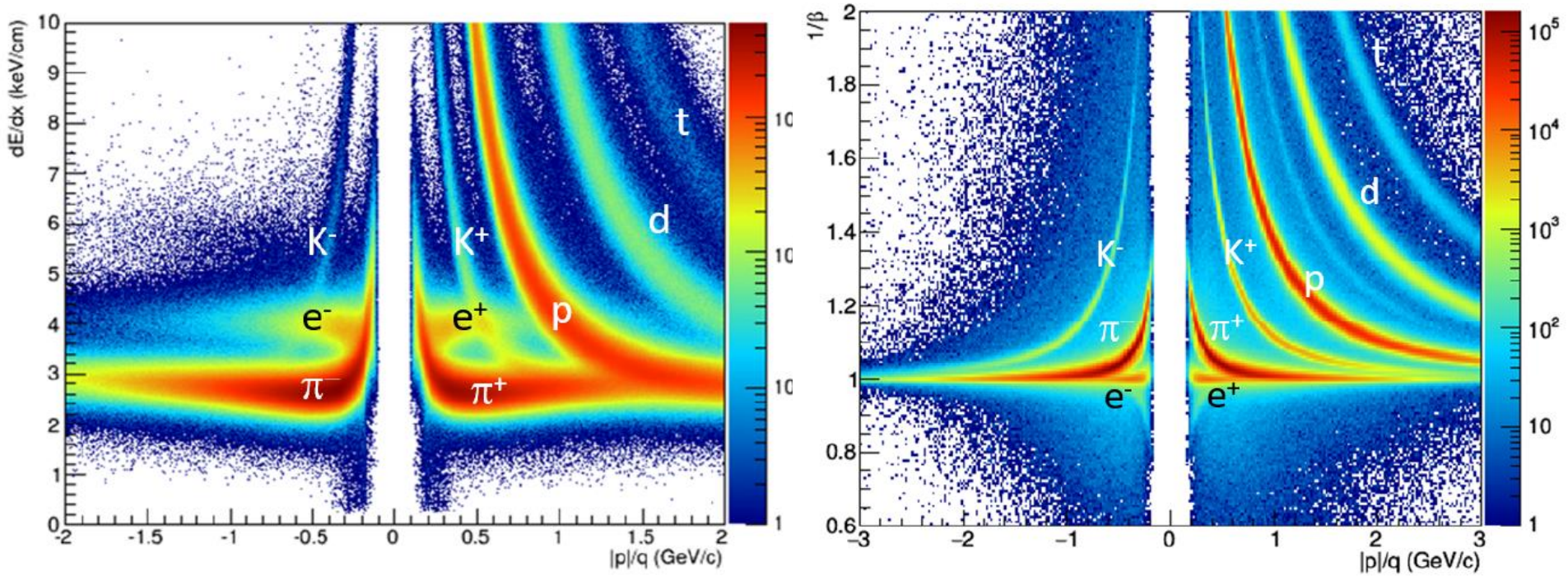

Acceptance for the FXT Program

FXT Energy $\sqrt{s_{NN}}$	Single Beam E_T (GeV)	Single beam E_k (AGeV)	Center-of-mass Rapidity	Chemical Potential μ_B (MeV)	Year of Data Taking
3.0	3.85	2.9	1.05	721	2018
3.2	4.59	3.6	1.13	699	2019
3.5	5.75	4.8	1.25	666	2020
3.9	7.3	6.3	1.37	633	2020
4.5	9.8	8.9	1.52	589	2020
5.2	13.5	12.6	1.68	541	2020
6.2	19.5	18.6	1.87	487	2020
7.2	26.5	25.6	2.02	443	2018
7.7	31.2	30.3	2.10	420	2020
9.1	44.5	43.6	2.28	372	2021
11.5	70	69.1	2.51	316	2021
13.7	100	99.1	2.69	276	2021

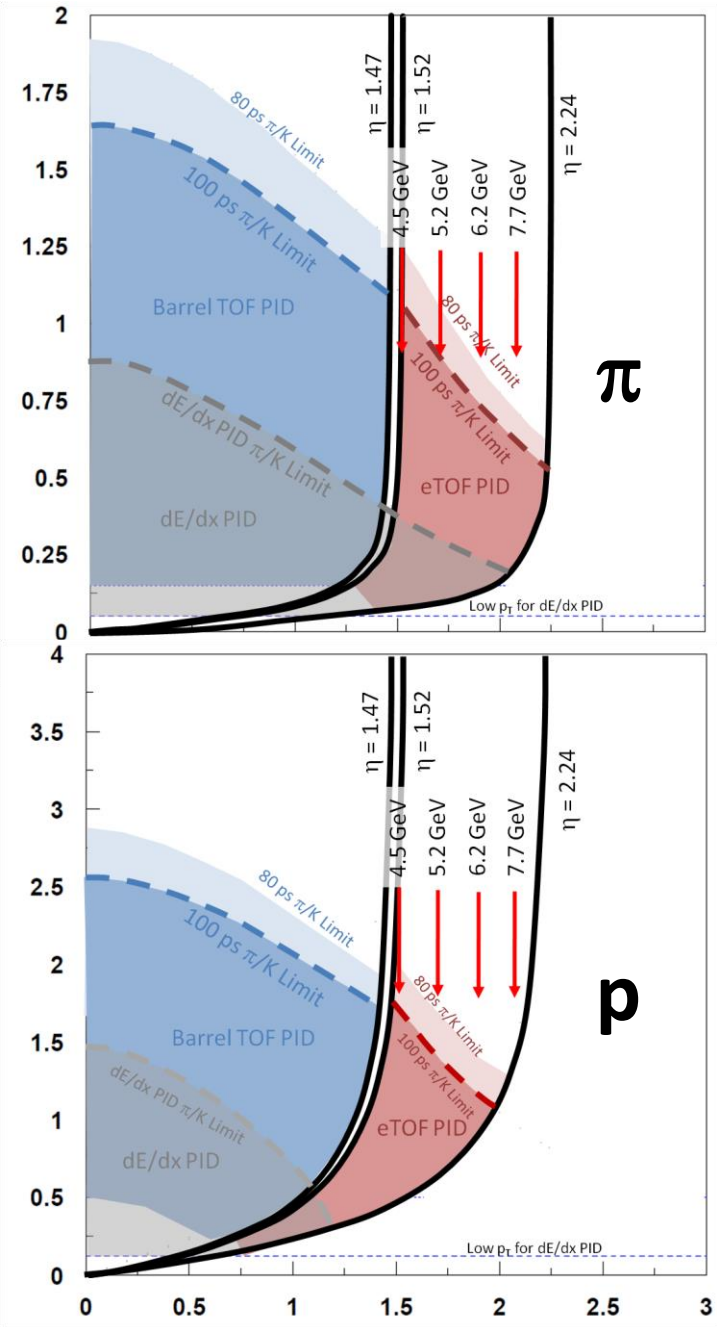

Beam Energy Scan Phase-II

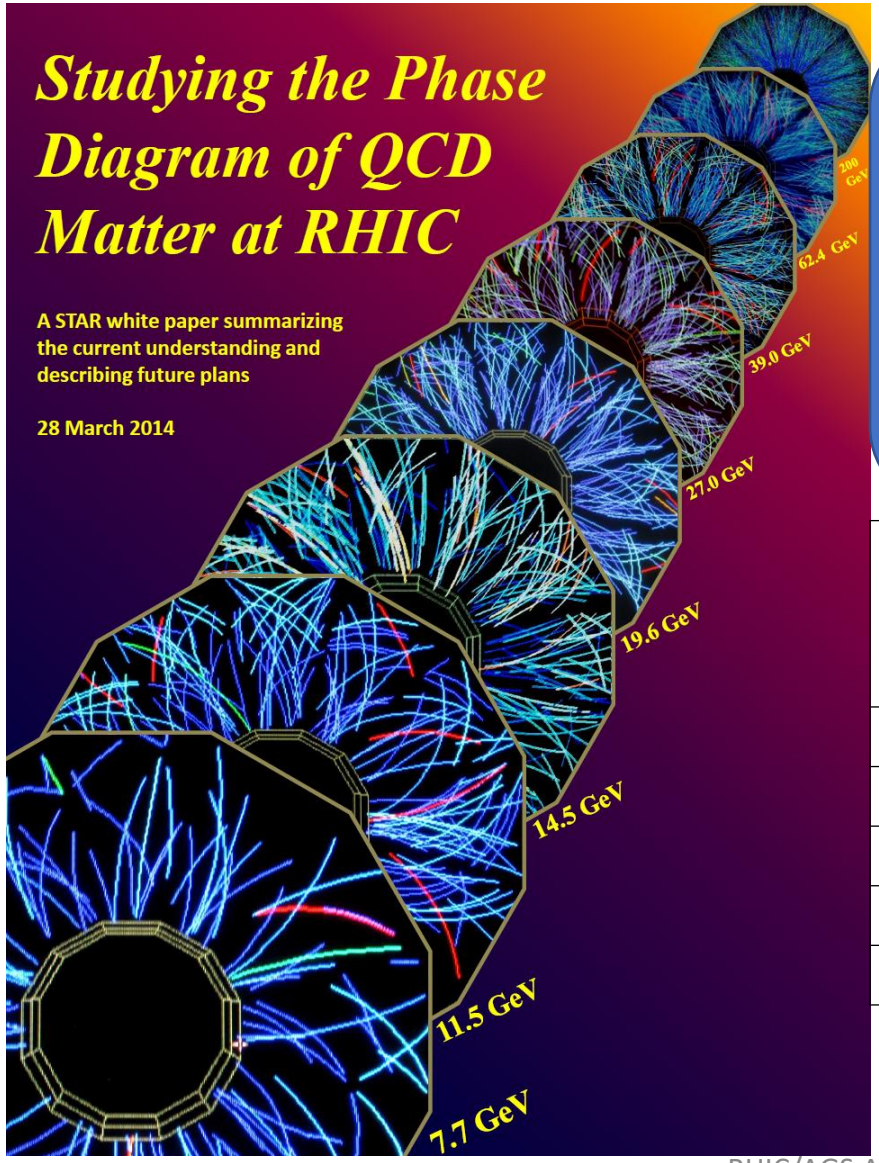

The Goals of the Beam Energy Scan Program:

1) Find the disappearance of QGP signatures
2) Find evidence of a first-order phase transition
3) Find the possible Critical Point

The Fixed-Target Program will extend the search range for all of these features of the QCD phase diagram up to μ_B = 720 MeV

Collision Energy (GeV)	Fixed Target $\sqrt{s_{NN}}$	Center of Mass Rapidity	Single Beam Kinetic	Chemical Potential Collider	Chemical Potential μ_B (MeV)
19.6	4.471	1.522	8.87	206	589
14.5	3.904	1.370	6.32	264	633
11.5	3.528	1.253	4.82	316	666
9.1	3.196	1.134	3.62	375	699
7.7	2.985	1.049	2.92	422	721

Overall Run Status (2018)

Energy	Start	Finish	First Run	Last Run	HLTgood	Target
3.85 FXT	May 31st	June 4th	19151029	19155022	258 M	100 M
26.5 FXT	June 5th	June 18th	19156034	19169017	155 M	none
27 GeV	May 10th	June 17th	19139960	19168040	558 M	1000 M

Overall Run Status (2019)

Energy	Start	Finish	First Run	Last Run	HLTgood	Target
19.6	Feb 25th	April 3rd	20056032	20093036	582 M	400 M
14.6	April 4th	June 3rd	20094048	20154013	324 M	310 M
3.85 FXT	June 9th	June 9th	20160024	20160027	3.7 M	5 M
7.3 FXT	June 18th	June 18th	20169029	20169055	52.7 M	50 M
7.7	June 3rd	June 27th	20154047	20178014	2.9 M	4 M
4.59 FXT	June 28th	July 2nd	20179040	20183025	200.6 M	200 M
9.2	June 28th	July 8th	20179016	20189017	1.0 M	none
31.2 FXT	July 8th	July 9th	20190006	20190024	50.6 M	50 M
200	July 11th	July 12th	20192001	20193026	138 M	140 M

Overall Run Status (2020)

Energy	Start	Finish	First Run	Last Run	HLTgood	Target
11.5 GeV	Dec 10th	Feb 24th	20056032	21055017	235 M	230 M
31.2 FXT	Jan 28th	Jan 29th	21028011	21029037	112.5 M	100 M
9.8 FXT	Jan29th	Feb 1st	21029051	21032016	108 M	100 M
19.5 FXT	Feb 1st	Feb 2nd	21032049	21033017	118 M	100 M
13.5 FXT	Feb 2nd	Feb 3rd	21033026	21034013	103 M	100 M
7.3 FXT	Feb 4th	Feb 5th	21035003	21036013	117 M	100 M
5.75 FXT	Feb 13th	Feb 14th	21044023	21045011	115.6 M	100 M
9.2 GeV	Feb 24th	Sep 1st	21055032	21245010	161.8 M	160 M
26.5 FXT	July 29th	Sep 14th	21211028	21258004	316.9 M	none
7.7 GeV	Sep 2nd	Sep 11th	21246012	21255021	3.2 M	none

FXT with eTOF (2020 and 2021)

Energy	Percent w/ eTOF	HLTgood total	Target w/ eTOF	
31.2 FXT	90.4 %	101.7 M	100 M	2020
19.5 FXT	68.1 %	80.4 M	80 M	
13.5 FXT	86.3 %	88.9 M	70 M	
9.8 FXT	67.3 %	72.7 M	65 M	
7.3 FXT	90.9 %	106.4M	50 M	
5.75 FXT	86.0 %	99.4 M	70 M	
26.5 FXT	94.3 %	298.7 M	none	
3.85 FXT	98.8 %	305.3 M	300 M	2021
44.5 FXT	93.3 %	50.3 M	50 M	
70 FXT	97.5 %	50.4 M	50 M	
100 FXT	99.8 %	50.6 M	50 M	
3.85 FXT				

Overall Run Status (2021)

Energy	Start	Finish	First Run	Last Run	HLTgood	Target
7.7 GeV	Jan 31st	May 1st	22031042	22121018	100.9 M	100 M
3.0 FXT	May 1st	May 5th	22121036	22125011	306.6 M	300 M
9.2 FXT	May 6th	May 6th	22126010	22126029	53.9 M	50 M
11.5FXT	May 7th	May 7th	22126045	22127018	51.7 M	50 M
13.7 FXT	May 8th	May 8th	22128001	22128011	50.7 M	50 M
O+O 200	May 11th	Min Bias	22131011	22136010	403.9 M	400 M
O+O 200	May 16th	Central	22136011	22141016	212.4 M	200 M
O+O 200	May 21st	Flip Field	22141039	22144006	125.0 M	100 M
17.3 GeV	May 25th	June 7th	22145017	22158019	256.1 M	250 M
3.0 FXT	June 7th	June 28th	22159051	22179022	1796 M	1.7 B
d+Au 200	June 28th	July 7th	22180043	22188007	216.9 M	200 M
7.2 FXT	June 3rd	July 3rd	22154936	22184019	88.6 M	none

Probing Strangeness Canonical Ensemble with K-, phi(1020) and Xi- Production in Au+Au Collisions at sqrt{s_NN} = 3 GeV
Submitted Dec. 23, 2021 , published May. 31, 2022
Phys. Lett. B 831 (2022) 137152

Light Nuclei Collectivity from 3 GeV Au+Au Collisions at RHIC
Submitted Dec. 8, 2021 , published Feb. 1, 2022

Measurements of Proton High Order Cumulants in sqrt{s_NN} = 3 GeV Au+Au Collisions and Implications for the QCD Critical Point
Submitted Dec. 2, 2021 , published May. 20, 2022
Phys. Rev. Lett. 128 (2022) 202303

Disappearance of partonic collectivity in 3 GeV Au+Au collisions at RHIC
Submitted Nov. 24, 2021 , published Mar. 10, 2022
Phys. Lett. B 827 (2022) 137003

Measurements of H3L and H4L Lifetimes and Yields in Au+Au Collisions in the High Baryon Density Region
Submitted Oct. 18, 2021 , published May. 17, 2022
Phys. Rev. Lett. 128 (2022) 202301

Global Lambda-hyperon polarization in Au+Au collisions at sqrt{sNN} =3 GeV
Submitted Aug. 4, 2021 , published Dec. 21, 2021
Phys. Rev. C 104 (2021) 61901

Measurement of the Sixth-Order Cumulant of Net-Proton Multiplicity Distributions in Au+Au Collisions at sqrt{sNN} = 27 , 54.4, and 200 GeV at
Submitted May. 31, 2021 , published Dec. 20, 2021
Phys. Rev. Lett. 127 (2021) 262301

First Observation of Directed Flow of Hypernuclei H3L and H4L in sqrt(sNN) = 3 GeV Au+Au Collisions at RHIC
Submitted Nov. 30, 2022 , published May. 26, 2023
Phys. Rev. Lett. 130 (2023) 212301

Higher-order cumulants and correlation functions of proton multiplicity distributions in sqrt{sNN} = 3 GeV Au + Au collisions at the RHIC STAR experiment
Submitted Sep. 26, 2022 , published Feb. 13, 2023
Phys. Rev. C 107 (2023) 24908

Search for the Chiral Magnetic Effect in Au+Au collisions at sqrt{sNN} = 27 GeV with the STAR forward Event Plane Detectors
Submitted Sep. 7, 2022 , published Mar. 1, 2023
Phys. Lett. B 839 (2023) 137779

Beam Energy Dependence of Fifth and Sixth-Order Net-proton Number Fluctuations in Au+Au Collisions at RHIC [3 GeV]
Submitted Jul. 21, 2022 , published Feb. 24, 2023
Phys. Rev. Lett. 130 (2023) 82301

Measurement of H4L and He4L binding energy in Au+Au collisions at sqrt(sNN) = 3GeV
Submitted Jul. 5, 2022 , published Sep. 17, 2022
Phys. Lett. B 834 (2022) 137449

Global polarization of Lambda and Lambdabar hyperons in Au+Au collisions at sqrt{s_NN} = 19.6 and 27 GeV
Submitted May. 17, 2023

Event-by-event correlations between Lambda (anti-Lambda) hyperon global polarization and handedness with charged hadron azimuthal separation in Au+Au collisions at sqrt(sNN) = 27 GeV from STAR
Submitted Apr. 21, 2023, published
Phys.Rev. C 108 (2023) 1, 014909

Observation of the electromagnetic field effect via charge-dependent directed flow in heavy-ion collisions at the Relativistic Heavy Ion Collider (27 GeV)
Submitted Apr. 11, 2023

Electric charge and strangeness-dependent directed flow splitting of produced quarks in Au+Au collisions (27 GeV)
Submitted Apr. 10, 2023

Elliptic Flow of Heavy-Flavor Decay Electrons in Au+Au Collisions at sqrt(sNN) = 27 and 54.4 GeV at RHIC
Submitted Mar. 8, 2023

Measurements of Dielectron Production in Au+Au Collisions at sqrt(sNN)= 27, 39, and 62.4 GeV from the STAR Experiment
Submitted Feb. 27, 2023 , published Jun. 1, 2023
Phys. Rev. C 107 (2023) 0

Probing Strangeness Canonical Ensemble with K-, phi(1020) and Xi- Production in Au+Au Collisions at sqrt{s_NN} = 3 GeV

Submitted Dec. 23, 2021 , published May. 31, 2022

Phys. Lett. B 831 (2022) 137152

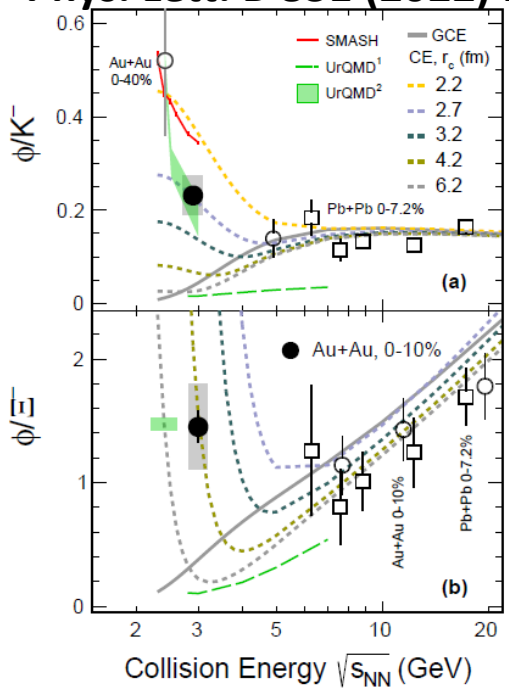

FIG. 5. ϕ/K^- (a) and ϕ/Ξ^- (b) ratio as a function of collision energy, $\sqrt{s_{\rm NN}}$. The solid black circles show the measurements presented here in 0-10% centrality bin, while empty markers in black are used for data from various other energies and/or collision systems [27–33, 57]. The vertical grey bands on the data points represent the systematic uncertainties. The grey solid line represents a THERMUS calculation based on the Grand Canonical Ensemble (GCE) while the dotted lines depict calculations based on the Canonical Ensemble (CE) with different values of the strangeness correlation radius (r_c) [20, 59]. The green dashed line, green shaded band and the solid red line show transport model calculations from the public versions UrQMD[1] [62, 63], modified UrQMD[2] [60] and SMASH [61], respectively.

In summary, we report the systematic measurements of K^-, $\phi(1020)$ and Ξ^- production yields and the ϕ/K^-, ϕ/Ξ^- ratios in Au+Au collisions at $\sqrt{s_{\rm NN}} = 3$ GeV with the STAR experiment at RHIC. The measured ϕ/K^- ratio is significantly larger than the statistical model prediction based on Grand Canonical Ensemble in the 0–10% central collisions. Both the results of ϕ/K^- ($r_c \sim 2.7$ fm) and ϕ/Ξ^- ($r_c \sim 4.2$ fm) ratios favor the Canonical Ensemble model for strangeness production in such collisions. Transport models, including the resonance decays, could reasonably describe our measured ϕ/K^- ratio at 3 GeV and the increasing trend of ϕ/Ξ^- at lower energies. The new results from this paper suggest a significant change in the strangeness production for $\sqrt{s_{\rm NN}} < 5$ GeV, providing new insights towards the understanding of the QCD medium properties at high baryon density.

Measurements of H3L and H4L Lifetimes and Yields in Au+Au Collisions in the High Baryon Density Region

Submitted Oct. 18, 2021 , published May. 17, 2022

Phys. Rev. Lett. 128 (2022) 202301

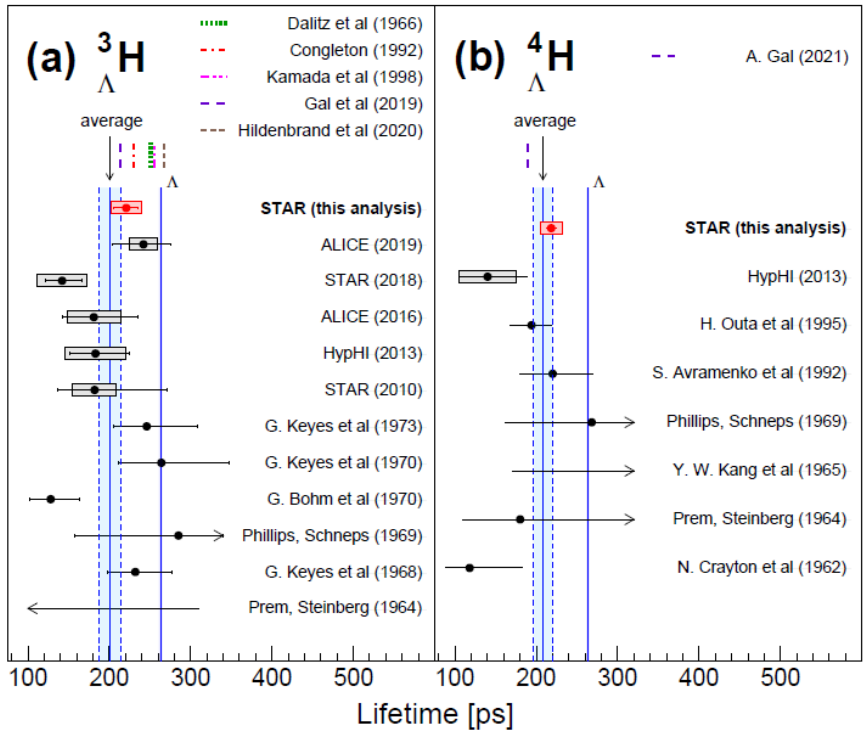

FIG. 2: $^3_\Lambda$H (a) and $^4_\Lambda$H (b) measured lifetime, compared to previous measurements [3–5, 7–11, 40–46], theoretical calculations [47–52] and τ_Λ [53]. Horizontal lines represent statistical uncertainties, while boxes represent systematic uncertainties. The experimental average lifetimes and the corresponding uncertainty of $^3_\Lambda$H and $^4_\Lambda$H are also shown as vertical blue shaded bands.

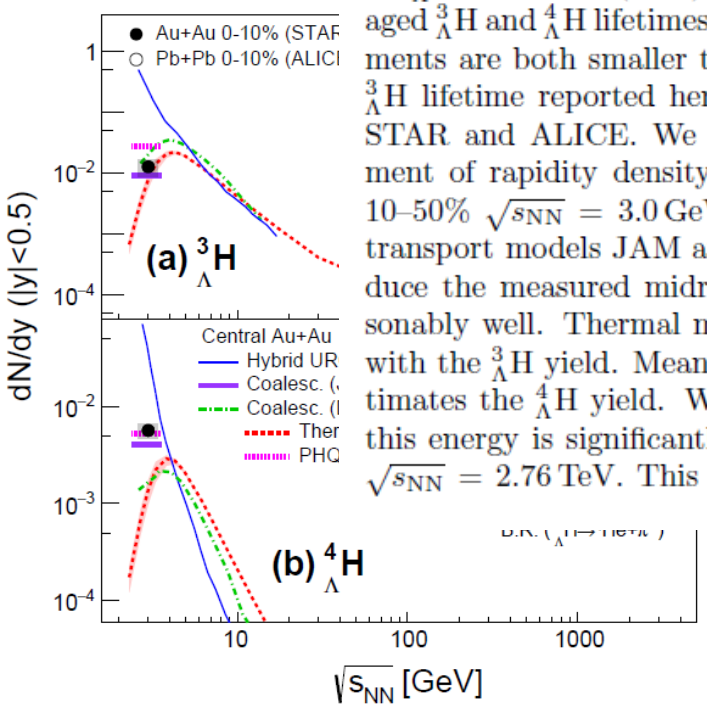

FIG. 4: (a) $^3_\Lambda$H and (b) $^4_\Lambda$H yields at $|y| < 0.5$ as a function of beam energy in central heavy-ion collisions. The symbols represent measurements [8] while the lines represent different theoretical calculations. The data points assume a B.R. of 25(50)% for $^3_\Lambda\mathrm{H}(^4_\Lambda\mathrm{H}) \rightarrow {}^3\mathrm{He}({}^4\mathrm{He}) + \pi^-$. The insets show the (a) $^3_\Lambda$H and (b) $^4_\Lambda$H yields at $|y| < 0.5$ times the B.R. as a function of the B.R.. Vertical lines represent statistical uncertainties, while boxes represent systematic uncertainties.

In summary, precise measurements of $^3_\Lambda$H and $^4_\Lambda$H lifetimes have been obtained using the data samples of Au+Au collisions at $\sqrt{s_{\mathrm{NN}}} = 3.0$ and 7.2 GeV. The lifetimes are measured to be $221 \pm 15(\mathrm{stat.}) \pm 19(\mathrm{syst.})$ ps for $^3_\Lambda$H and $218 \pm 6(\mathrm{stat.}) \pm 13(\mathrm{syst.})$ ps for $^4_\Lambda$H. The averaged $^3_\Lambda$H and $^4_\Lambda$H lifetimes combining all existing measurements are both smaller than τ_Λ by $\sim 20\%$. The precise $^3_\Lambda$H lifetime reported here resolves the tension between STAR and ALICE. We also present the first measurement of rapidity density of $^3_\Lambda$H and $^4_\Lambda$H in 0–10% and 10–50% $\sqrt{s_{\mathrm{NN}}} = 3.0$ GeV Au+Au collisions. Hadronic transport models JAM and PHQMD calculations reproduce the measured midrapidity $^3_\Lambda$H and $^4_\Lambda$H yields reasonably well. Thermal model predictions are consistent with the $^3_\Lambda$H yield. Meanwhile, the same model underestimates the $^4_\Lambda$H yield. We observe that the $^3_\Lambda$H yield at this energy is significantly higher compared to those at $\sqrt{s_{\mathrm{NN}}} = 2.76$ TeV. This observation establishes low energy collision experiments as a promising tool to study exotic strange matter.

Measurement of H4L and He4L binding energy in Au+Au collisions at sqrt(sNN) = 3GeV

Submitted Jul. 5, 2022 , published Sep. 17, 2022

Phys. Lett. B **834** (2022) 137449

BES- Re/FXT Result

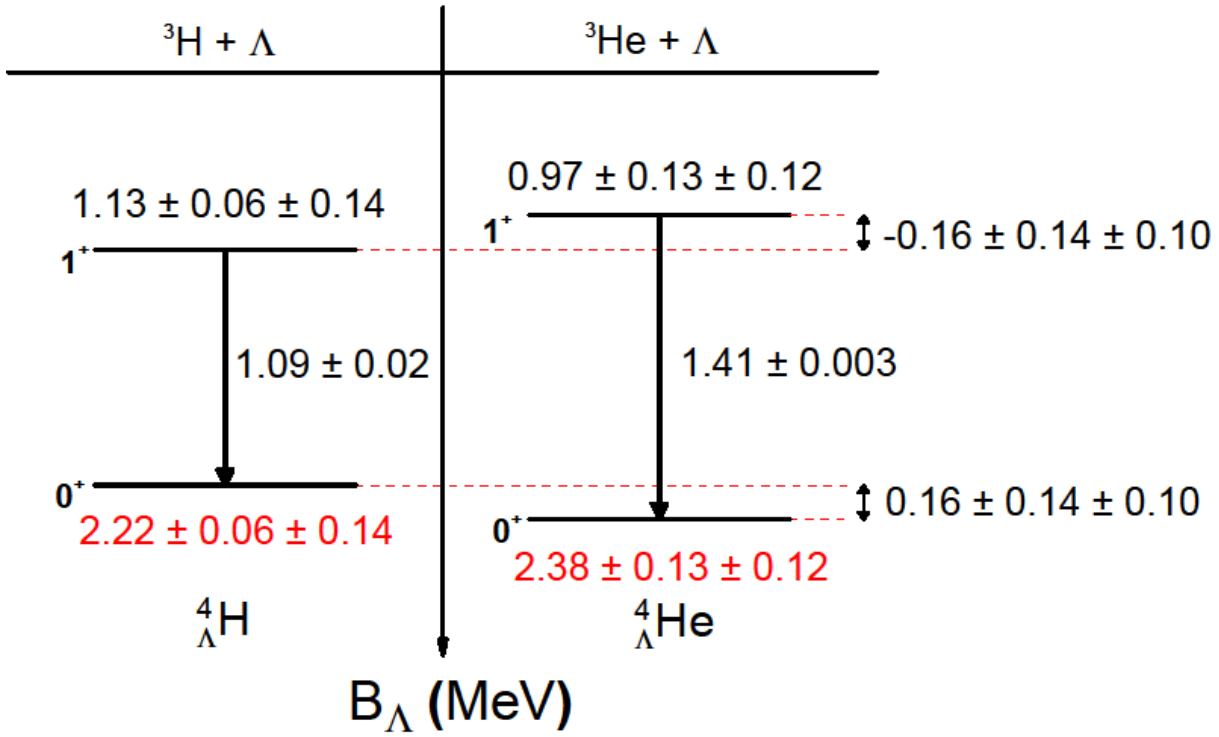

The masses and the binding energies of the mirror hypernuclei, 4HL and 4HeL, are measured at 3 GeV.

The binding energies and excited states are extracted.

Provides a new avenue to study the Charge Symmetry Breaking in heavy-ion collision experiments.

First Observation of Directed Flow of Hypernuclei H3L and H4L in sqrt(sNN) = 3 GeV Au+Au Collisions at RHIC

Submitted Nov. 30, 2022 , published May. 26, 2023

Phys. Rev. Lett. 130 (2023) 212301

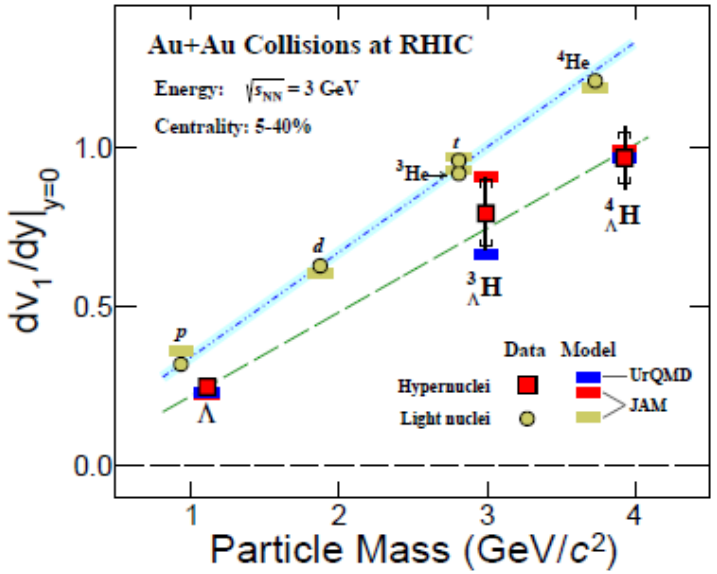

FIG. 4. Mass dependence of the midrapidity v_1 slope, dv_1/dy, for Λ, $^3_\Lambda$H and $^4_\Lambda$H from the $\sqrt{s_{\rm NN}} = 3$ GeV 5%-40% midcentral Au+Au collisions. The statistical and systematic uncertainties are presented by vertical lines and square brackets, respectively. The slopes of p, d, t, ^{3}He, and ^{4}He from the same collisions are shown as black circles. The blue and dashed green lines are the results of a linear fit to the measured light nuclei and hypernuclei v_1 slopes, respectively. For comparison, calculations of transport models plus coalescence afterburner are shown as gold and red bars from the JAM model, and blue bars from the UrQMD model.

To summarize, we report the first observation of hypernuclei $^3_\Lambda$H and $^4_\Lambda$H v_1 from $\sqrt{s_{\rm NN}} = 3$ GeV midcentral 5%-40% Au+Au collisions at RHIC. The rapidity dependences of their v_1 are compared with those of Λ, p, d, t, ^{3}He and ^{4}He in the same collisions. It is found that, within uncertainties, the mass dependent v_1 slope of hypernuclei, $^3_\Lambda$H and $^4_\Lambda$H is similar to that of light nuclei, implying that they follow the baryon mass scaling. Calculations from transport models (JAM and UrQMD) plus coalescence afterburner can qualitatively reproduce the rapidity dependence of v_1 and the mass dependence of the v_1 slope. These observations suggest that coalescence of nucleons and hyperon Λ could be the dominant mechanism for the hypernuclei $^3_\Lambda$H and $^4_\Lambda$H production in the 3 GeV collisions. Model calculations suggest that baryon density at freeze-out may depend on collision energy [51–53]. High statistics data at different energies, especially at the high baryon density region, will help in extracting the information on Y-N interaction and possibly its density dependence in the future.

Global Lambda-hyperon polarization in Au+Au collisions at sqrt{sNN} =3 GeV

Submitted Aug. 4, 2021 , published Dec. 21, 2021

Phys. Rev. C 104 (2021) 61901

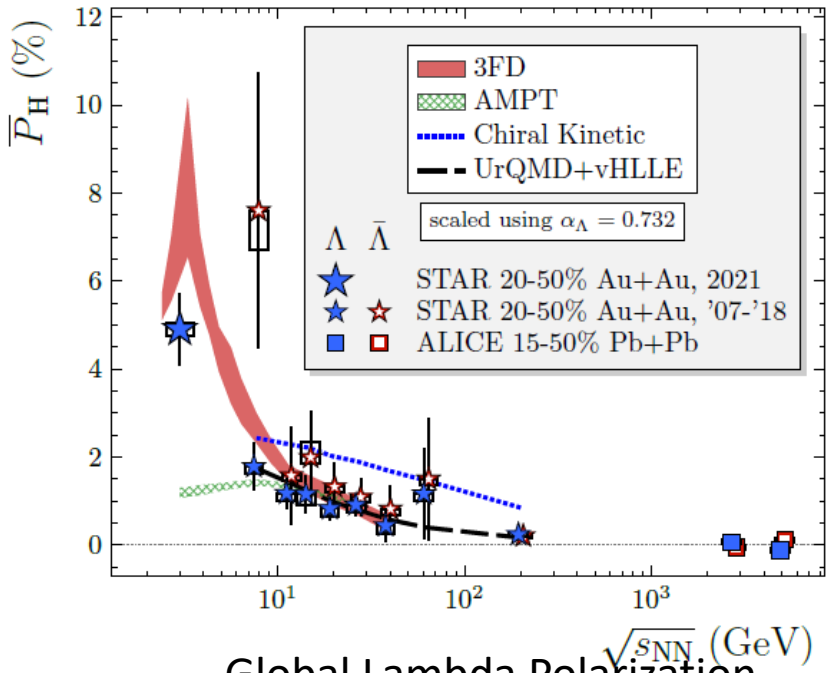

Global Lambda Polarization

FIG. 3. Global hyperon polarization as a function o
in mid-central heavy-ion collisions. The trend of in
$\overline{P}_H$ with decreasing $\sqrt{s_{NN}}$ is maintained at the low
of $\sqrt{s_{NN}} = 3$ GeV. Statistical uncertainties are repr
with lines while systematic uncertainties are represent
boxes. Previous experimental results[9–11, 17] are s
using the currently accepted[31] decay parameter α_Λ =
Calculations with a hybrid model (UrQMD+vHLLE)
chiral-kinetic transport[21] are compared to the highe
data only, while others have been extended to lower
The AMPT model[20] matches higher-energy data w
dramatically underestimating $\overline{P}_\Lambda$ at $\sqrt{s_{NN}} = 3$ Ge
hydrodynamic 3FD model[40] with two separate equa
state (crossover and first-order phase transition) pr
sharply rising $\overline{P}_\Lambda$ below $\sqrt{s_{NN}} = 7.7$ GeV. The model
use an impact parameter of 8 fm.

Our measurement of nonzero $\overline{P}_\Lambda$ at $\sqrt{s_{NN}} = 3$ GeV demonstrates that vorticity aligned with $\hat{J}$ is at a maximum below $\sqrt{s_{NN}} = 7.7$ GeV. The data agree roughly with calculations made using the 3FD model, integrated over mid-rapidity, but are dramatically larger than such calculations made using the partonic-transport model AMPT. As in Ref. [17], we observe a significant centrality dependence of $\overline{P}_\Lambda$ that is consistent with increasing $\vec{J}$. Our measurement of the dependence of $\overline{P}_\Lambda$ on y is uniquely valuable because we have access to the most forward-rapidity Λ hyperons. Interestingly, despite the variety of model calculations predicting quite strong dependence of $\overline{P}_H$ on y [19, 42, 43, 45, 48–52], we see no statistically significant dependence. A migration of $\overline{P}_H$ towards forward rapidity has been offered as a potential explanation of the monotonic fall of $\overline{P}_H$ with $\sqrt{s_{NN}}$[45]. Given our observation, such an explanation may be incorrect, though this does not dispel such arguments as the state of the system at higher energy is notably different;

measurements of $\overline{P}_H$ using the STAR forward upgrade will provide indispensable comparisons to the work presented here.

Global polarization of Lambda and Lambdabar hyperons in Au+Au collisions at sqrt{s_NN} = 19.6 and 27 GeV

Submitted May. 17, 2023 •2305.08705 [nucl-ex]

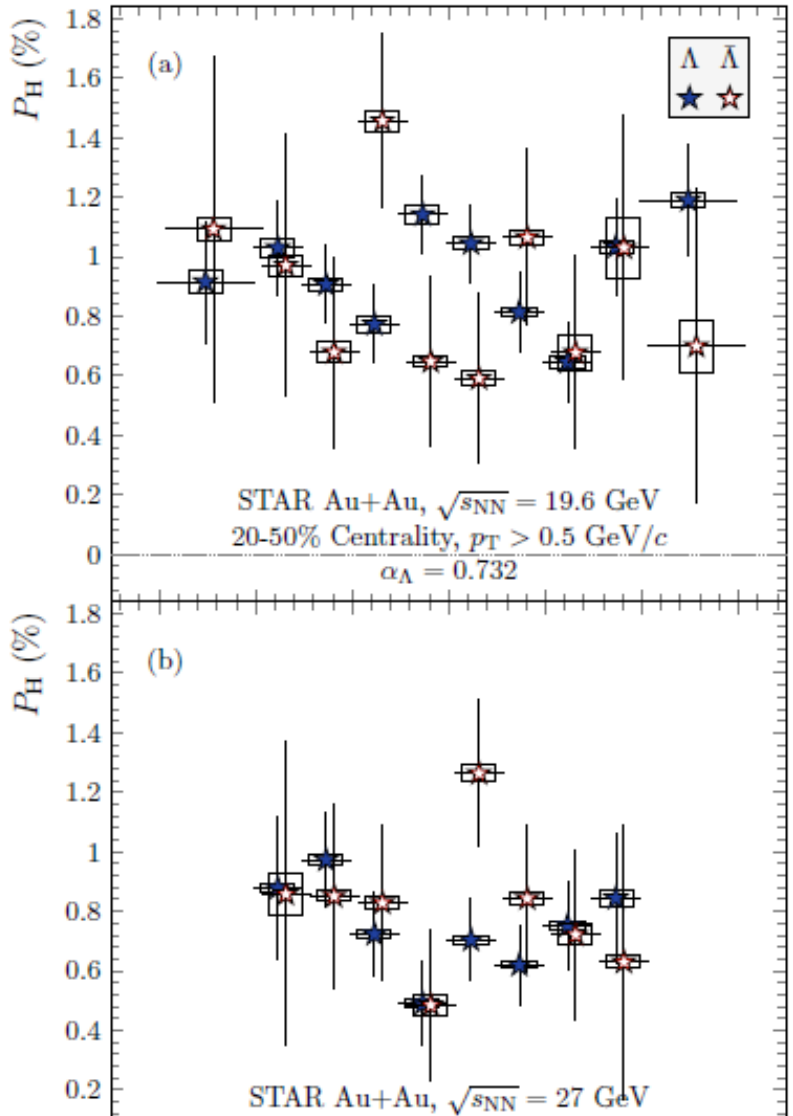

The observation of global polarization in heavy-ion collisions has prompted intense investigations, both experimentally and theoretically, into the vortical flow structure of the QGP. One of the main questions raised in this context is that of the late-stage magnetic field sustained by the QGP through its finite conductivity and how $P_{\bar{\Lambda}} - P_\Lambda$ might serve to measure it. While competing theories offer differing views on the interpretation of $P_{\bar{\Lambda}} - P_\Lambda$, its measurement nevertheless provides valuable insight. In this study, we take advantage of upgraded subsystems within the STAR detector and recent high-statistics data sets at $\sqrt{s_{\rm NN}} = 19.6$ and 27 GeV in order to serve a precision measurement of $P_{\bar{\Lambda}} - P_\Lambda$. With the naïve assumptions, we place an upper limit on the late-stage magnetic field of $B < 9.4 \times 10^{12}$ T and $B < 1.4 \times 10^{13}$ T at a 95% confidence level for the measurements at $\sqrt{s_{\rm NN}} = 19.6$ and 27 GeV, respectively. Still, through a more detailed approach, the $P_{\bar{\Lambda}} - P_\Lambda$ reported here may be found to correspond to a significant and positive late-stage magnetic field. We also report here measurements of $P_{\rm H}$ with respect to collision centrality and $p_{\rm T}$ and find $P_{\rm H}$ rising with centrality but no significant dependence on $p_{\rm T}$; these are consistent with previous observations. Of more interest is a changing $P_{\rm H}$ with y, which has been predicted but not yet measured. Our measurement of $P_{\rm H}$ with respect to y can accommodate an enhancement at larger $|y|$, consistent with numerous model predictions, but is not statistically significant. The findings reported here call for a better theoretical understanding of the relevance of $P_{\bar{\Lambda}} - P_\Lambda$ to the late-stage magnetic field and for future high-statistics studies of $P_{\rm H}$.

Elliptic Flow of Heavy-Flavor Decay Electrons in Au+Au Collisions at sqrt(sNN) = 27 and 54.4 GeV at RHIC

Submitted Mar. 8, 2023

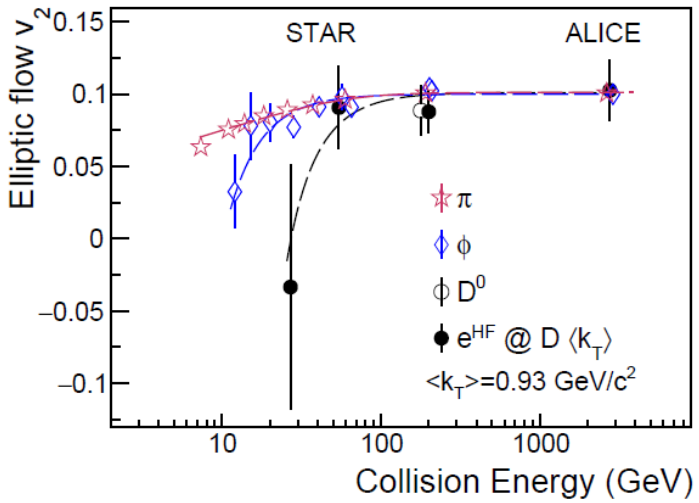

Figure 7: Energy dependence of v_2 for $\pi^{\pm}$, ϕ, D^0 and e^{HF} at the same transverse mass value $\langle k_T \rangle = \langle m_T - m_0 \rangle = 0.93$ GeV/c^2. The data points are from or interpolated from STAR [52, 75, 76] and ALICE [77, 78] measurements. The e^{HF} v_2 shown here is at the same parent D^0 meson transverse mass position using the decay kinematics calculated from PYTHIA6. Data points at the same energy are shifted horizontally for clarity. Error bars depict combined statistical and systematic uncertainties. The lines are for eye guidance.

In summary, new results of heavy-flavor decay electron (e^{HF}) elliptic flow v_2 at mid-rapidity ($|y| < 0.8$) in Au+Au collisions at $\sqrt{s_{NN}}$ = 27 and 54.4 GeV from STAR are reported. The e^{HF} v_2 in Au+Au collisions at $\sqrt{s_{NN}}$ = 27 GeV is consistent with zero within large uncertainties, whereas for $\sqrt{s_{NN}}$ = 54.4 GeV collisions a significant non-zero v_2 is observed for $p_T < 2$ GeV/c. The e^{HF} v_2 in Au+Au $\sqrt{s_{NN}}$ = 54.4 GeV is comparable to that at $\sqrt{s_{NN}}$ = 200 GeV. TAMU and PHSD transport model calculations underestimate the measured e^{HF} v_2 in both $\sqrt{s_{NN}}$ = 200 and 54.4 GeV at $p_T < 1$ GeV/c. Within the uncertainties, the magnitude of e^{HF} v_2 at $\sqrt{s_{NN}}$ = 54.4 GeV and produced electron $p_T > 1$ GeV/c is consistent with the scenario that their parent D meson v_2 follows the NCQ scaling with light-flavor hadrons in the same collision energy. This suggests that charm quarks gain significant collectivity through the interactions with the expanding QGP medium such that they may reach local thermal equilibrium in Au+Au collisions at $\sqrt{s_{NN}}$ = 54.4 GeV. Our new results are expected to provide new constraints on the charm quark spatial diffusion coefficient, especially its temperature dependence. The energy dependence of measured v_2 from various particles ($\pi/\phi/D^0/e^{HF}$) shows a hint of quark-mass dependence. Future measurements on v_2 at lower energies, as well as bottom quark v_2 results at RHIC and the LHC, will shed new insights into particle collectivity and medium thermalization in heavy-ion collisions.

Beam Energy Dependence of Triton Production and Yield Ratio (NtNp/N2d) in Au+Au Collisions at RHIC

Submitted Sep. 19, 2022 , published May. 16, 2023

Phys. Rev. Lett. **130** (2023) 202301

BES-I Result

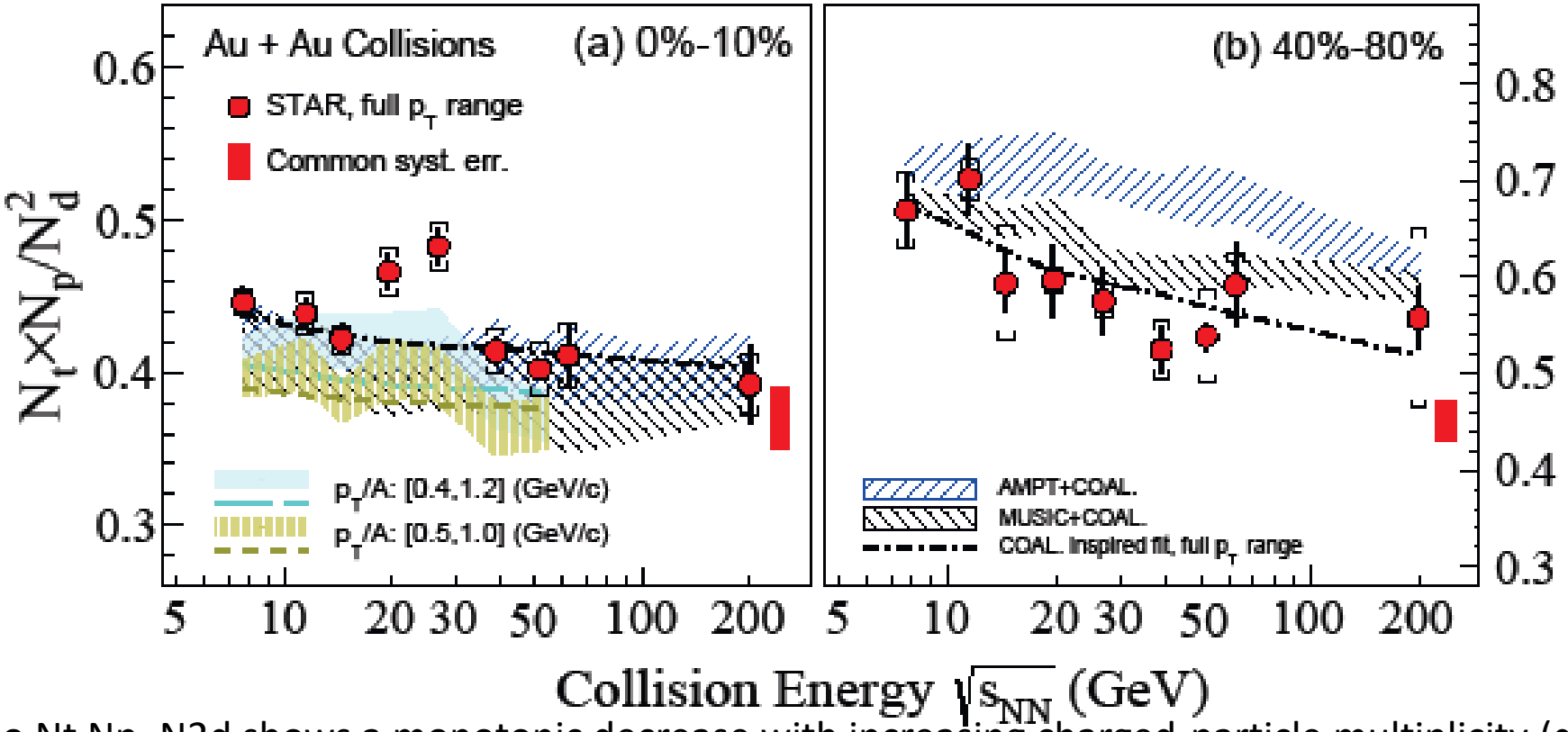

The yield ratio Nt Np=N2d shows a monotonic decrease with increasing charged-particle multiplicity (dNch=dh) and exhibits a scaling behavior, which can be attributed to the formation of deuteron and triton via nucleon coalescence.

In the most central Au+Au collisions at 19.6 and 27 GeV, Nt Np=N2d shows enhancements.

Enhancements may be due to large baryon density fluctuations near the critical point of the QCD phase diagram.

Electric charge and strangeness-dependent directed flow splitting of produced quarks in Au+Au collisions (27 GeV)

Submitted Apr. 10, 2023

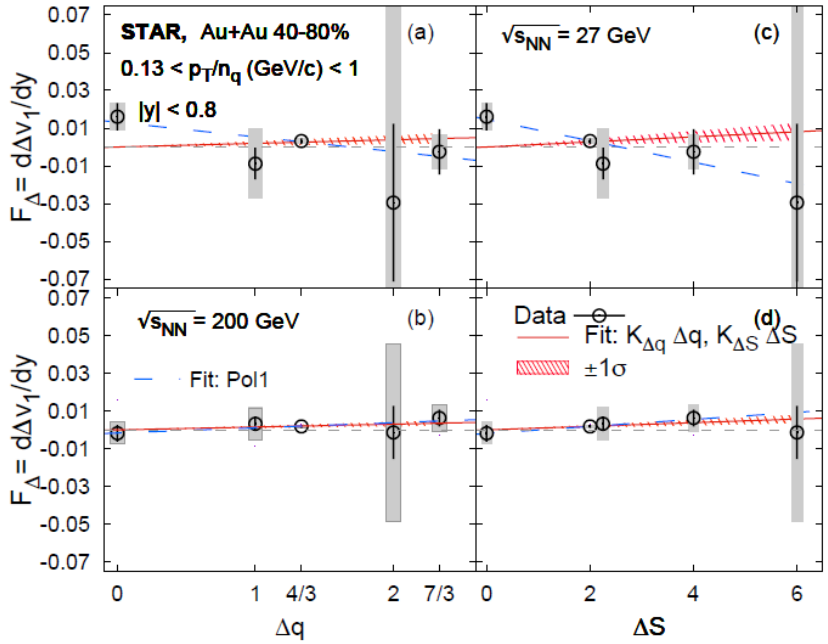

FIG. 6: Midrapidity Δv_1 slope versus Δq (a, b), ΔS (c, d) in 40-80% Au+Au at 27 (a, c) and 200 (b, d) GeV, respectively. The dashed curves show AMPT calculations. The vertical bars and shaded bands denote statistical and systematic uncertainties, respectively. There are two degenerate points at $\Delta S = 2$; one is displaced horizontally for better visualization.

In summary, we first report the measurements of $v_1(y)$ of multistrange baryons (Ξ and Ω) in Au+Au collisions at $\sqrt{s_{NN}} = 27$ and 200 GeV. We focus on seven produced particle species: K^-, $\bar{p}$, $\bar{\Lambda}$, ϕ, $\bar{\Xi}^+$, Ω^- and $\bar{\Omega}^+$, none of whose constituent quarks is transported from the colliding nuclei, and study the difference (splitting), $F_\Delta = d\Delta v_1/dy$, between pairs of particle combinations with similar quark content but varying electric charge difference Δq and strangeness difference ΔS. For $\Delta q = \Delta S = 0$, consistency with the coalescence sum rule is observed at 10-40% centrality. For $\Delta q \neq 0$ and $\Delta S \neq 0$, a nonzero average F_Δ is observed with over 5σ significance, dominated by the $(\Delta q, \Delta S)$=(4/3, 2) pair. This splitting appears to increase with increasing Δq and ΔS. However, the increase is not statistically significant without assuming the coalescence sum rule. With this assumption, the one-parameter linear fit as a function of Δq and ΔS yields a positive slope, respectively 4.8σ and 4.6σ away from zero for $\sqrt{s_{NN}} = 27$ GeV. This splitting is stronger at 27 GeV than at 200 GeV. The

AMPT model (where no EM fields are implemented) fails to describe the data. These midcentral 10-40% data are therefore consistent with electromagnetic effects, where the positive slope suggests a dominance of Hall effect over Faraday+Coulomb effect. Our peripheral 40-80% data statistics are insufficient to yield firm conclusions. On the other hand, a companion analysis [26] by STAR, which considers hadrons involving both produced and transported quarks, finds that in peripheral collisions, Faraday+Coulomb effects dominate the v_1 splitting of hadrons with light (anti-)quarks, such as pions and protons. Additionally, the v_1 splitting of kaons is predominantly influenced by the Hall effect acting on the strange (anti-)quarks. Therefore, the combined inference from Ref. [26] and the present study is that a competition between the Hall effect and the Faraday+Coulomb effect exists, and that the observed pattern of v_1 splitting may be influenced by the particle species and centrality dependence of this competition.

Observation of the electromagnetic field effect via charge-dependent directed flow in heavy-ion collisions at the Relativistic Heavy Ion Collider (27 GeV)

Submitted Apr. 11, 2023

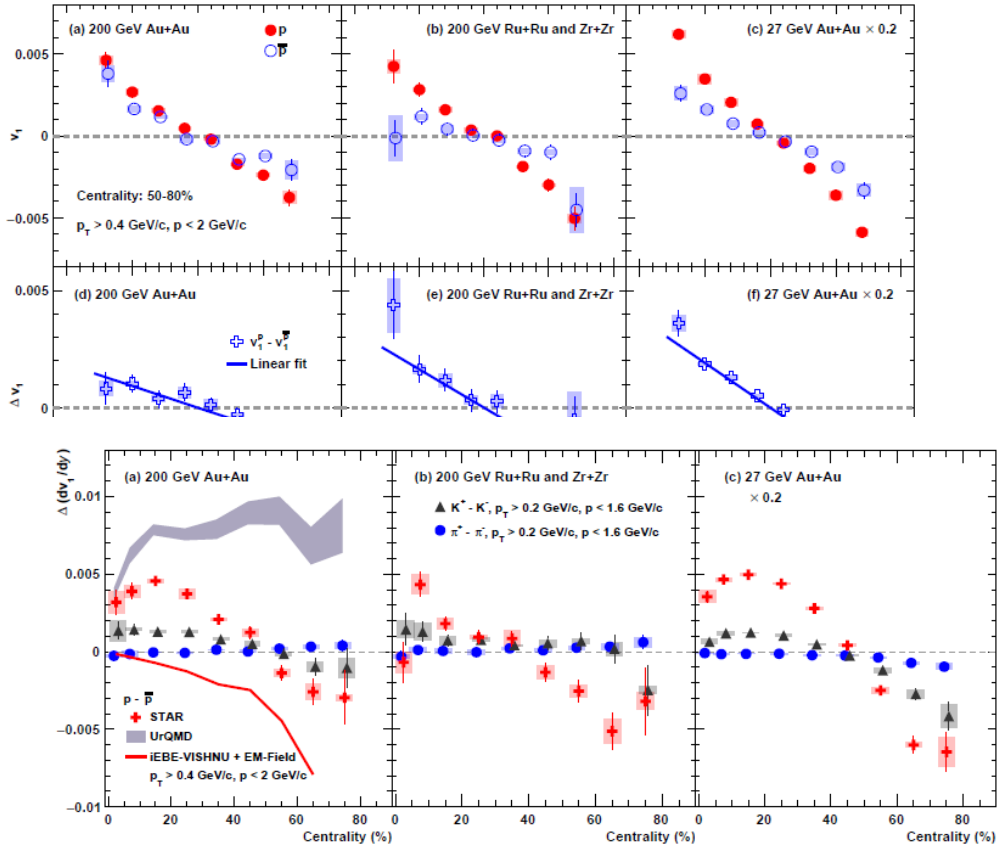

FIG. 6: $\Delta(dv_1/dy)$ between positively and negatively charged pions, kaons and protons as a function of centrality in (a) Au+Au collisions at $\sqrt{s_{NN}} = 200$ GeV, (b) isobar collisions at $\sqrt{s_{NN}} = 200$ GeV and (c) Au+Au collisions at $\sqrt{s_{NN}} = 27$ GeV. The lavender band indicates UrQMD simulations of the proton $\Delta dv_1/dy$ in Au+Au collisions at 200 GeV. In comparison, a solid curve is added correspondingly for the electromagnetic field calculation [26].

The charge-dependent directed flow provides a probe to the transported quarks, as well as the Hall, Faraday, and Coulomb effects in heavy-ion collisions. We have presented the v_1 measurements for $\pi^{\pm}$, $K^{\pm}$, and $p(\bar{p})$ in Au+Au and isobar (Ru+Ru and Zr+Zr) collisions at $\sqrt{s_{NN}} = 200$ GeV, and Au+Au collisions at $\sqrt{s_{NN}} = 27$ GeV. The slope difference, $\Delta(dv_1/dy)$, between protons and anti-protons, as well as between K^+ and K^-, changes from positive values in central collisions to negative in peripheral collisions. The measured proton $\Delta(dv_1/dy)$ values in the centrality range of 50–80% are $[-1.89 \pm 0.35(\text{stat.}) \pm 0.09(\text{syst.})] \times 10^{-3}$ in Au+Au collisions at 200 GeV, $[-3.28 \pm 0.53(\text{stat.}) \pm 0.27(\text{syst.})] \times 10^{-3}$ in isobar collisions at 200 GeV, and $[-1.91 \pm 0.13(\text{stat.}) \pm 0.03(\text{syst.})] \times 10^{-2}$ in Au+Au collisions at 27 GeV. While the positive $\Delta(dv_1/dy)$ for protons and kaons in central collisions can be attributed to the transported-quark contributions, the significant negative values in peripheral events are consistent with the electromagnetic field effects with the dominance of the Faraday induction + Coulomb effect [26, 27]. This charge splitting is stronger in collisions at $\sqrt{s_{NN}} = 27$ GeV, corroborating the idea that the electromagnetic field decays more slowly at low energies. Compared with protons, pions and kaons have smaller $\Delta(dv_1/dy)$ magnitudes, which is understandable in view of factors such as mean p_T and the formation time. A companion STAR analysis [66] assumes the coalescence sum rule using combinations of hadrons without transported quarks and concludes that the presence of the EM-field dominated by the Hall effect in mid-central events explains the observed v_1 splitting. The combined inference from Ref. [66] and the current work is that a competition between the Hall effect and the Faraday+Coulomb effect, its flavor and centrality dependence may lead to the observed v_1 splittings. Further studies on the beam energy dependence of this observable are underway, with more data accumulated in the RHIC BES-II program.

Event-by-event correlations between Lambda (anti-Lambda) hyperon global polarization and handedness with charged hadron azimuthal separation in Au+Au collisions at sqrt(sNN) = 27 GeV from STAR

Submitted Apr. 21, 2023, Pubished Phys.Rev.C 108 (2023) 1, 014909

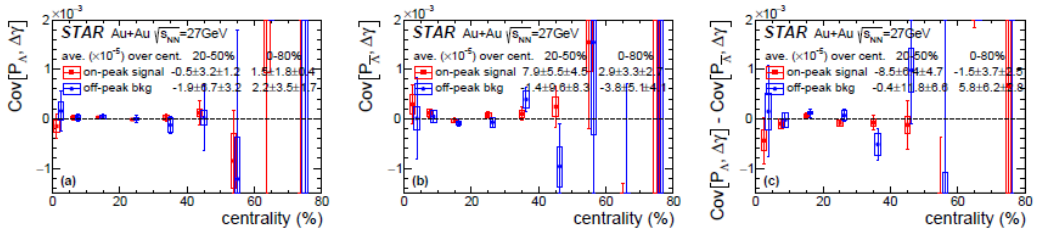

FIG. 10. Covariances between the parity-even observables P_Λ and $\Delta\gamma$ (left), between $P_{\bar{\Lambda}}$ and $\Delta\gamma$ (middle), and their difference (right) as functions of centrality in Au+Au collisions at $\sqrt{s_{\rm NN}} = 27$ GeV. Hadrons used to reconstruct Λ or $\bar{\Lambda}$ in the mass peak region are excluded from $\Delta\gamma$. The statistical uncertainty is shown by error bars, while the systematic uncertainty is shown by hollow boxes. The on-peak signal data points are shifted slightly to the left along the x-axis, while the off-peak background to the right symmetrically, for better visualization.

In conclusion, this paper reports measurements of event-by-event correlations between the observed Λ handedness and the charged hadron Δa_1, and between Λ polarizations and charged hadron $\Delta\gamma$, in Au+Au collisions at $\sqrt{s_{\rm NN}} = 27$ GeV using the STAR detector. These correlation observables have been deployed to measure the chiral magnetic effect and the presence of a strong magnetic field in heavy-ion collisions.

Neither of these measurements has yielded a non-zero correlation result within the statistical precision of the present dataset. However, looking toward the future, these correlation measurements should be largely insensitive to the typical physics backgrounds that plague measurements of CME-senstitive observables, and it is possible that such correlation measurements will ultimately offer better sensitivity than individual measurements of these quantities to investigate the chiral magnetic effect.

Search for the Chiral Magnetic Effect in Au+Au collisions at sqrt{sNN} = 27 GeV with the STAR forward Event Plane Detectors

Submitted Sep. 7, 2022 , published Mar. 1, 2023

Phys. Lett. B 839 (2023) 137779

See later talk by Zhiwan Xu

QM2023: 7.7, 14.6, and 19.6 GeV results

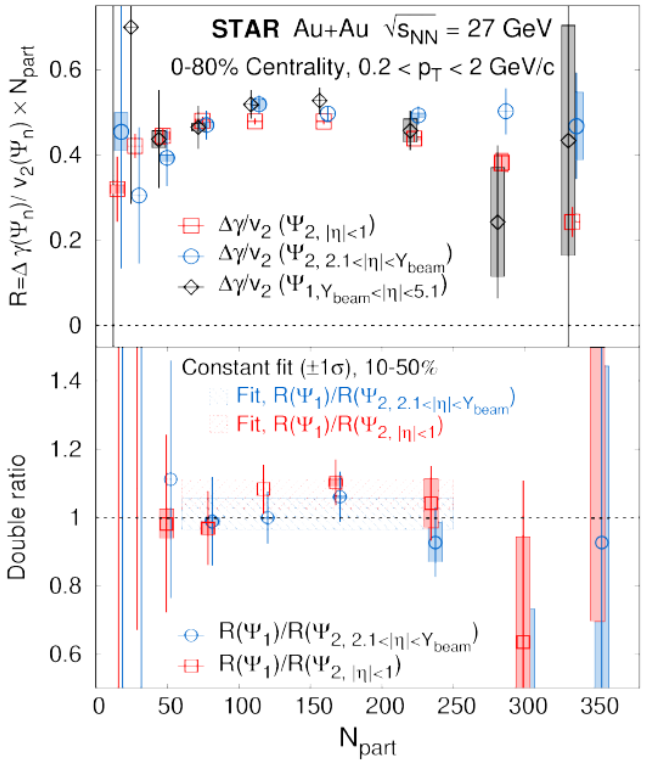

In this letter, we present measurements of charge separation with respect to reaction plane using Au+Au $\sqrt{s_{NN}}$ =27 GeV collisions. At this collision energy, the STAR forward EPDs can measure the event plane associated with a large directed flow from beam fragments with high resolution. This directed flow plane (Ψ_1) is expected to be more correlated with the direction of magnetic field than the elliptic flow planes (Ψ_2) of produced particles as shown in UrQMD simulations. Therefore, we measured the charge separation scaled by ellipticity $R(\Psi_n)$ across the Ψ_1 determined at forward rapidity and compare it with the corresponding measurements using Ψ_2 reconstructed out of produced particles at both forward and mid-rapidity. Within our measurement uncertainties we find the ratio $R(\Psi_1)/R(\Psi_2)$ to be consistent with unity, which agrees with the expectations from a flow driven background scenario. For further quantification, we derive an upper limit at the 95% confidence level on the quantity $\mathcal{D} = R(\Psi_1)/R(\Psi_2) - 1$ for possible deviation from a flow driven background scenario. In 10-50% centrality we find the upper limits of $\mathcal{D}$ to be 10% and 16% using Ψ_2 at forward and mid-rapidity, respectively. In this analysis we argued that the information of the directed flow near the beam rapidity using EPDs and the elliptic flow at mid-rapidity allows us to control the flow driven CME background in 27 GeV Au+Au collisions and explore effects beyond background. Due to the acceptance of the EPDs ($2.1 < \eta < 5.1$), the same can be done for several data sets ($\sqrt{s_{NN}}$ = 9.2, 11.5, 13.7, 14.5, 17.3, 19.6 GeV) collected by the STAR under RHIC Beam Energy Scan Phase II program. The use of forward event planes in this work not only pioneers a high-precision CME search from the RHIC Beam Energy Scan Phase II program, but also opens up opportunities to search for other magnetic field driven effects at RHIC.

Figure 4: (Upper panel) The quantity R obtained by estimating the charge separation measured by the difference between opposite-sign and same-sign γ correlator ($\Delta\gamma$) and then scaling by v_2 times $N_{\rm part}$. The measurements are shown for all three different event planes. (Lower panel) The ratio of the quantity R shown on upper panel between Ψ_1 plane and Ψ_2 plane. The error bars indicate the statistical uncertainty, the shadowed bars indicate the systematic uncertainty. The results of the fit including 1σ fitting uncertainties are shown by bands with dashed border for $10-50\%$ centrality in lower panel. Points are shifted horizontally for clarity.

Measurements of Proton High Order Cumulants in sqrt{s_NN} = 3 GeV Au+Au Collisions and Implications for the QCD Critical Point

Submitted Dec. 2, 2021 , published May. 20, 2022

Phys. Rev. Lett. 128 (2022) 202303

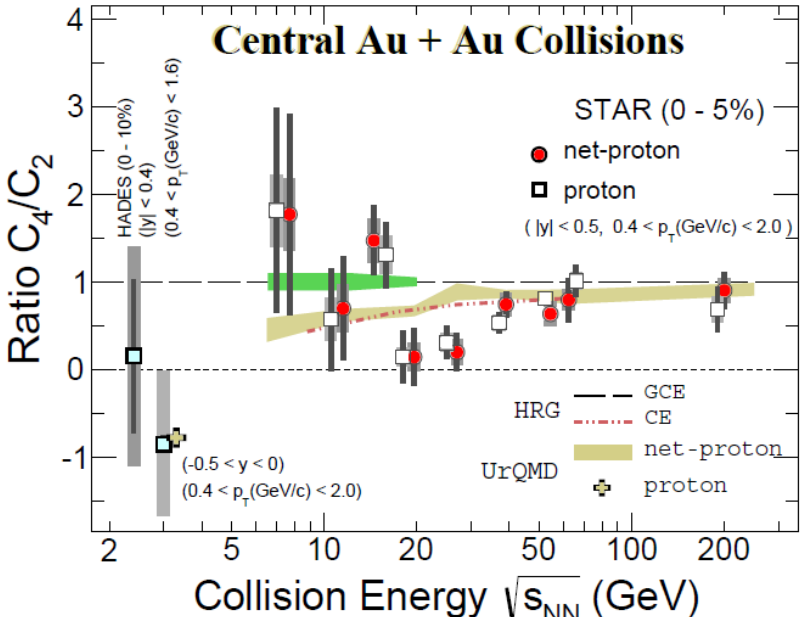

FIG. 5. Collision energy dependence of the ratios of cumulants, C_4/C_2, for proton (squares) and net-proton (red circles) from top 0%–5% Au+Au collisions at RHIC [14, 15]. The points for protons are shifted horizontally for clarity. The new result for proton from $\sqrt{s_{\rm NN}} = 3.0$ GeV collisions is shown as a filled square. HADES data of $\sqrt{s_{\rm NN}} = 2.4$ GeV 0%–10% collisions [50] is also shown. The vertical black and gray bars are the statistical and systematic uncertainties, respectively. In addition, results from the HRG model, based on both Canonical Ensemble (CE) and Grand-Canonical Ensemble (GCE), and transport model UrQMD are presented.

In summary, cumulant ratios of proton multiplicity distribution from $\sqrt{s_{\rm NN}} = 3.0$ GeV Au+Au collisions are reported. The new data are measured by the STAR experiment configured in fixed-target mode. At this collision energy, large effects due to the initial volume fluctuation are observed in the cumulant ratios except in the most central 0%–5% bin. The protons are measured with the acceptance $-0.5 < y < 0$ and $0.4 < p_{\rm T} < 2.0$ GeV/c. The rapidity and transverse momentum dependencies of the cumulant ratios C_2/C_1, C_3/C_2, and C_4/C_2 are presented. A suppression with respect to the Poisson baseline is observed in proton $C_4/C_2 = -0.85 \pm 0.09$ (stat) ± 0.82 (syst) in the most central 0%–5% collisions at 3 GeV and the UrQMD model reproduces the observed trend in the centrality dependence of the cumulant ratios including $C_2/C_1, C_3/C_2$, and C_4/C_2. This new result is consistent with fluctuations driven by baryon number conservation at the high baryon density region.

Measurement of the Sixth-Order Cumulant of Net-Proton Multiplicity Distributions in Au+Au Collisions at sqrt{sNN} = 27 , 54.4, and 200 GeV at RHIC

Submitted May. 31, 2021 , published Dec. 20, 2021

Phys. Rev. Lett. 127 (2021) 262301

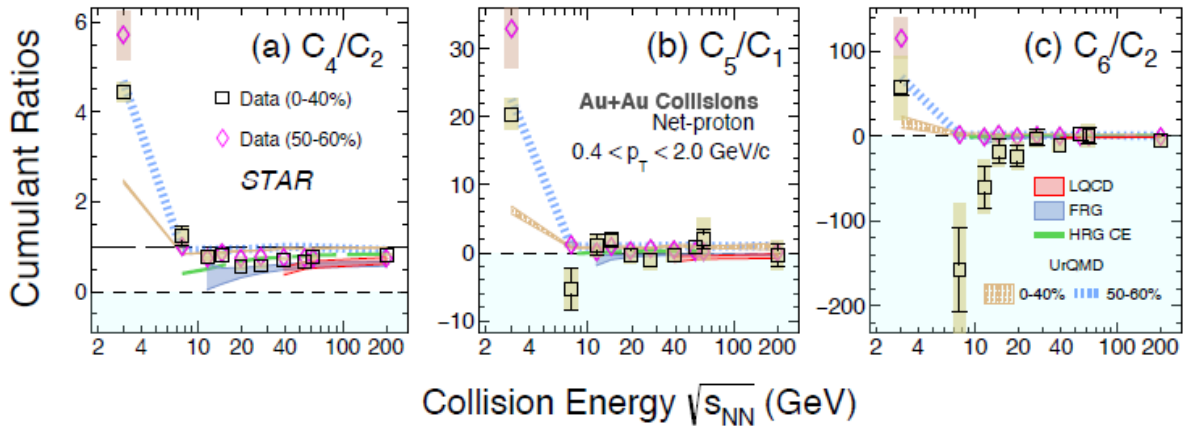

FIG. 3. C_4/C_2 (a), C_5/C_1 (b) and C_6/C_2 (c) of the net-proton distribution in Au+Au collisions from 3 GeV to 200 GeV. The results are shown for 0-40% (squares) and 50-60% (diamonds) centralities. The bars and bands on the data points represent the statistical and systematic uncertainties, respectively. LQCD (39 – 200 GeV) [26], FRG (11.5 – 200 GeV) [27], UrQMD (0-40%, 50-60%), and HRG model calculations (7.7 – 200 GeV) with canonical ensemble [52] (HRG CE) are shown as red, gray, brown bands, blue and green dashed lines, respectively.

In conclusion, measurements of net-proton C_5/C_1 and C_6/C_2 and proton κ_5 and κ_6 are reported in Au+Au collisions over a broad range of collision energies from 3 GeV to 200 GeV corresponding to a μ_B range of 750 MeV to 24 MeV. The data are presented for 0-40% and 50-60% collision centralities. For the first time, we test the ordering of cumulant ratios $C_3/C_1 > C_4/C_2 > C_5/C_1 > C_6/C_2$ expected from QCD thermodynamics. While the overall measured trend for cumulant ratios from 7.7 GeV to 200 GeV seem to follow this hierarchy, a reverse ordering is seen at 3 GeV. C_6/C_2 for 0-40% centrality is increasingly negative with decreasing energy, except at 3 GeV where it is positive. Their deviations from zero at each energy are within $1.7\sigma_{\rm tot}$. The significance of finding negative C_6/C_2 (0-40%) at more than half of the collision energies over the range 7.7 GeV to 200 GeV was found to be 1.7σ. The negative sign of C_6/C_2 is consistent with QCD calculations ($\mu_B \leq 110$ MeV) that include a crossover quark-hadron transition. In contrast, the peripheral 50-60% data, and calculations from the UrQMD model which does not include any QCD transition, are either positive or consistent with zero.

Proton factorial cumulants κ_4, κ_5, κ_6 (0-40%) are presented as sensitive observables to probe a possible first-order phase transition [30]. The measurements indicate the possibility of a sign change at low collision energies, although the uncertainties are large. For energies above 7.7 GeV, the measured proton κ_n within uncertainties do not support the two-component (Poisson+Binomial) shape of proton distributions that is expected from a first-order phase transition. Peripheral 50-60% data do not show a sign change with increasing order and are consistent with calculations from the UrQMD model at all energies. The agreement between the presented data and UrQMD at 3 GeV suggests that matter is predominantly hadronic at such low collision energies. Taken together, the hyper-order proton number fluctuations suggest that the structure of QCD matter at high baryon density,

Disappearance of partonic collectivity in 3 GeV Au+Au collisions at RHIC

Submitted Nov. 24, 2021 , published Mar. 10, 2022

Phys. Lett. B 827 (2022) 137003

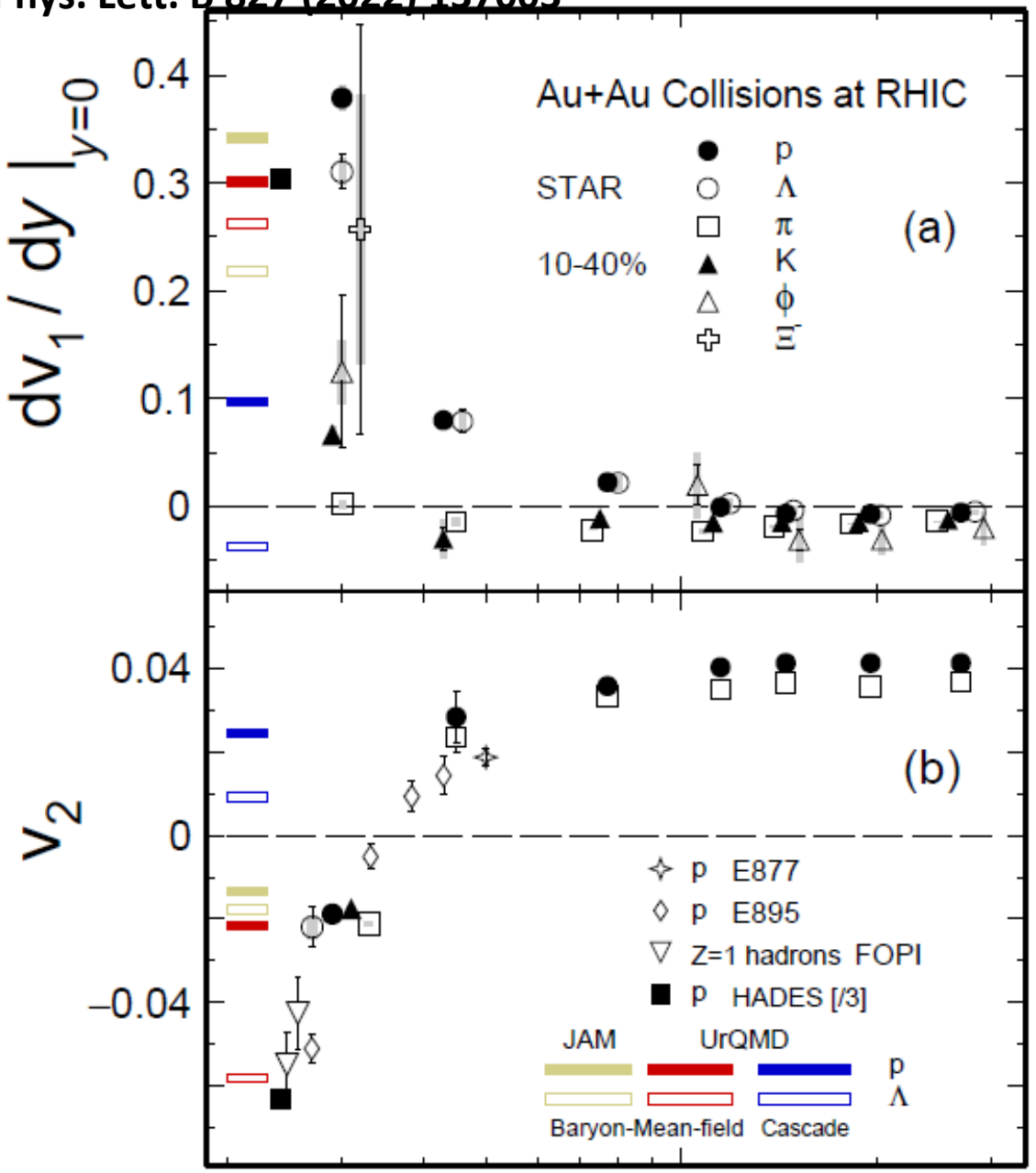

FIG. 5. Collision energy dependence of (top panel) directed flow slope $dv_1/dy|_{y=0}$ for p, Λ, π(combined from $\pi^{\pm}$), K(combined from $K^{\pm}$ and K^0_S), ϕ and Ξ^-, and (bottom panel) elliptic flow v_2 for p, π(combined from $\pi^{\pm}$) in heavy-ion collisions [18, 19, 21, 22, 26]. Collision centrality for all data from RHIC is 10-40%, except for 4.5 GeV where 10-30% is for $dv_1/dy|_{y=0}$ and 0-30% is for v_2. Note that the HADES [35] results of proton $dv_1/dy|_{y=0}$ and v_2 from 20-30% scaled by a factor of 3 are from $1 < p_T < 1.5$ (GeV/c), which is in a higher p_T region compared to our data ($0.4 < p_T < 2.0$ (GeV/c)). Statistical and systematic uncertainties are shown as bars and gray bands, respectively. Some uncertainties are smaller than the data points. The JAM and UrQMD results are shown as colored bands: golden, red and blue bands stand for JAM mean-field, UrQMD mean-field and UrQMD cascade mode, respectively. For clarity the x-axis value of the data points have been shifted.

In summary, we have reported on the p_T and rapidity differential and integral measurements for directed flow v_1 and elliptic flow v_2 of identified hadrons $\pi^{\pm}$, $K^{\pm}$, K^0_S, ϕ, p, Λ and Ξ^- from the 10-40% centrality Au+Au collisions at $\sqrt{s_{\rm NN}}$ = 3 GeV, and the high statistics measurements for v_2 of $\pi^{\pm}$, $K^{\pm}$, p and $\bar{p}$ at $\sqrt{s_{\rm NN}}$ = 27 and 54.4 GeV. The NCQ scaling of v_2 is observed for collision energies $\geq$ 7.7 GeV. Due to the formation of the QGP at center-of-mass collision energies larger than 10 GeV, one finds that each hadron's v_2 is positive while all slopes of v_1 are negative. For Au+Au collisions at 3 GeV, the NCQ scaling is absent and the opposite collective behavior is observed: the elliptic flow of all hadrons at midrapidity is negative; the slope of the directed flow of all hadrons, except π^+, at midrapidity is positive. Furthermore, transport models JAM and UrQMD calculations with a baryonic mean-field qualitatively reproduced these results. These observations imply the vanishing of partonic collectivity and a new EOS, likely dominated by baryonic interactions in the high baryon density region.

Users Meeting
note)

Light Nuclei Collectivity from 3 GeV Au+Au Collisions at RHIC

Submitted Dec. 8, 2021 , published Feb. 1, 2022,

Phys.Lett.B 827 (2022) 136941

•*Phys.Lett.B* 827 (2022) 136941

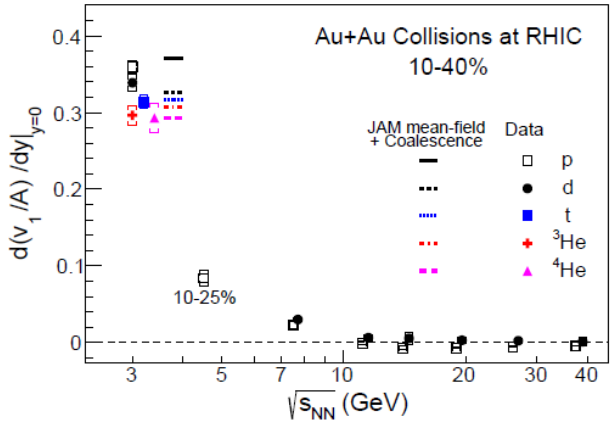

FIG. 6. Light nucleus scaled v_1 slopes $\left(d(v_1/A)/dy|_{y=0}\right)$ as a function of collision energy in 10-40% mid-central Au+Au collisions. Statistical and systematic uncertainties are represented by vertical lines and open boxes, respectively. The data points above 7 GeV are taken from [13]. The proton result at $\sqrt{s_{\rm NN}} = 4.5$ GeV is for 10-25% Au+Au collisions [34]. For clarity, the data points are shifted horizontally. Results of the JAM model in the mean-field mode plus coalescence calculations are shown as color bars.

In summary, we present the directed flow v_1 and elliptic flow v_2 of d, t, ^{3}He, and ^{4}He for 10-40% centrality in Au+Au collisions at $\sqrt{s_{\rm NN}} = 3$ GeV. The light nucleus v_1, as function of both transverse momentum and particle rapidity, follow an approximate atomic mass number A scaling at rapidity $-0.5 < y < 0$, consistent with the nucleon coalescence model calculations. On the other hand, the light nucleus v_2 do not follow the simple A scaling, even after taking into account the contribution from the comparable magnitude of v_1^2. At mid-rapidity $-0.1 < y < 0$, the value of v_2 is negative for all light nuclei, implying a shadowing effect due to the longer passage time of the spectators. Away from the mid-rapidity, the values of light nucleus v_2 become positive and the corresponding proton v_2 remains negative. The JAM model, with the baryon mean-field (incompressibility parameter $\kappa = 380$ MeV and a momentum dependent potential), and a nucleon coalescence qualitatively reproduce both the v_1 and v_2 as functions of rapidity for all reported light nuclei. On the other hand, the results from the JAM cascade mode plus coalescence fail to describe the data. Our results suggest that the light nuclei are likely formed via the coalescence of nucleons at $\sqrt{s_{\rm NN}} = 3$ GeV Au+Au collisions, where baryonic interactions dominate the collision dynamics.

Measurements of Dielectron Production in Au+Au Collisions at sqrt(sNN)= 27, 39, and 62.4 GeV from the STAR Experiment

Submitted Feb. 27, 2023 , published Jun. 1, 2023

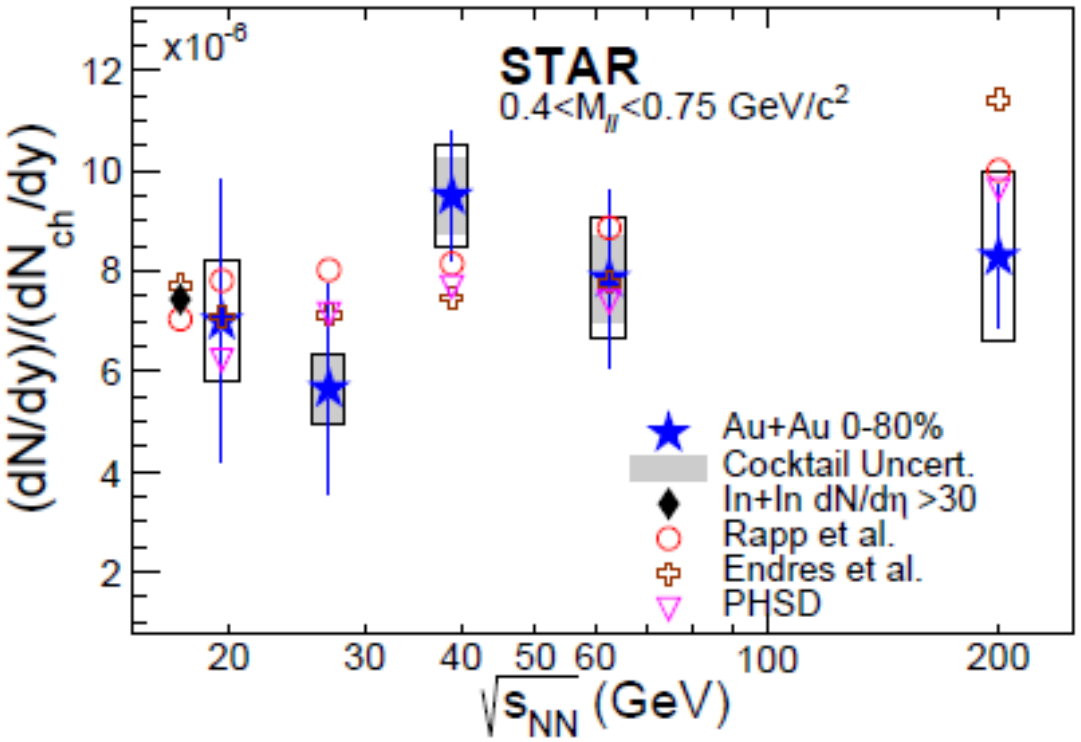

The normalized integrated excess yields show no statistically significant collision-energy dependence for the 0-80% most-central Au+Au collisions.

This may be because dilepton production in the medium is determined by the strong coupling of the rho-meson to baryons, rather than to mesons.

We know that the total baryon density remains approximately unchanged for minimum-bias Au+Au collisions with collision energies above 20 GeV.

The models and our data are statistically consistent even though the model predictions display modest energy dependence.

SciPost Phys. Proc. 10, 040 (2022)

Light Nuclei Production in Au+Au Collisions at $\sqrt{s_{NN}} = 3$ GeV from the STAR experiment

Hui Liu[1*]

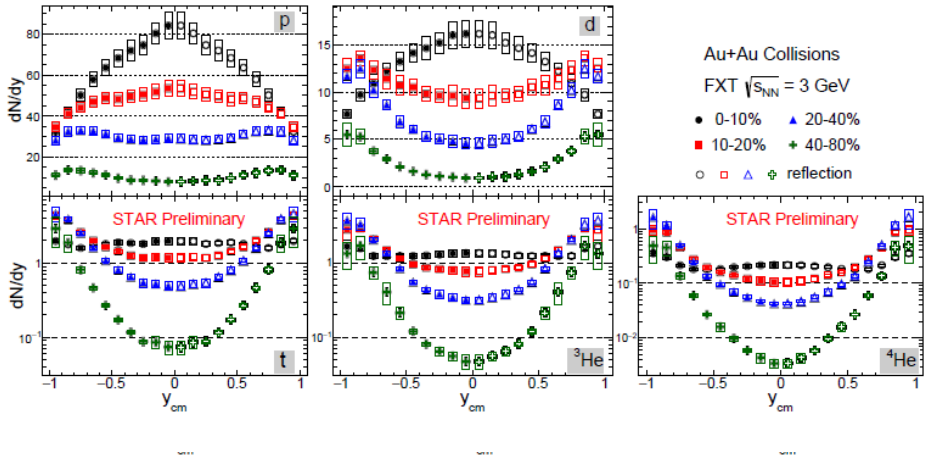

Figure 2: (top) dN/dy and (bottom) $\langle p_T \rangle$ distribution of proton, deuteron, triton, ^{3}He, and ^{4}He in Au+Au collisions at $\sqrt{s_{NN}} = 3$ GeV. Solid markers obtained by real data, open markers are reflected by measured ranges. The boxes indicate the systematical uncertainties.

We report the measurements of the proton and light nuclei (d, t, ^{3}He, and ^{4}He) production in Au+Au collisions at $\sqrt{s_{NN}} = 3$ GeV from the STAR experiment. The p_T spectra, dN/dy and $\langle p_T \rangle$ distributions with various rapidity windows at 0-10%, 10-20%, 20-40% and 40-80% centrality are presented.

Furthermore, an intriguing finding based on the blast-wave model is that we have observed that the distribution of $T_{\rm kin}$ *vs.* $\langle \beta_T \rangle$ at $\sqrt{s_{NN}} = 3$ GeV exhibits a completely different trend compared to high energies. These results reflect the different bulk properties at kinetic freezeout,